Control of gain in conjugated polymers and perylene dyes

A.K. Sheridan

Control of Gain in Conjugated Polymers and Perylene Dyes

Anna Sheridan

March 26, 2001

A thesis submitted to the Faculty of Science, at the University of Durham, for the degree of Doctor of Philosophy.

Abstract

Control of Gain in Conjugated Polymers and Perylene Dyes

This thesis presents an investigation into the factors which control the gain and amplification properties in conjugated materials. Conjugated polymers and perylene dyes are highly fluorescent, are easy to process into thin films, and exhibit strong amplification over a broad gain bandwidth making them ideal for use in lasers and amplifiers. The stimulated emission created when thin films of the red emitting polymer poly(2-methoxy-5-(2'-ethylhexyloxy)-*p*-phenylenvinylene) (MEH-PPV) were photoexcited with high energy laser pulses was investigated. This was characterised by a dramatic narrowing of the emission spectrum which has been assigned to amplified spontaneous emission (ASE). The emission was found to have a gaussian profile and the gain coefficient was found to be 4 cm^{-1}.

The temperature dependence of the absorption, photoluminescence and ASE of films of MEH-PPV was measured. The effect of film morphology on the photophysical properties was investigated by using films cast from two spinning solvents, chlorobenzene (CB) and tetrahydrofuran (THF). Film morphology was found to greatly affect the temperature dependence.

A particularly important property is the spectral position of the ASE and the factors which affect it. By controlling the film thickness close to the cut-off thickness for waveguiding in the polymer film it was shown that the peak position of the ASE could be tuned by 31 nm. Modelling of the waveguide modes in the polymer films was used to explain this effect. The cut-off wavelength for each film was measured and good agreement with the theory was found.

In order to investigate ways in which energy transfer could be used to

control the emission, two perylene dyes were used as a donor-acceptor pair in a host matrix of poly methymethacralate (PMMA). The position of the ASE was found to depend on the acceptor concentration. Measurements of the photoluminescence quantum yield and time-resolved luminescence measurements showed that the energy transfer coefficient was $5\times10^{11}\text{mol}^{-1}\text{dm}^3$.

Contents

Declaration

The material in this thesis has not been submitted for examination for any other degree of part thereof at the University of Durham or another institution. The material in this thesis is the work of the author except where formally acknowledged by reference.

Acknowledgements

I would like to dedicate this thesis to my parents and thank them for their support, encouragement and for the mobile phone.

I am very grateful to my supervisor Prof. Ifor Samuel without whose help during the past three years, this thesis would not have been possible and to Corning (formerlly BICC) for funding this project.

I would also like to thank everyone in the electronics, and mechanical workshops and most of all to technicians Norman and Davey for solving endless problems with equipment.

I am grateful to all the members of my research group especially Ben, Alexei, LO, Mary and Nancy-Ann (for female support), John (for his humour), Graham (for his laser expertise), Ma, Wang, Geetha and Phil (for introducing me to LaTeX) and all my other office-mates for their sense of humour.

Also a huge thank you to all the friends I have made while here in Durham especially to Deborah (for everything bright and cheerful), Ali+Ben (for providing hotel standard accommodation and of course accurate train information), Nick (for making clocks),Frank+Conny and Claire (for many German conversations), Mark and Kevin and Mary (for video evenings and food), Roberto (for being interested in all things Jewish), Patrick (for theological discussions and trips to the vic), to my housemates, Helen, Helen and Corinne (for putting up with me), and to Steve and Antony for introducing me to Seasons cafe. Finally, thanks to Phil - for providing food and friendship when I've needed it most.

Chapter 1

Introduction

Although relatively new, the field of conjugated polymers is an exciting, fast moving area, which incorporates many areas of physics, chemistry and material science.

Conjugated materials are an important class of semi-conducting plastics. They have an extended system of delocalised π electrons, which gives rise to semiconducting optical and electronic properties making electrical conduction possible. In fact it was just over 10 years ago, in 1989, when organic electroluminescence was achieved using the conjugated polymer PPV [1]. This discovery quickly made conjugated polymers the subject of a great deal of interest from companies such as Cambridge Display Technology (CDT), Uniax, Phillips and many others, and also from many research groups throughout the world.

Although these materials were known to be highly luminescent, early experiments in thin films suggested that it would not be possible to observe stimulated emission [2–4] . However in 1992 Moses demonstrated laser action in solutions of MEH-PPV (poly(2-methoxy-5-(2'-ethylhexyloxy)-*p*-phenylenvinylene)) [5]. A few years later Hide et al. observed stimulated emission from polymers doped with titania nanoparticles [6] and the first

microcavity laser was fabricated using PPV [7]. It is partly due to improvements in the quality of the polymer that these advances could be made.

The mechanism for the dramatic narrowing of the emission spectrum has been a matter of much debate. Overwhelming evidence points to the mechanism of amplified spontaneous emission (ASE) [6, 8–13], however there are still those who support cooperative emission mechanisms such as superfluorescence (SF) and superradiance (SR) [14]. Optically pumped lasers in various different forms have been fabricated, including microcavity lasers [7], whispering gallery mode lasers [15] and a flexible DFB (distributed feedback) laser [16].

Conjugated polymers have been shown to exhibit strong amplification over a broad gain bandwidth [12, 17–19]. They are easy to process and by chemically altering the polymers, tuning over a wide spectral range is possible. The emission wavelength can also be controlled by using energy transfer between a host and an acceptor [20, 21].

For these reasons, there is hope that electrically pumped diode lasers will be possible. One problem yet to be overcome is that of the high threshold required for stimulated emission. The density of charge carriers injected into the polymer must be high enough to produce a population inversion, without damaging the polymer film. Thresholds for stimulated emission can be reduced by introducing feedback such as in distributed feedback structures [22]. There has however been some evidence that polaron formation can create an additional absorption in the same spectral region as the gain [23, 24] which will quench the gain. More recent work has shown that in single crystals of tetracene, electrically pumped laser action is possible [25].

Conjugated polymers also have the potential to be used in amplifiers in the communications industry. All-polymer optical fibre networks are now being developed, which have the advantage that information can be transferred quickly and efficiently. An ideal amplifier for this application would emit at

650 nm, where polymer optical fibres are transparent. Conjugated polymers are therefore ideal for this application as they are easy to incorporate into fibres, and they can demonstrate high gain at suitable wavelengths. However for any of these applications to be realised, an understanding of the factors which affect the gain is vital.

In this thesis the factors which affect and control the gain in conjugated polymers and in perylene dyes are investigated.

The first two chapters introduce the theory required to understand the optical properties of these materials and how that relates to amplification in thin film waveguides. Chapter 2 examines the theory of conjugated materials including the process of photoexcitation and quenching mechanisms. Chapter 3 introduces the concepts of spontaneous and stimulated emission. The principles behind a 4-level laser system are examined and the theory of waveguiding in thin films is discussed. Finally, the possible mechanisms for spectral line-narrowing are presented.

In chapter 4 the experimental procedures used to characterise the materials are outlined. Measurements of absorption and photoluminescence give basic information about the polymers and the species formed under photoexcitation. The method for determining the photoluminescence quantum yield - a measure of how efficient the luminescence is from a polymer, is described. The most important experiment in this thesis is the spectral-line narrowing set-up which is used to measure and characterise the gain. This is described in some detail.

In chapter 5 two novel perylene dyes are introduced. The optical properties of these materials and the commonly used polymer MEH-PPV are measured and they are all assessed for their suitability as the active medium in laser and amplification devices. The threshold for spectral-line narrowing (SLN) in MEH-PPV is measured. The second part of the chapter explores some of the factors which can affect the SLN behaviour such as the excitation

wavelength, the angular dependence of the emission and the excitation intensity. The gain coefficient and the loss coefficient at 620 nm are measured for MEH-PPV. The results from this chapter show that the mechanism for SLN is likely to be amplified spontaneous emission (ASE).

Chapter 6 explores the effect of temperature and film morphology on the ASE in films of MEH-PPV. The absorption, photoluminescence and ASE spectra over the temperature range 77 K- 298 K are measured and the effect of the temperature on the position of the peak of the ASE for all three measurements are compared. These measurements are carried out for films spun from the spinning solvents chlorobenzene (CB) and tetrahydrofuran (THF) to investigate the effect of film morphology on the ASE behaviour.

Chapter 7 presents the most exciting and important results regarding the control of the gain in conjugated polymers. The results show that the position of the peak of the ASE can be tuned by over 30 nm by changing the film thickness close to the cut-off thickness for waveguiding. The results are modelled using the standard waveguide theory for waveguide modes in a simple three layer asymmetric structure. In addition the cut-off wavelength for each waveguide is measured as a function of film thickness.

Chapter 8 examines the concept of energy transfer using two perylene dyes (lumogen red and lumogen orange) in the host matrix PMMA. The peak position of the ASE as a function of doping concentration is studied and a discontinuity is observed at 10% lumogen red:lumogen orange. The ASE is found to originate from the donor at low doping concentrations and from the acceptor at high doping concentrations. The dynamics of the energy transfer are measured using photoluminescence quantum yield measurements and time-resolved luminescence measurements. These experiments lead to an estimate of the rate of energy transfer in this system.

Bibliography

[1] J.H. Burroughes, D.D.C. Bradley, A.R. Brown, R.N. Marks, K.D. Mackay, R.H. Friend, P.L. Burn, and A.B. Holmes. *Nature*, 347:539, 1990.

[2] M. Yan, L. J. Rothberg, E. W. Kwock, and T. M. Miller. *Physical Review Letters*, 75(10):1992–1995, 1995.

[3] M. Yan, L. J. Rothberg, F. Papadimitrakopoulos, M. E. Galvin, and T. M. Miller. *Physical Review Letters*, 72(7):1104–1107, 1994.

[4] L.J. Rothberg, M. Yan, F. Papadimitrakopoulos, M.E. Galvin, W.E. Kwock, and T.M. Miller. *Synthetic Metals*, 78:231, 1996.

[5] D. Moses. *Applied Physics Letters*, 60(26):3215–3216, 1992.

[6] F. Hide, B. J. Schwartz, M. A. Diazgarcia, and A. J. Heeger. *Chemical Physics Letters*, 256(4-5):424–430, 1996.

[7] N. Tessler. *Advanced Materials*, 11(5):363–370, 1999.

[8] F. Hide, M. A. Diazgarcia, B. J. Schwartz, M. R. Andersson, Q. B. Pei, and A. J. Heeger. *Science*, 273(5283):1833–1836, 1996.

[9] C. Zenz, W. Graupner, S. Tasch, G. Leising, K. Mullen, and U. Scherf. *Applied Physics Letters*, 71(18):2566–2568, 1997.

[10] M. D. McGehee, R. Gupta, S. Veenstra, E. K. Miller, M. A. DiazGarcia, and A. J. Heeger. *Physical Review B-Condensed Matter*, 58(11):7035–7039, 1998.

[11] G. J. Denton, N. Tessler, M. A. Stevens, and R. H. Friend. *Advanced Materials*, 9(7):547, 1997.

[12] V. Doan, V. Tran, and B. J. Schwartz. *Chemical Physics Letters*, 288(2-4):576–584, 1998.

[13] A. Schulzgen, C. Spiegelberg, M. M. Morrell, S. B. Mendes, P. M. Allemand, Y. Kawabe, M. Gonokami, S. Honkanen, M. Fallahi, B. Kippelen, and N. Peyghambarian. *Optical Engineering*, 37(4):1149–1156, 1998.

[14] S. V. Frolov, M. Ozaki, W. Gellermann, M. Shkunov, Z. V. Vardeny, and K. Yoshino. *Synthetic Metals*, 84(1-3):473–474, 1997.

[15] M. Berggren, A. Dodabalapur, Z. N. Bao, and R. E. Slusher. *Advanced Materials*, 9(12):968, 1997.

[16] C. Kallinger, M. Hilmer, A. Haugeneder, M. Perner, W. Spirkl, U. Lemmer, J. Feldmann, U. Scherf, K. Mullen, A. Gombert, and V. Wittwer. *Advanced Materials*, 10(12):920, 1998.

[17] G. Kranzelbinder, H. J. Byrne, S. Hallstein, S. Roth, G. Leising, and U. Scherf. *Physical Review B-Condensed Matter*, 56(3):1632–1636, 1997.

[18] C. W. Lee, K. S. Wong, J. D. Huang, S. V. Frolov, and Z. V. Vardeny. *Chemical Physics Letters*, 314(5-6):564–569, 1999.

[19] N. D. Kumar, J. D. Bhawalkar, P. N. Prasad, F. E. Karasz, and B. Hu. *Applied Physics Letters*, 71(8):999–1001, 1997.

[20] U. Lemmer, A. Ochse, M. Deussen, R. F. Mahrt, E. O. Gobel, H. Bassler, P. H. Bolivar, G. Wegmann, and H. Kurz. *Synthetic Metals*, 78(3):289–293, 1996.

[21] V. G. Kozlov, V. Bulovic, P. E. Burrows, M. Baldo, V. B. Khalfin, G. Parthasarathy, S. R. Forrest, Y. You, and M. E. Thompson. *Journal Of Applied Physics*, 84(8):4096–4108, 1998.

[22] M. D. McGehee, M. A. DiazGarcia, F. Hide, R. Gupta, E. K. Miller, D. Moses, and A. J. Heeger. *Applied Physics Letters*, 72(13):1536–1538, 1998.

[23] V. G. Kozlov, P. E. Burrows, G. Parthasarathy, and S. R. Forrest. *Applied Physics Letters*, 74(8):1057–1059, 1999.

[24] N. Tessler, N.T. Harrison, and R.H. Friend. *Advanced Materials*, 10:64, 1998.

[25] J.H. Schön, Ch. Kloc, A. Dodabalapur, and B. Batlogg. *Science*, 289:599, 2000.

Chapter 2

Theory of Conjugated Materials

2.1 Introduction

In this chapter the basic physical properties of conjugated polymers will be discussed.

Conjugated polymers are a unique class of semiconducting polymers which have a range of useful electronic and optical properties. These properties arise from the conjugation i.e. the alternating single and double bonds along the backbone of the polymer. Carbon has a valency of 4, therefore carbon tends to form bonds with 4 other atoms. For instance, in the case of methane (CH_4) the carbon is bonded to 4 hydrogen atoms. The carbon atoms in conjugated polymers are unsaturated, which means that they form double rather than single bonds, and each carbon atom bonds to only 3 or less other atoms. The molecule ethene (C_2H_4) will be used to explain how this effects the electron conjugation and leads to the electronic properties associated with conjugated polymers. The schematic diagram in figure 2.1 shows how the electron configuration changes when 2 distinct carbon atoms form a double bond as in

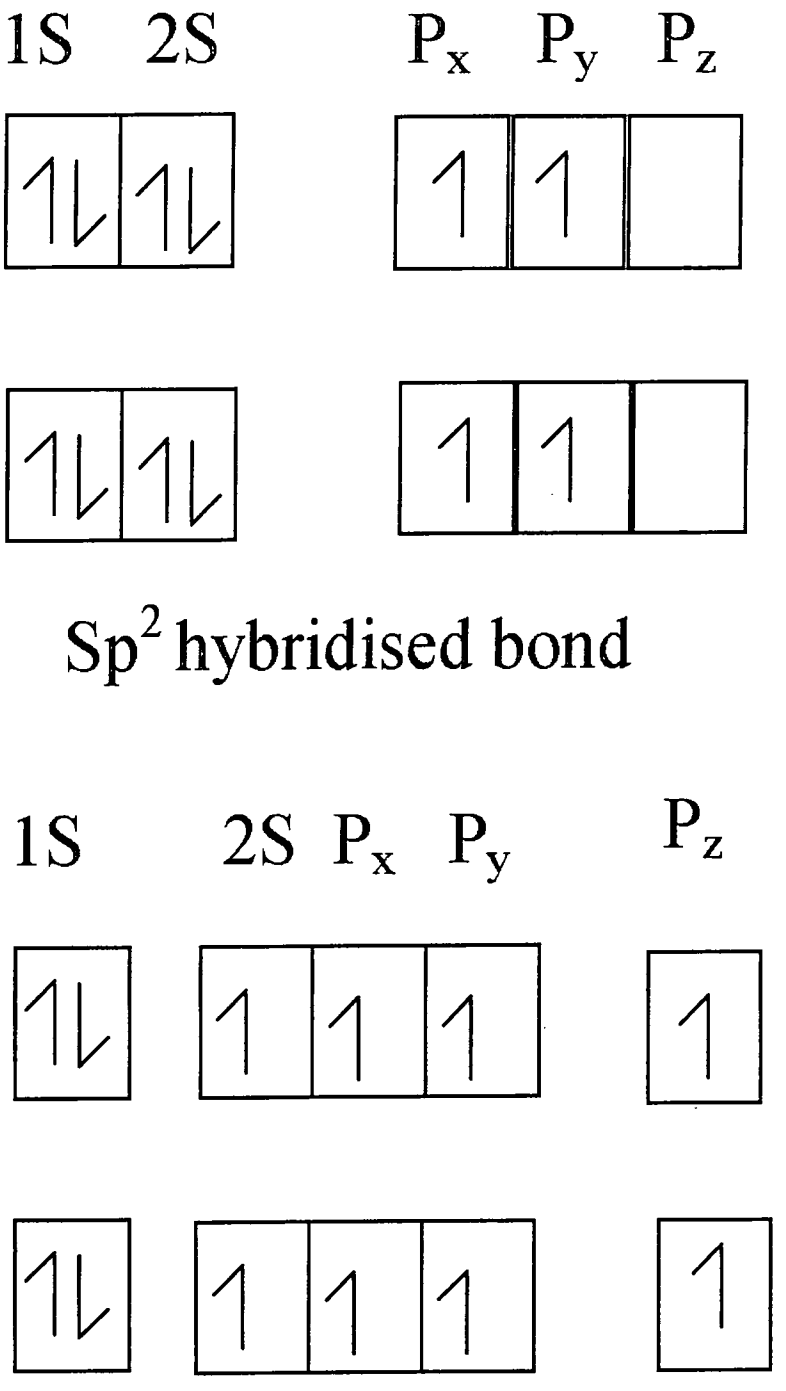

Figure 2.1: Electronic configuration of two distinct carbon atoms (upper panel) and two carbons forming a double bond (lower panel) by sp^2 hybridisation.

the molecule ethene [1]. The electrons in a ground state carbon atom can be written in the configuration $1s^2 2s^2 2p^2$ which is shown in the top part of figure 2.1. Due to Pauli's exclusion principle, the electrons in the p orbitals are not paired. This leaves only two free electrons. For carbon to bond to 4 other atoms, one of the $2s^2$ electrons is promoted into the p orbital. Although this promotion to a higher energy state requires energy, it is vastly outweighed by the energy produced by forming two extra bonds. The single electrons in each of the 2s, p_x and p_y orbitals form what is known as an sp^2 hybridised bond. The remaining p_z electrons remain unhybridised and form a π bond.

In conjugated polymers the electrons in the π bond are free to move along the back bone of the polymer chain. The bonds are formed by the combining of the atomic orbitals to form two molecular orbitals [2]. One of these has less energy, and one has more energy than the two separate atomic orbitals. These are termed bonding and anti-bonding orbitals and it is this which gives rise to the electrical conductivity properties of conjugated polymers.

In these systems the electronic coupling along the polymer backbone is much stronger than the coupling between chains. This means that the system can be considered one-dimensional.

2.2 Non-degenerative Ground State Polymer

Most conjugated polymers, including the ones used in this work are non-degenerate ground state polymers. This means that a change in the bond alternation (interchanging single and double bonds) leads to a change in the energy of the polymer. A theory for describing the degenerate ground state polymer *trans* polyacetylene was developed by Su, Schrieffer and Heeger (SSH model) [3, 4] and is discussed in detail elsewhere [5].

In non-degenerate ground state polymers, three important excitations that can be formed are shown in figure 2.2; a polaron (negative or positive),

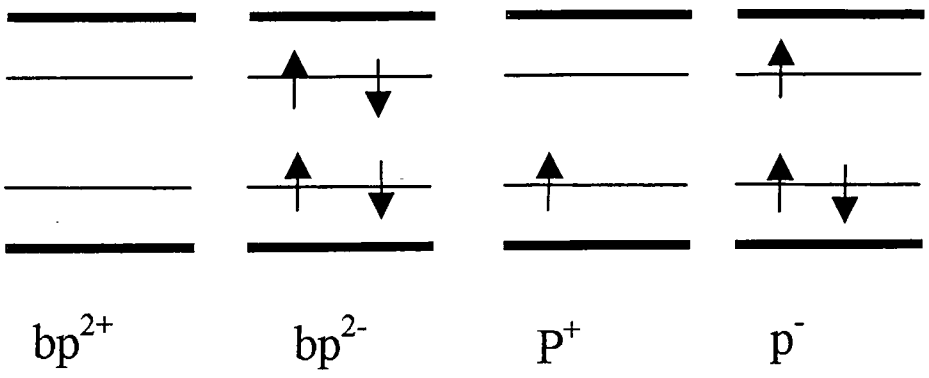

Figure 2.2: Energy levels of positive and negative bipolarons, and positive and negative polarons.

a bipolaron (negative or positive), or a neutral polaron-exciton are formed when states are created in the energy gap which are occupied by 0,1,2,3 or 4 electrons. These polarons give rise to new energy levels within the band gap which are symmetrically placed in the centre of the gap.

Neutral polarons which have two electrons, are of particular interest since they are formed by photoexcitation. Negative and positive polarons are important in the electroluminescence process. The single polaron exciton (generally referred to as an exciton) may decay radiatively, emitting light as it does so.

2.3 Photoexcitation

The study of the photoexcitation process in conjugated polymers can give information about the predominant species formed and therefore how the structure of the polymer is related to its optical properties. Direct optical

excitation is a useful way of generating excitons. These can then be studied by steady state, or time-resolved techniques. In this work, both the spontaneous emission and the stimulated emission are investigated.

The diagram in figure 2.3 shows the transitions typical of an organic molecule that give rise to absorption and emission spectra. A molecule excited with sufficient energy within the π-π^* transition will be excited from the ground state S_0 to a higher excited state S_1. Each energy state consists of vibronic sublevels which are strongly coupled to the electronic transitions. The transitions can be represented as straight vertical lines, as for organic molecules it can be assumed that the electronic transitions take place on a much faster time scale ($\sim 10^{-15}$ s) than the nuclear motions ($\sim 10^{-13}$ s). Therefore most electronic transitions are completed before the nucleus can alter its configuration. This is the Frank-Condon principle. The graph at the bottom of figure 2.3 shows an absorption and emission spectra with the vibronic structure clearly seen, which is due directly to the vibronic sublevels. The 'mirror symmetry' observed between the absorption and photoluminescence spectra is the ideal case for organic molecules. The energy shift between the absorption and emission is termed the Stokes' shift.

Typical absorption spectra of conjugated polymers are however significantly broader with less vibronic structure. Figure 2.4 shows the photoluminescence and absorption spectra measured for a film of MEH-PPV at room temperature. This is partly due to the fact that polymers have a random distribution of conjugation lengths, which all contribute to the spectrum - the absorption spectra sample all conjugated segments. Each individual chain gives rise to an electronic structure, with a corresponding absorption spectrum. It has been suggested that the absorption spectrum of a polymer can be thought of as the superposition of the contributions from each of the different conjugation lengths [7].

The disorder in the sample is also an important factor which affects the

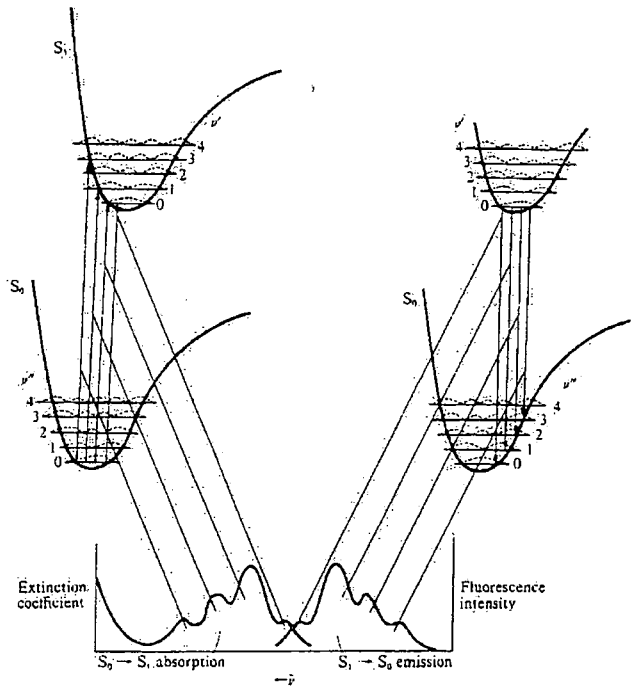

Figure 2.3: Jablonski configuration coordinate diagram from Kearwell and Wilkinson [6].

shape of the spectrum. In an ordered sample the vibronic lines become sharper, this therefore reveals the underlying vibronic structure which is not observed in a disordered sample. As conjugated polymers are cooled down, this increase in the vibronic structure is seen in the spectra. This is because conjugated polymers at room temperature have twists around the phenylene rings which break the conjugation and shorten the effective chain length. As the sample is cooled, the chains become more planar, and therefore more ordered, which leads to an observed increase in the vibronic features. The temperature dependence of conjugated polymers has been studied by Pichler and Yu [8, 9]. A red shift of the spectrum is also seen, as the emission from longer chain lengths is at lower energy. The effect of film morphology in

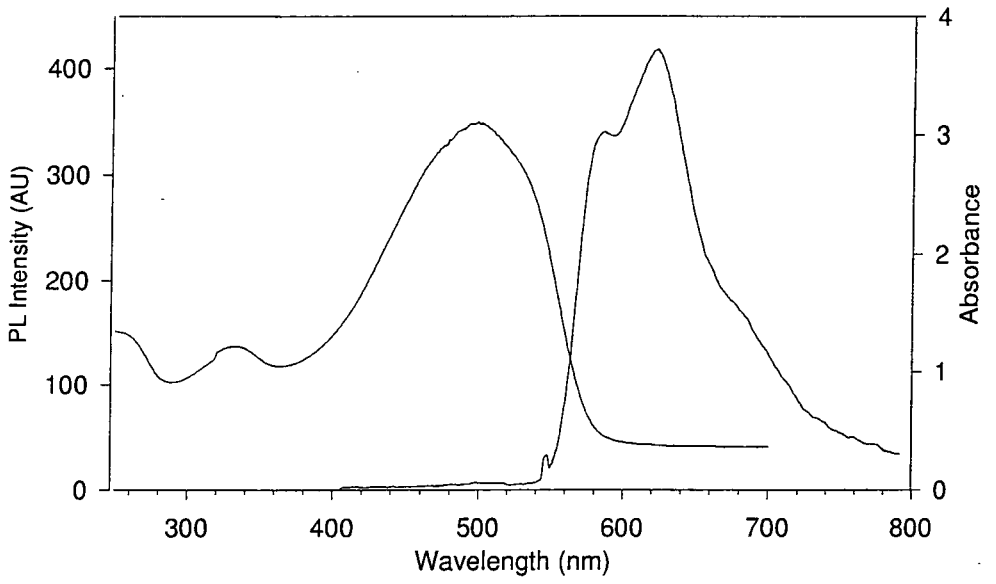

Figure 2.4: Photoluminescence and absorbance spectra of film of MEH-PPV.

MEH-PPV has been studied by Hagler et al. [10]. The effect of temperature and morphology on MEH-PPV films is discussed in more detail in chapter 6.

The spectrum is also affected by broadening mechanisms. These can be homogeneous and inhomogeneous in nature. Inhomogeneous broadening is due to the random nature of the conjugated polymers - the chains experience a statistically varying environment. This results in a distribution of the interaction energies (van der Waals) between the excited state of a molecule and the dipoles induced in the surrounding molecules [11]. A broadening of the absorption and the emission profiles is therefore seen. In contrast a line broadening mechanism is termed homogeneous broadening when it affects each individual molecule. This process is also called natural or intrinsic broadening and is dominant in conjugated polymers where the molecules are

rigidly fixed. Homogeneous broadening is related to the lifetime of a system and can be described with a Lorentzian line-shape [12].

2.4 Excitons

An exciton is a bound electron-hole pair which forms either through direct optical excitation or through electrical excitation. One of the most convenient ways to generate excitons is through optical excitation. Absorption and photoluminescence spectroscopy are therefore useful ways of studying the nature of the photoexcitations in these materials. An exciton can be thought of as a bound electron hole pair. There are two main types of exciton - Frenkel excitons where the electron-hole pair is located on one molecular unit and Mott-Wannier excitons where it extends over many molecular units. It is also possible to have the intermediate state, where an exciton extends over only a few molecular units, this is called a charge transfer exciton. A typical radius for Wannier excitons is between 4 and 10 nm.

Excitons are formed under optical or electrical excitation. Time-resolved luminescence work has shown that after excitons are created they migrate from the shorter (higher energy) chain segments to longer (lower energy) chain segments on a picosecond timescale [13–15]. This effect is well known in molecular organic systems and it is used to explain the blue shift observed from emission measured on short timescales after photoexcitation compared to steady state emission spectra.

Excitons may exist as triplets or as singlets depending on their spin configuration. Singlet excitons can be formed through optical excitation or through injection of electrons and holes of a device. Triplet excitons can only be directly formed by electrical excitation however they are also formed through intersystem crossing from the singlet exciton, which is discussed in section 2.5. The singlet state has an antisymmetric spin wavefunction, whereas the

triplet has a symmetric wavefunction. The possible combinations of spins are shown below. There are three possible superpositions which give rise to triplets but only one which gives rise to the singlet state. The arrows represent the spin state of the electrons in the wavefunction.

$$singlet = \frac{1}{\sqrt{2}}[(\uparrow\downarrow) - (\uparrow\downarrow)] \tag{2.1}$$

$$triplet = \frac{1}{\sqrt{2}}[(\uparrow\downarrow) + (\uparrow\downarrow)] \tag{2.2}$$

$$triplet = (\uparrow\uparrow) \tag{2.3}$$

$$triplet = (\downarrow\downarrow) \tag{2.4}$$

2.5 Quenching Mechanisms

The photoluminescence quantum yield of conjugated polymers (PLQY) can be as high as 50 % [16]. However, the fact that the PLQY is not 100 % implies that non-radiative decay channels compete with the radiative decay.

The photoluminescence quantum yield is related to the radiative and non-radiative rate constants by:

$$\phi_{pl} = \frac{k_R}{k_R + k_{NR}} \tag{2.5}$$

where ϕ_{pl} is the PLQY, k_R is the radiative decay rate and k_{NR} is the non-radiative decay rate.

Therefore the rate of non-radiative decay is of great importance, as a fast non-radiative decay will have an adverse affect on the quantum yield of the polymer.

Possible non-radiative decay mechanisms are multiple phonon emission, and charge separation (through intermolecular energy transfer) which are discussed in more detail elsewhere [17]. Another non-radiative decay mechanism is the migration of excitons to quenching sites formed for instance by aggregates of excimers.

The formation of triplet states through intersystem crossing can lead to luminescence, however, as this is very weak, any intersystem crossing may reduce the overall luminescence efficiency of the polymer. The diagram in figure 2.5 shows how excitons photoexcited through optical pumping can form triplet excitons. Triplet excitons are long lived excited states for which the decay to the ground state is a forbidden transition. The triplet exciton therefore decays on time-scales from milliseconds to seconds. The emission from triplets (phosphorescence) is extremely weak, however it has recently been observed in polymer systems [18]. As the direct formation of triplets is spin forbidden, they are only formed by intersystem crossing from singlet excitons. The long lifetime of the triplet can however lead to quenching of the excitation.

The triplet energies have recently been measured for a variety of polymers using pulse radiolysis by Monkman et al [19].

2.6 Intermolecular Interactions

Although conjugated polymers can often be considered to be one-dimensional, interactions between the chains do exist, and just as in organic dye systems, the optical properties can be vastly modified when this interaction is present. In the case of conjugated polymers, there are two important intermolecular interactions. Aggregates, also called physical dimers (in the case of two molecules) are a ground state species, and excimers which are excited state dimers [11]. There is evidence for such intermolecular interactions (although

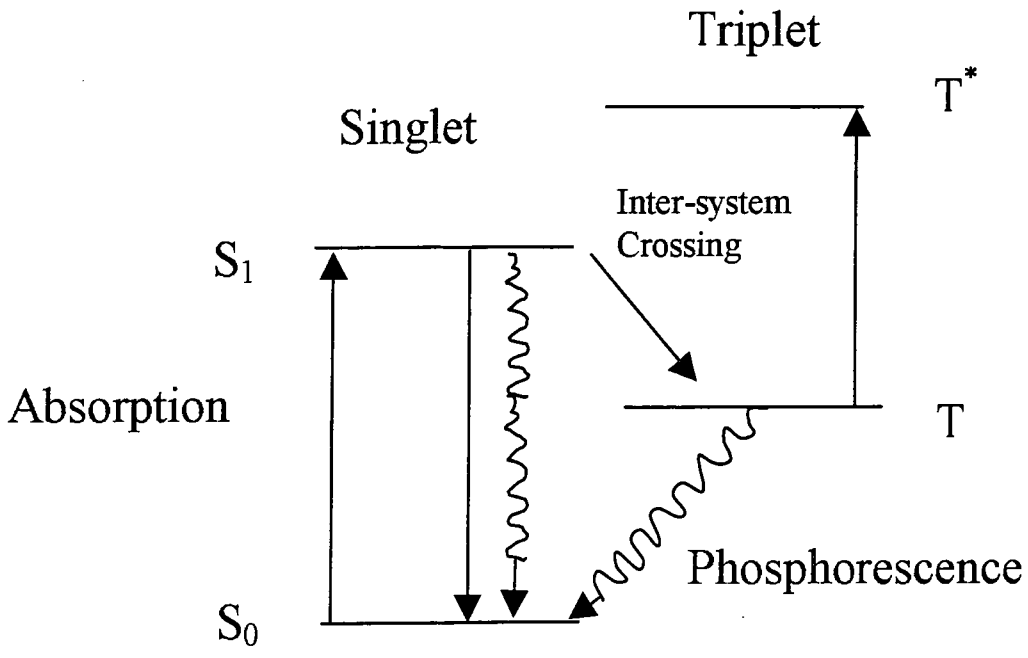

Figure 2.5: Electronic transitions showing singlet and triplet states

it is not clear whether they are aggregates or excimers) in polymers such as CN-PPV [20].

Aggregates result from the overlap between the wavefunctions of two identical closely spaced molecules. These molecules dimerise, causing a splitting of the exciton into a lower and an upper energy level. The orientation of the transition dipoles determines the optical transitions, i.e. if the dipoles are parallel, transition to one of the levels is forbidden, if they are not parallel then both transitions are allowed. In general, aggregates have a broad emission spectrum which is shifted to the red of the absorption spectrum. Aggregates are also characterised by a long emission lifetime and a broad

absorption spectrum in comparison to the solution absorption.

In contrast to aggregates, the absorption spectrum in molecules that form excimers is that which is expected for the monomer, but they also show a broad structureless emission spectrum. These excimers form between an excited molecule and a molecule in the ground state. The repulsive force between the ground and excited state molecules causes the broad emission spectrum. There has been a great deal of interest in intermolecular interactions and how they affect the optical properties of polymers [20–23]. It has been proposed that inter-chain excitations are less mobile than intra-chain excitations possibly because inter-chain excitations are more localised on the region where the dimer is formed [11].

The effect of intermolecular interaction on the gain is extremely important in the context of this thesis and on the future of conjugated polymer electrically pumped lasers. Work by Kozlov and Tessler [24, 25] has shown that in both small organics and conjugated polymers polaron pairs are formed which, under electrical excition can introduce an absorption in the same spectral region as the gain. This could quench the gain and therefore hinder laser action. However, recently lasing was observed in a single crystal of tetracene [26].

Bibliography

[1] J. McMurry. *Organic Chemistry.* Brooks/Cole Publishing, 1984.

[2] P. Sykes. *A Guidebook to Mechanism in Organic Chemistry.* Longman, 1961.

[3] W.P. Su and J.R. Schrieffer. *Proc. Natl. Acad. Sci*, 77:5626, 1980.

[4] W.P. Su, J.R. Schrieffer, and A.J. Heeger. *Physical Review Letters*, 42:1698, 1979.

[5] N.C. Greenham. *Electroluminescence in Conjugated Polymers.* PhD thesis, 1995.

[6] A. Kearwell and F. Wilkinson. *Transfer and Storage of Energy by Molecules.* Wiley, New York, 1969.

[7] B.E. Kohler and I.D.W. Samuel. *Chemical Physics Letters*, 213:472, 1993.

[8] K. Pichler, D. A. Halliday, D. D. C. Bradley, P. L. Burn, R. H. Friend, and A. B. Holmes. *Journal Of Physics-Condensed Matter*, 5(38):7155–7172, 1993.

[9] J. W. Yu, M. Hayashi, S. H. Lin, K. K. Liang, J. H. Hsu, W. S. Fann, C. I. Chao, K. R. Chuang, and S. A. Chen. *Synthetic Metals*, 82(2):159–166, 1996.

[10] T. W. Hagler, K. Pakbaz, K. F. Voss, and A. J. Heeger. *Physical Review B-Condensed Matter*, 44(16):8652–8666, 1991.

[11] I.D.W. Samuel. *Primary Photoexcitations in Conjugated Polymers: Molecular Exciton versus Semiconductor Band Model.* World Scientific, 1998. Chapter 7.

[12] O. Svelto. *Principles of Lasers.* Plenum Press, 1982.

[13] G. R. Hayes, I. D. W. Samuel, and R. T. Phillips. *Physical Review B-Condensed Matter*, 52(16):11569–11572, 1995.

[14] I. D. W. Samuel, B. Crystall, G. Rumbles, P. L. Burn, A. B. Holmes, and R. H. Friend. *Synthetic Metals*, 54(1-3):281–288, 1993.

[15] B. Mollay, U. Lemmer, R. Kersting, R.F. Mahrt, H. Kurz, H.F. Kuffman, and H. Bässler. *Physical Review B*, 50:10769, 1994.

[16] N. C. Greenham, I. D. W. Samuel, G. R. Hayes, R. T. Phillips, Yarr Kessener, S. C. Moratti, Holmesm A.B., and R.H. Friend. *Chemical Physics Letters*, 241(1-2):89–96, 1995.

[17] R.H. Friend, D.D.C. Bradley, and P.D. Townsend. *Journal of Physics D*, 20:1367, 1987.

[18] Y.V. Romanovskii, A. Gerhard, B. Schweitzer, U. Scherf, R.I. Personov, and H. Bassler. *Physical Reveiw Letters*, 84:1027, 2000.

[19] A. P. Monkman, H. D. Burrows, M. D. Miguel, I. Hamblett, and S. Navaratnam. *Chemical Physics Letters*, 307(5-6):303–309, 1999.

[20] I. D. W. Samuel, G. Rumbles, C. J. Collison, S. C. Moratti, and A. B. Holmes. *Chemical Physics*, 227(1-2):75–82, 1998.

[21] I. D. W. Samuel, G. Rumbles, and C. J. Collison. *Physical Review B-Condensed Matter*, 52(16):11573–11576, 1995.

[22] M. Yan, L. J. Rothberg, E. W. Kwock, and T. M. Miller. *Physical Review Letters*, 75(10):1992–1995, 1995.

[23] M. Yan, L. J. Rothberg, F. Papadimitrakopoulos, M. E. Galvin, and T. M. Miller. *Physical Review Letters*, 72(7):1104–1107, 1994.

[24] V. G. Kozlov, P. E. Burrows, G. Parthasarathy, and S. R. Forrest. *Applied Physics Letters*, 74(8):1057–1059, 1999.

[25] N. Tessler, N.T. Harrison, and R.H. Friend. *Advanced Materials*, 10:64, 1998.

[26] J.H. Schön, Ch. Kloc, A. Dodabalapur, and B. Batlogg. *Science*, 289:599, 2000.

Chapter 3

Theory of Stimulated Emission in Conjugated Materials

3.1 Introduction

Organic lasers were first reported in the 1960's using both organic molecules [1] and later dye doped polymers [2, 3]. However it was not until 1992 that evidence emerged that it would be possible to observe stimulated emission in conjugated polymers [4, 5].

In this chapter the basic principles of stimulated emission and laser operation are discussed. Conjugated polymers can be thought of as 4-level laser systems similar to dye laser systems. Since the observation of spectral line narrowing (SLN) in conjugated polymers, (the dramatic narrowing of the emission spectrum at higher excitation densities) there has been much discussion in the literature concerning the mechanism for this phenomenon. The main types of mechanism (amplified spontaneous emission (ASE), superfluorescence (SF) and superradiance (SR)) will be outlined. The thin films used in this work are asymmetric waveguides therefore in the last part of this chapter the general properties of waveguides and the theory behind the

cut-off thickness for TE and TM modes are discussed.

3.2 Spontaneous and Stimulated Emission

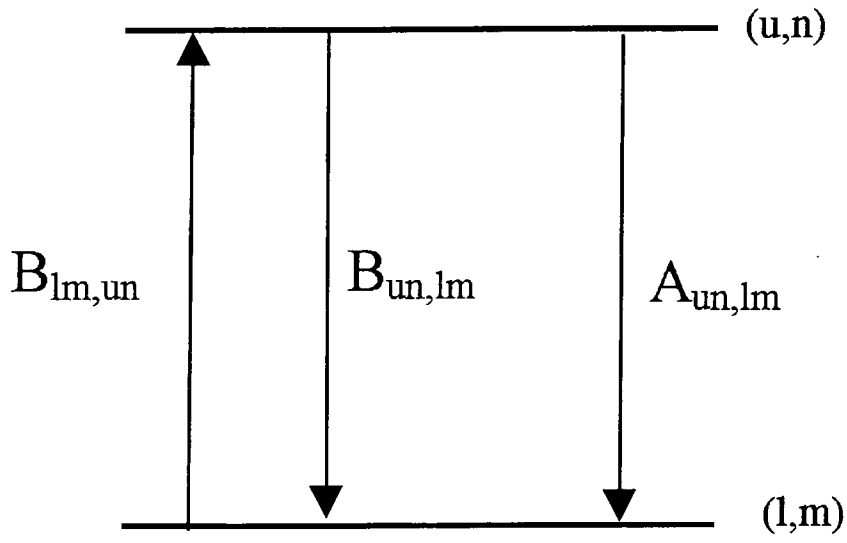

Figure 3.1: Illustration of Einstein Coefficients from Pope and Swenberg [6].

The process of absorption and photoemission in conjugated materials was described in chapter 2. Einstein developed a formalism for the rate of transitions between two energy levels. The diagram in figure 3.1 [6] represents two electronic levels where the subscripts lm represent the mth vibrational level of the lth electronic state and un represent the nth vibrational level of the uth electronic state. The absorption of light is represented by $B_{lm,un}$. Fol-

lowing the initial photoexcitation there are two emissive processes possible, the first is the process of spontaneous emission, where the rate is given by $A_{un,lm}$. This is a random process that determines the normal radiative decay of the excited state.

Spontaneous emission occurs when an atom, excited to a higher energy state by the absorption of a photon, undergoes a relaxation back to the ground state in which a photon of energy $h\nu = E_2 - E_1$ is emitted. The average number of atoms undergoing this spontaneous transition from state 2 with a population N_2 to state 1 per unit time is:

$$\frac{-dN_2}{dt} = A_{21}N_2 = \frac{N_2}{(t_{spont})_{21}} \tag{3.1}$$

where A_{21} is the spontaneous transition rate and $t_{(spont)21}$ is the spontaneous emission lifetime associated with the transition 2→1

The second radiative decay mechanism is stimulated emission, for which the rate constant is given by $B_{un,lm}$. For stimulated emission to occur, a photon with an energy equal to the energy gap of the two states must interact with an electron in the excited level *un*. Stimulated emission can occur at nearly the same rate as the absorption process and it was shown by Einstein that:

$$B_{un,lm} = B_{lm,un} \tag{3.2}$$

and

$$\frac{A_{un,lm}}{B_{un,lm}} = \frac{8\pi\nu^3 n_0^3}{c^3} \tag{3.3}$$

where ν is the frequency of the transition, n_o the index of refraction of the medium and c the speed of light.

3.3 Laser Operation

The work in this thesis is not concerned with making a conjugated polymer laser, rather with studying the gain in the polymers, and ways in which the gain can be controlled. Although there is still some controversy over the mechanism for the spectral line narrowing seen from these materials in thin film waveguides, it is thought *not* to be due to laser action, as there is not sufficient feedback from the edges of the film. Experiments have shown that roughening the edges of the film does not affect the emission properties [7]. However, some of the phenomena associated with lasers, such as a population inversion, threshold for stimulated emission and gain saturation, are relevant to the structures used in this work.

The word LASER is an acronym which stands for 'light amplification by stimulated emission of radiation'; however a laser is more than a device for amplifying light. In general a laser consists of an optical amplifier and a feedback mechanism of some sort. A cavity can be formed by the partially reflecting mirrors as in a ruby laser, the sides of a crystal, as in a semiconductor laser or by a grating arrangement. Common ways to introduce feedback in organic semiconductor lasers are distributed Bragg reflectors (DBR) [8–10], distributed feedback (DFB) waveguides [11] and whispering gallery mode structures [12]. One of the main features of a laser is that it emits coherent light. Coherent emission occurs when a photon interacts with the excited molecule causing another photon to be emitted. This photon will have the same phase and direction as the other photons present.

By considering the populations N_1 in level 1 and N_2 in level 2 of a system, it can be shown that the rate of change of emission intensity per unit length is given by [13]:

$$\frac{dI(\nu)}{dz} = (N_2 - N_1)Cg(\nu)I_\nu \tag{3.4}$$

where C is a constant which depends on the speed of light, the refractive index, the frequency of the emission and the spontaneous decay time; I_ν is the emission intensity and $g(\nu)$ is the photoluminescence spectral line-shape.

This has the solution :

$$I_\nu(z) = I_\nu(0)e^{\gamma(\nu)z} \tag{3.5}$$

where $\gamma(\nu)$ is the exponential gain constant and is given by:

$$\gamma(\nu) = (N_2 - N_1)Cg(\nu) \tag{3.6}$$

A population inversion is defined as when the excited state is more highly populated than a state of lower energy, i.e. when $N_2 > N_1$. Equation 3.5 shows that the intensity grows exponentially if the population is inverted, or attenuated if the population is not inverted ($N_2 < N_1$). In the case where the population is inverted, amplification of the incident wave occurs. This is required for laser operation and is described through the exponential gain coefficient $\gamma(\nu)$. A typical value for the gain coefficient, for instance in a ruby laser where the difference in the populations between level 1 and level 2 is 5×10^{17} cm^{-3}, is 5×10^{-2} cm^{-1}. This implies that a wave passing through the ruby rod of 1 cm will be amplified by approximately 5% [14].

The equation above implies that light intensity will increase without bound if a population inversion exists. However, in practice, gain saturation limits the amplification which is possible. When a light wave is very strongly amplified a substantial fraction of the excitations are depleted. Any further increase in the pump intensity does not increase the amplification. There is in fact a decrease in the gain coefficient when gain saturation takes place [13].

A defining feature of laser operation is a threshold pump intensity, below which only spontaneous emission is observed and above which stimulated

emission is produced. In a laser the threshold is reached when the round trip gain exceeds the round trip losses in the cavity.

3.4 4-level Lasers

Laser dyes are essentially large conjugated molecules which are known to behave as 4-level systems [14]. The stimulated emission observed in conjugated polymers has therefore been assigned to 4-level laser systems [7, 15]. This section describes the underlying principles of a 4-level laser system.

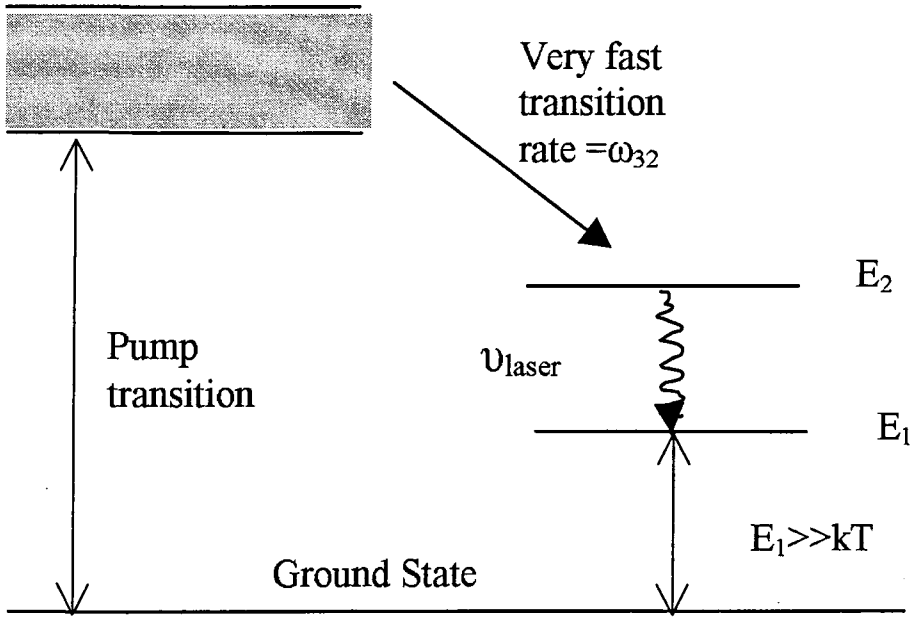

Figure 3.2: A 4-level laser system.

The diagram in figure 3.2 shows the energy levels present in a 4-level laser system. A pump source is used to excite the dye molecule, which,

by absorbing the pump light undergoes a transition into a higher excited state. Most of the dye molecules will then relax quickly to the state E_2. This happens on a very fast time-scale, on the order of 10^{-15} s and is a radiationless transition. The lifetime of the state E_2 is much longer - this allows the population to build up until the population in E_2 is greater than the population in E_1. Stimulated emission then occurs from E_2 to E_1 with the emission of a photon. Finally there is another fast, radiationless transition back to the ground state. In a conjugated polymer system the lower two levels correspond to the S_0 ground state and the upper two levels correspond to the S_1 first excited state. The fast radiationless transitions are vibronic transitions to the lowest level in each state. The diagram in figure 3.3 below shows how the conjugated polymer energy level diagram corresponds to a 4-level laser system.

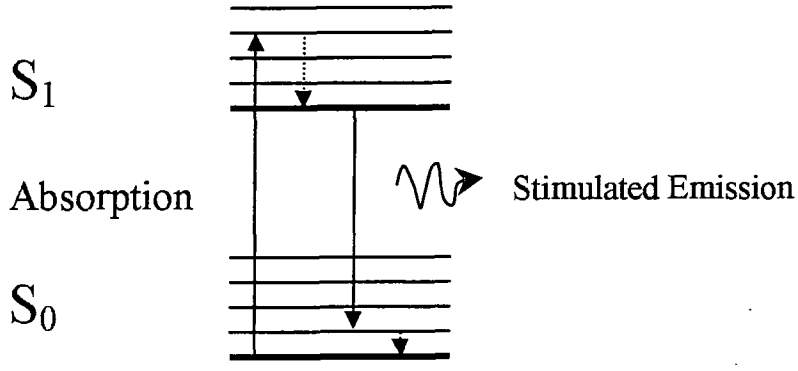

Figure 3.3: 4-level laser system

3.5 Mechanisms for Spectral Line-narrowing

3.5.1 ASE

Spectral line-narrowing is the dramatic narrowing of the broad emission spectrum seen when organic materials are photoexcited with high excitation densities. The widely accepted explanation for the observation of the narrowing of the emission spectrum in conjugated polymers is amplified spontaneous emission (ASE) [16–19]. This phenomenon has been studied extensively in dye lasers [14], however it is normally thought of only as being in competition with the lasing mode, and much effort goes into reducing the ASE. In ASE, photons which are spontaneously emitted in a photoexcited region cause a radiative de-activation of other emitters as they propagate through the medium. The overall gain experienced by an emitted photon propagating through the excited region is given by G:

$$G = e^{g(\lambda)l} \tag{3.7}$$

where g is the gain coefficient and l is the path length inside the sample. The ASE intensity therefore depends on the length of the pump stripe used to excite the polymer film. The importance of waveguiding is also obvious from this equation - the further the photon travels, the more it can be amplified. As equation 3.7 shows, the gain coefficient is a function of the frequency (and hence the wavelength) of the light. As the pump intensity increases, the wavelengths at the peak of the gain will experience a greater amplification, at the expense of the light at other wavelengths. This leads to a dramatic narrowing of the emission spectrum and very intense emission. The peak of the ASE is therefore determined by the peak of the net gain, where the net gain depends on the material gain and ground state and excited state

absorption. The line-width of the ASE in conjugated polymers is generally 6-10 nm.

The pump geometry used in spectral-line narrowing experiments is shown below in figure 3.4. A cylindrical lens is used to form a long stripe length. In ASE waveguiding is very important to confine the optical field over a long gain length. It is therefore necessary for the polymer to have a higher refractive index than both the substrate and the superstrate.

The ASE threshold is a useful way of characterising different gain materials and is very important for the design of electrically pumped lasers, where a low threshold will be essential. It is defined as the incident intensity at which the stimulated emission output becomes as large as the spontaneous emission output.

The effect of the waveguide structure on the spectral line narrowing is discussed in chapter 5 and chapter 7.

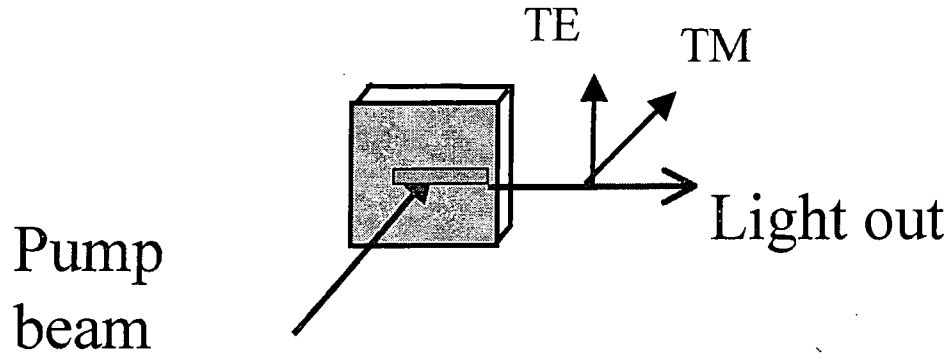

Figure 3.4: Excitation geometry used for the spectral line narrowing experiment.

3.5.2 Co-operative Emission Processes

There are two types of cooperative emission process - superfluorescence (SF) and superradiance (SR), both of which have been assigned to the spectral line-narrowing in conjugated polymers [20–23]. In co-operative emission processes a 'super dipole', which gives rise to extremely rapid coherent emission and narrowed spectra [24] is formed.

SF takes place after an induction time when individual dipoles couple together. There is a time delay in the emission before a rapid decay, which is expected to be of the order of 10^{-13} s for a disordered material such as a conjugated polymer [23].

SR typically arises from aggregates which are coupled to the ground state, however it is usually found in materials with narrow absorption bands and small Stokes shifts which makes it unlikely to be the mechanism for spectral line narrowing in conjugated polymers. Work by Frolov et al. states that the important characteristics of SR are the existence of a threshold intensity and a decrease in the spontaneous emission lifetime [22]. They argue that ASE cannot be responsible for the spectral line narrowing and they show from a simple calculation that the position of the gain should be blue shifted as the thickness of the film is decreased, which they do not see. There is however more recent evidence which shows that a blue shift of the gain spectrum *is* seen as the film thickness is decreased [25].

3.6 Bimolecular Exciton Annihilation

Bimolecular exciton annihilation is a non-radiative process that occurs at high excitation densities and is therefore a competing process to stimulated emission. An understanding of the dynamics of bimolecular exciton annihilation is very important for the realisation of laser devices, as devices must

operate well below the threshold for any competing non-radiative process. An additional factor of $-\gamma N^2$ must be added to rate equations to take account of this process where γ is the bimolecular annihilation coefficient [26].

3.7 Analysis of Waveguide Modes

The films discussed in this thesis can be considered as thin film optical waveguides. A diagram of such a waveguide is shown below in figure 3.5. The polymer layer is sandwiched between the substrate (glass or quartz) and the superstrate (air). For light to propagate in the waveguide, the polymer films must have a higher refractive index than both the substrate and the superstrate.

In order to analyse the modes in the waveguide it is necessary to use the slab (planar) model, which assumes that there is no variation in one direction (in this case the y direction) and that the modes propagate in the z direction [13]. All fields in the waveguide will satisfy the standard Helmholz equation [27]:

$$\nabla^2\mathbf{E}(\mathbf{r}) + \left(\frac{2\pi}{\lambda}\right)^2 n^2(r)\mathbf{E}(\mathbf{r}) = 0 \tag{3.8}$$

Where n is the index of refraction in each layer, λ is the wavelength of light in free space and $\mathbf{E}(\mathbf{r})$ is the electric field as a function of distance r.

In order to solve this equation solutions of the form:

$$\mathbf{E}(r,t) = \mathbf{E}(x,y)e^{i(\omega t - \beta z)} \tag{3.9}$$

are used with the boundary conditions that there is continuity of the tangential component of $\mathbf{E}$ and $\mathbf{H}$ at the air/polymer and polymer/glass interfaces.

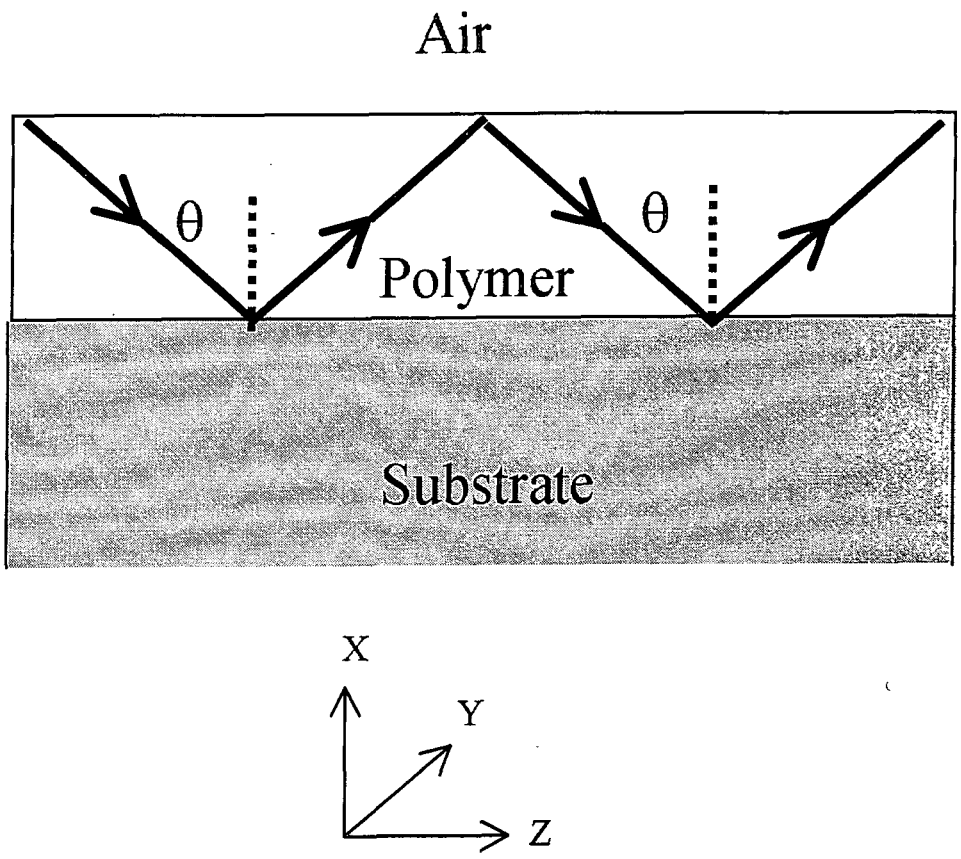

Figure 3.5: Schematic diagram of a waveguide.

There are a number of different solutions to this equation all shown in figure 3.6.

Figure 3.6*a* shows the results for the case where $\beta > k_0 n_2$. β is the propagation constant and k_0 is the free space propagation constant. Here the field increases without bound on either side of the waveguide. This solution is not physically realizable. Figure 3.6 *b* and *c* show solutions for the case where $k_0 n_3 < \beta < k_0 n_2$. These graphs have exponential decays in both the substrate and superstrate and a sinusoidal solution in the polymer region

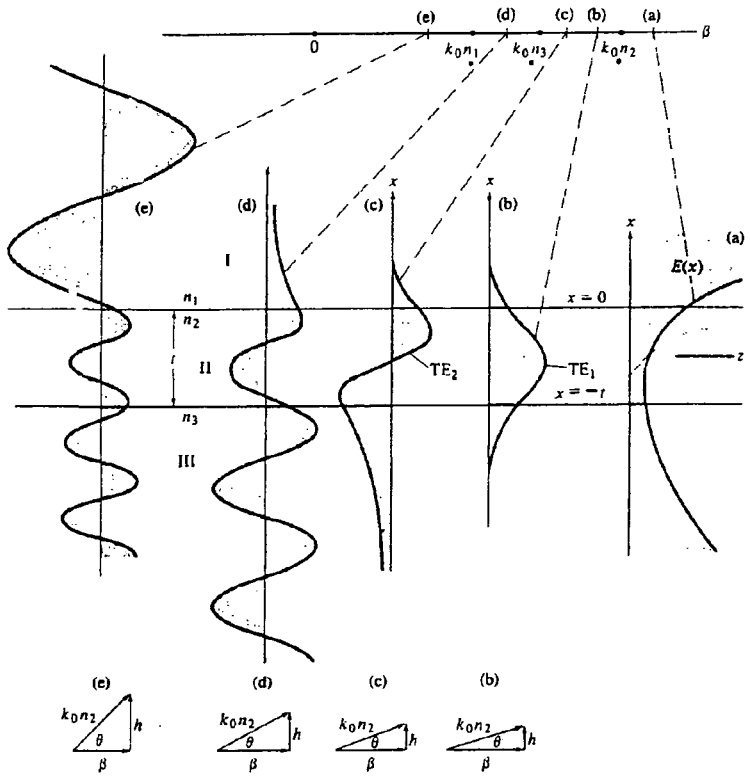

Figure 3.6: Mode Structure from Yariv [13].

and therefore these represent two possible solutions. In these solutions the energy carried by the modes is confined to the vicinity of the guiding layer and they are therefore referred to as bound guided modes. Consequently, in order for modes to be guided in a waveguide, the guiding layer must have a higher refractive index than both the sub- and superstrate regions. For polymers such as MEH-PPV which have a refractive index of about 1.9 at 600 nm, fused silica (n=1.46) or glass (n=1.5) substrates give good refractive index contrast. However there have been reports that no ASE was observed when a sapphire substrate (n=1.8) was used with a similar polymer [7].

By solving the Helmholz equation for the guided mode in an asymmetric waveguide where the guiding layer has a thickness t, the following results are obtained [13]:

$$E_y = Ce^{-qx} \tag{3.10}$$

$$E_y = C\left(\cos(hx) - \frac{q}{h}sin(hx)\right) \tag{3.11}$$

$$E_y = C\left(\cos(hx) + \frac{q}{h}sin(hx)\right)e^{p(x+t)} \tag{3.12}$$

Equation 3.10 is valid for the substrate region, equation 3.11 is for the guiding layer and equation 3.12 is for the superstrate region. The variables h,p and q are given by:

$$h = \sqrt{n_p^2\left(\frac{2\pi}{\lambda}\right)^2 - \beta^2} \tag{3.13}$$

$$p = \sqrt{\beta^2 - n_s^2\left(\frac{2\pi}{\lambda}\right)^2} \tag{3.14}$$

$$q = \sqrt{\beta^2 - n_a^2\left(\frac{2\pi}{\lambda}\right)^2} \tag{3.15}$$

n_s is the refractive index of the substrate, n_p is the refractive index of the polymer and n_a is the refractive index of the air.

This leads to the following equation:

$$\tan ht = \frac{p+q}{h\left(1 - pq/h^2\right)} \tag{3.16}$$

There are two types of bound mode possible in a waveguide. The first is the

TE (transverse electric) mode which is polarized with the electric field in the y-direction. The field components are therefore E_y,H_z,H_x where E denotes the electric field and H denotes the magnetic field. The direction of propagation is the z-direction as shown in figure 3.5. Similarly the TM (transverse magnetic) mode has the magnetic field component in the y-direction and therefore has the field components H_y,E_z,E_x.

If the refractive index is known, the mode profile of the first order TE mode (or any other mode), for a given thickness of the polymer layer and at a given wavelength can be calculated. The software package Mathcad is used to determine the value of β, the propagation coefficient for the waveguide. This is then used in the solutions of the Helmholz equations given above to calculate the field profile required. A typical graph showing the mode profile for a 100 nm thick film of MEH-PPV at 620 nm is shown below in figure 3.7.

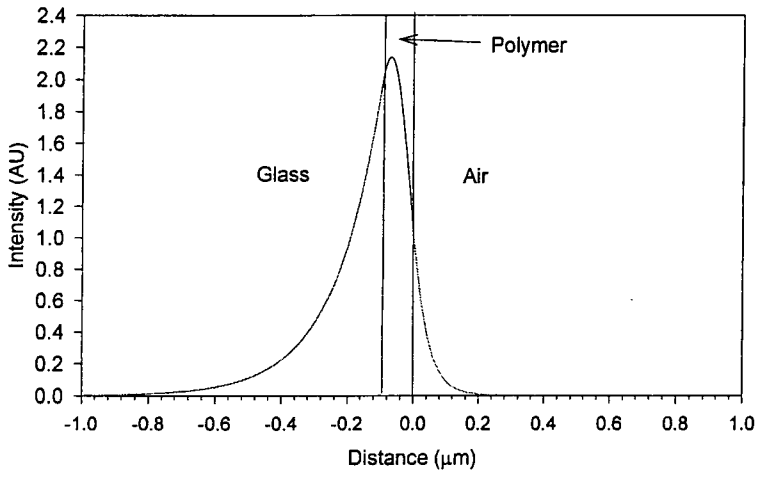

Figure 3.7: First order TE mode in a 100 nm thick MEH-PPV film at 620 nm.

In symmetric waveguides i.e. waveguides with a sub- and superstrate of

identical refractive indices, there is no cut-off thickness for the lowest order TE and TM modes and so light of any wavelength will be guided in these modes. However, for an asymmetric waveguide, a distinct cut-off thickness exists for a given wavelength, below which light of this wavelength will not be guided. At the cut-off thickness, the effective refractive index of the mode ($\beta\lambda/2\pi$) is equal to the refractive index of the substrate (n_s). Therefore p, in equation (3.14) is zero.

Rearranging equation 3.16 with p=0 yields the expression for the cut-off of an asymmetric guide:

$$t = \frac{1}{h} tan^{-1}\left(\frac{q}{h}\right) \tag{3.17}$$

Measurement of the cut-off thickness and the effect it has on the spectral-line narrowing are investigated in more detail in chapter 7.

3.8 Summary

In this chapter the principles of laser operation have been described. A 4-level laser system has been examined and discussed in relation to the energy levels in conjugated polymers. The process of waveguiding has been examined in detail and the possible mechanisms for spectral line-narrowing have been described.

Bibliography

[1] D.J. Moranta, B.G. White, and A.J.C. Wright. *Jounal of Chemical Physics*, 37:2041, 1962.

[2] B.H. Soffer and B.B. McFarland. *Applied Physics Letters*, 10:266, 1967.

[3] H. Kogelnik and C.V. Shank. *Applied Physics Letters*, 18:152, 1971.

[4] D. Moses. *Applied Physics Letters*, 60(26):3215–3216, 1992.

[5] N. Tessler. *Advanced Materials*, 11(5):363–370, 1999.

[6] M. Pope and C.E. Swenberg. *Electronic Processes in Organic Crystals and Polymers*. Oxford Science Publications, 2nd edition, 1999.

[7] X. A. Long, A. Malinowski, D. D. C. Bradley, M. Inbasekaran, and E. P. Woo. *Chemical Physics Letters*, 272(1-2):6–12, 1997.

[8] N. Tessler, G. J. Denton, and R. H. Friend. *Nature*, 382(6593):695–697, 1996.

[9] V. Bulovic, V. B. Khalfin, G. Gu, P. E. Burrows, D. Z. Garbuzov, and S. R. Forrest. *Physical Review B-Condensed Matter*, 58(7):3730–3740, 1998.

[10] A. Schulzgen, C. Spiegelberg, M. M. Morrell, S. B. Mendes, B. Kippelen, N. Peyghambarian, M. F. Nabor, E. A. Mash, and P. M. Allemand. *Applied Physics Letters*, 72(3):269–271, 1998.

[11] C. Kallinger, M. Hilmer, A. Haugeneder, M. Perner, W. Spirkl, U. Lemmer, J. Feldmann, U. Scherf, K. Mullen, A. Gombert, and V. Wittwer. *Advanced Materials*, 10(12):920, 1998.

[12] M. Berggren, A. Dodabalapur, Z. N. Bao, and R. E. Slusher. *Advanced Materials*, 9(12):968, 1997.

[13] A. Yariv. *Optical Electronics in Modern Communications.* Saunders College Publishing, 5th edition, 1997.

[14] F.J. Duarte and L.W. Hillman. *Dye Laser Principles.* Academic Press, 1990.

[15] A. Schulzgen, C. Spiegelberg, M. M. Morrell, S. B. Mendes, P. M. Allemand, Y. Kawabe, M. KuwataGonokami, S. Honkanen, M. Fallahi, B. Kippelen, and N. Peyghambarian. *Optical Engineering*, 37(4):1149–1156, 1998.

[16] V. Doan, V. Tran, and B. J. Schwartz. *Chemical Physics Letters*, 288(2-4):576–584, 1998.

[17] F. Hide, M. A. DiazGarcia, B. J. Schwartz, M. R. Andersson, Q. B. Pei, and A. J. Heeger. *Science*, 273(5283):1833–1836, 1996.

[18] C. Zenz, W. Graupner, S. Tasch, G. Leising, K. Mullen, and U. Scherf. *Applied Physics Letters*, 71(18):2566–2568, 1997.

[19] M. D. McGehee, R. Gupta, S. Veenstra, E. K. Miller, M. A. DiazGarcia, and A. J. Heeger. *Physical Review B-Condensed Matter*, 58(11):7035–7039, 1998.

[20] S. V. Frolov, Z. V. Vardeny, and K. Yoshino. *Physical Review B-Condensed Matter*, 57(15):9141–9147, 1998.

[21] S. V. Frolov, M. Ozaki, W. Gellermann, M. Shkunov, Z. V. Vardeny, and K. Yoshino. *Synthetic Metals*, 84(1-3):473–474, 1997.

[22] S. V. Frolov, W. Gellermann, Z. V. Vardeny, M. Ozaki, and K. Yoshino. *Synthetic Metals*, 84(1-3):471–472, 1997.

[23] S. V. Frolov, W. Gellermann, M. Ozaki, K. Yoshino, and Z. V. Vardeny. *Physical Review Letters*, 78(4):729–732, 1997.

[24] R. Bonifacio and L.A. Lugiato. *Physical Review A*, 11:1507, 1975.

[25] A.K. Sheridan, G.A. Turnbull, A.N. Safanov, and I.D.W. Samuel. *Physical Review B*, 62(18):R11929, 2000.

[26] A. Haugeneder, M. Neges, C. Kallinger, W. Spirkl, U. Lemmer, and J. Feldman. *Jounal of Applied Physics*, 85:1124, 1999.

[27] D. Marcuse. *Theory of Dielectric Optical Waveguides.* Academic Press, 1974.

Chapter 4

Experimental Techniques

4.1 Introduction

In this chapter the main experimental techniques which were used to investigate new materials, to assess their usefulness as amplification media, and to characterise the gain observed, are discussed. The first section deals with the preparation of high quality thin films for optical measurements. The polymers used in this work were supplied as a powder from a variety of sources. The MEH-PPV was supplied by Covion and was synthesised via a Heck reaction. The novel PPV derivatives investigated in chapter 5 were made by Andreas Bacher and Andreas Bleyer at Sheffield University. The two perylene dyes used in the energy transfer experiments in chapter 9 were supplied by BASF in Germany and were used in the host matrix poly-methylmethacralate (PMMA). The methods of optical charaterisation; absorption and photoluminescence, will be described. The technique of measuring the photoluminescence quantum yield is then discussed in detail. In the final section, the experimental set-up used to investigate gain in thin film waveguides is described. The observation of a sharp decrease in the line-width of the emission spectrum at high excitation densities (spectral-

line-narrowing) is a characteristic feature of gain in conjugated materials. This technique is a useful way of probing the excited state dynamics.

4.2 Film Preparation

The main techniques used for producing good quality thin films of conjugated polymers or small organics in a host matrix are spin coating or drop casting. Drop casting produces thick films, however the optical quality is not as good as the films produced by spin coating and the thickness of the films, is not uniform, especially at the centre and the edge of the substrate. All the films used in this work were produced by spin casting as high optical quality was required. This was especially important in the SLN experiments where imperfections in the film could affect the waveguiding necessary to produce ASE.

Two different substrates were used in the experiments; the quartz substrates were circular with a diameter of 12 mm and were always used in absorption measurements as quartz is transparent up to 6 eV. The glass substrates were made from microscope slides cut using a diamond scribe to squares 12 mm$\times$12 mm. These were then cleaned in acetone and isopropanol and dried using a nitrogen line.

Choosing the right substrate for the experiment is very important. For some SLN experiments quartz was used as it has a lower refractive index (1.46) than glass (1.51). In the SLN experiments it is vital to form a substrate/polymer/air waveguide in which the polymer has a refractive index larger than the substrate. While polymers have a relatively high refractive index, the perylene dyes, doped into PMMA have a refractive index lower than 1.51. It was therefore necessary to use quartz substrates for these experiments. However for the experiments with MEH-PPV, glass substrates were used. It was found that films on glass were of better optical quality,

in particular no edge bead formed at the edges of the film as with quartz substrates.

In order to prepare films of conjugated polymers, solutions with a concentration of about 5 mg/ml were made. A suitable solvent was used for example, toluene, tetrahodrofuran (THF) or chlorobenzene (CB). Once the polymer was dissolved the solution was pipetted onto a substrate and spun at between 1000 and 2500 rpm. The substrate was held on the chuck by a vacuum. Films of between 50 and 300 nm could easily be formed. The perylene dyes used in this work were doped into a host polymer matrix of PMMA. PMMA with a molecular weight of 120 000 was used as supplied by Aldrich. A typical solution of 200 mg of PMMA doped with 4 mg of dye in 1 ml of toluene would form films of around 3 μm. The solutions were left to stir overnight.

4.2.1 Measurement of Film Thickness

The thickness of the films was measured using an alpha step surface profilometer. A small section of the polymer film was removed using a scalpel blade. The stylus of the profilometer was drawn across the film, tracing the height at each point. An average could then be obtained between the level of the top of the film and the level of the substrate, thereby giving a measure of the film thickness. It is also possible to get an estimate of the film thickness if an accurate measurement of the absorption coefficient is made. This is discussed below.

4.3 Optical Characterisation

4.3.1 Absorption

Absorption and photoluminescence measurements are important techniques for the characterisation of polymers. Together with time-resolved luminescence measurements, information about the type of ground and excited state species and the inter- and intra-chain interactions can be gained [1–4]. The absorption spectra were measured using a dual beam lambda 19 absorption spectrometer. A reference sample of quartz or glass was placed in one arm of the spectrometer and the sample in the other. Absorbances up to about 2.5 could be measured accurately. A tungsten lamp was used for the long wavelength light to 319 nm and a deuterium lamp was used for shorter wavelengths. The light passed through a monochromator before hitting the sample and was then detected using a photo-multiplier tube (PMT) detector.

In order to measure the absorption coefficient accurately for MEH-PPV 4 films with different thicknesses were made. These were placed in pairs in the two arms of the absorption spectrometer. This technique avoids the problem of reflection from the polymer air interface which causes an overestimate of the absorption. The thickness of the films was measured using the surface profilometer. The relation $\Delta A = \alpha \Delta L$ where ΔA is the change in absorbance, α is the absorption coefficient, and ΔL is the change in thickness for a pair of samples, was used to calculate the absorption coefficient. The graph in figure 4.1 below shows a plot of ΔA at the peak (550 nm) against ΔL. The gradient of this graph and therefore the absorption coefficient for MEH-PPV at 550 nm is 1.1×10^5 cm^{-1}. This can be used to estimate the thickness of an MEH-PPV film if the peak absorbance is known.

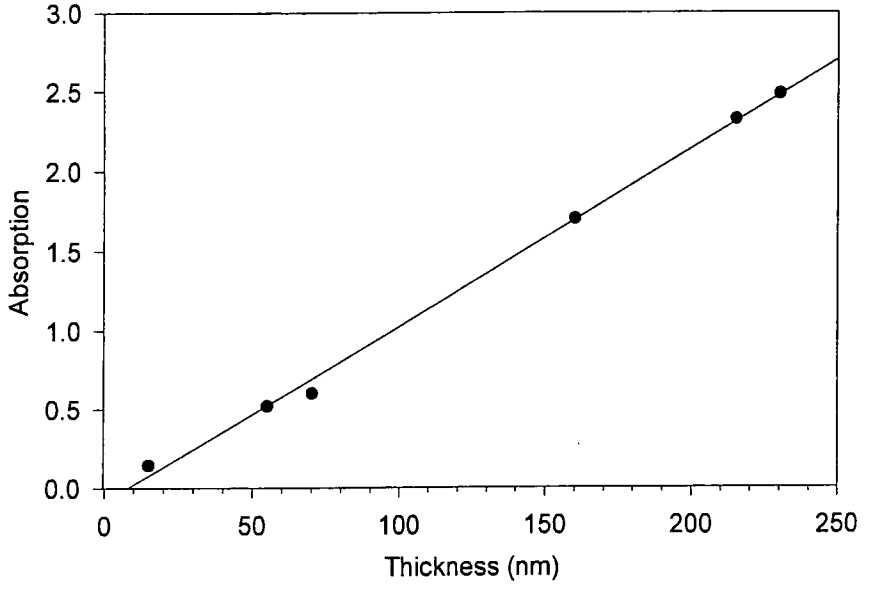

Figure 4.1: Absorbance differences at 550 nm against thickness differences for pairs of films of MEH-PPV.

4.3.2 Photoluminescence

Photoluminescence spectra were measured using the fibre coupled CCD (charge coupled device) spectrograph from Instruments SA. The samples were excited using an Argon Ion laser at a suitable wavelength. The CCD spectrograph consists of a flexible quartz fibre which carries the light into the heart of the CCD. The light passes from the fibre through the entrance slit which determines the resolution of the spectra and then hits a diffraction grating which spatially splits the light into its constituent wavelengths. This light then falls onto the front of the CCD and electron-hole pairs are generated. The number

of electrons generated is proportional to the light intensity. The integration time and the slit width can be used to control the amount of light which is incident on the CCD. A calibration curve supplied by the manufacturer was used to calibrate the intensity of the spectra.

For some photoluminescence measurements, the Instruments SA fluoromax flourimeter was used. This consists of a xenon lamp which is monochromated before it hits the sample, followed by another monochromator and finally a Hamamatsu 928 PMT detector. This instrument has the advantage that photoluminescence excitation (PLE) spectra could also be measured. PLE spectra are produced when the excitation wavelength is scanned and the emission is detected at one chosen wavelength. PLE spectra can give useful information about the type of species formed under excitation, for instance the presence of aggregates can be detected [5].

4.4 Photoluminescence Quantum Yield

The photoluminescence quantum yield (PLQY) is defined as the number of photons emitted by the sample divided by the number of photons absorbed. In conjugated polymers luminescence is the result of radiative decay of singlet excitons. However, this process competes with other non-radiative decay processes and it is the ratio of the rates of radiative (k_r) and non-radiative (k_{nr}) processes which determines the efficiency of the luminescence. In terms of these rate constants the photoluminescence quantum yield is given by:

$$\phi_{pl} = \frac{k_r}{k_r + k_{nr}} = \frac{\tau}{\tau_r} \tag{4.1}$$

where ϕ_{pl} is the PLQY, τ is the overall lifetime which can be measured using the time-correlated single photon counting technique and τ_r is the natural

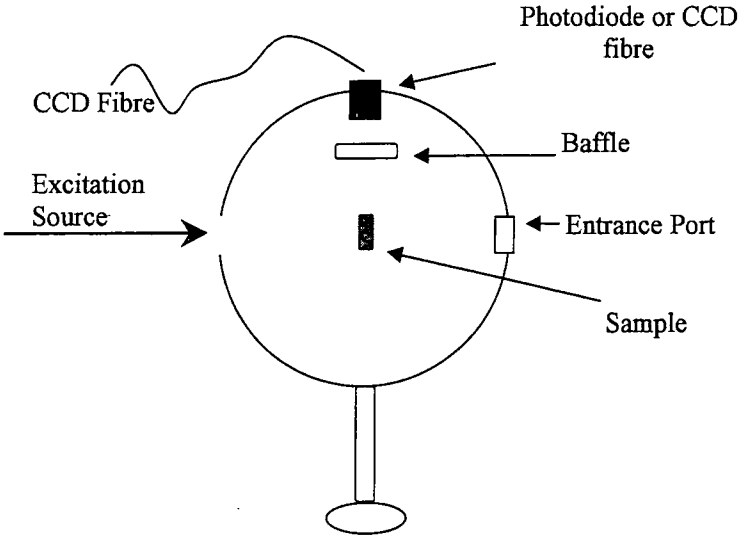

Figure 4.2: The integrating sphere.

radiative lifetime. If these quantities are measured, the rate constants can be deduced. The measurement of the PLQY is described below.

4.5 Measurement of PLQY

4.5.1 Theory

In this section two methods for measuring the PLQY of thin films are described in detail. The measurement of an absolute quantum yield for films is not a straightforward process. In contrast to solutions, which can be treated as sources which emit light equally in all directions, films are anisotropic emitters. The standard technique used for solutions, in which the emission intensity is compared to a standard solution with a known PLQY, cannot be used for films. Films do not emit light isotropically, partly because the

dipoles tend to align along the plane of the film. There is also the problem, that there is no suitable standard film with a known quantum yield. Waveguiding of light down the polymer film and refraction of light also play a role. For this reason the PLQY of films is measured in an integrating sphere which collects all the light emitted in every direction. The technique for measuring the PLQY of films in an integrating sphere was developed by Greenham et al. [6]. An integrating sphere is a hollow sphere coated white inside with a highly reflective and diffusive coating so that light is reflected equally in all directions. The flux of light which reaches the detector is therefore always directly proportional to the flux of light emitted from the sample. This technique also has the advantage that it gives an absolute measure of the PLQY without the need for comparison with standards as in the typical method for measuring the quantum yield of solutions.

Experimental measurements of the PLQY were performed using a Bentham IS4 integrating sphere shown in figure 8.12. The sphere has an entrance slit approximately 2 mm in diameter for the excitation light which is either a laser or the monochromated light from a xenon lamp. The samples were held in the centre of the sphere with the front face perpendicular to the incoming beam. Above the sample, before the collection port is a baffle which is there to prevent light from being scattered directly into the collection apparatus. The samples used had optical densities near 1 at the excitation wavelength. The excitation power was controlled using metal neutral density filters. The light emitted from the sample was collected in a port above the sample. In the method developed by Greenham et al. a calibrated photodiode was used to collect the light. In order to stop the excitation light from being detected at the same time as the emission from the sample, a cut-off filter was placed in front of the photodiode. Kodak Wratten Gelatin filters were used as there have been reports that other filters can fluoresce and therefore add to the measured luminescence intensity [6].

4.5.2 Photodiode Method

In order to measure the PLQY a measurement of the incident laser intensity without the sample (X_{laser}), and a measurement of the photoluminescence intensity with the sample in the sphere is required (X_{sample}). However not all the laser light is absorbed by the film, therefore the absorption at the excitation wavelength is also required. This is given by 1-R-T where R and T are the reflectance and the transmission of the sample respectively. These were measured for each sample by using a photodiode and a laser beam. Greenham et al. [6] derived the following equation for the quantum yield X, in terms of measurable parameters:

$$X = \frac{X_{sample} - (R+T)\,X_{sphere}}{X_{laser}\,(1-R-T)} \tag{4.2}$$

The term (X_{sphere}) is required to account for the light which passes through the sample but is then re-absorbed, leading to an increase in the luminescence. This is measured by tilting the sample out of the path of the laser beam so that direct excitation is avoided.

In order to achieve a correct PLQY value, further corrections have to be applied to account for the response of the photodiode, the transmission of the sphere and the effect of the cut-off filters. This correction Y, is given by:

$$Y = \frac{\int S_{sphere} L(\lambda) G(\lambda) F(\lambda) d\lambda}{S_{sphere}(\lambda_{ex}) G(\lambda_{ex}) \int L(\lambda) d\lambda} \tag{4.3}$$

where S_{sphere} is the transmission of the sphere, G is the quantum efficiency of the calibrated photodiode, F is the transmission of the filter and L is the emission spectrum of the sample and λ_{ex} is the excitation wavelength. The PLQY is then given by:

$$\phi = \frac{X}{Y} \tag{4.4}$$

This technique has been used to measure the PLQY of many conjugated polymer thin films [7]. Many polymers are very sensitive to exposure to air and light and the photoluminescence quantum yield will decrease rapidly if the samples are not stored in vacuum or nitrogen and in the dark. This process is believed to be due to photo-oxidation. In order to overcome the problems of photo-oxidation [8], freshly made samples were used in the experiments and the integrating sphere was flushed with nitrogen to remove most of the oxygen. The temporal decay of the PLQY of some polymers in air, nitrogen and in vacuum have been measured using a computer controlled time dependent measurement [9].

4.5.3 CCD method

An alternative method was developed by de Mello in 1997 [10], in which a CCD spectrograph is used as the detector instead of a calibrated photodiode. In this technique, two spectra are recorded. The first spectrum is of the laser beam, attenuated so that the CCD is not saturated. The second spectrum is measured with the sample in the integrating sphere. Therefore both the photoluminescence spectrum and a laser signal are recorded.

This has the benefit that both the laser and the photoluminescence spectra are measured simultaneously and there is therefore no need for a cut-off filter. There is also no need to measure the reflection and transmission separately as the absorption of the sample is simply given by the reduction in integrated intensity of the laser signal. The PLQY is therefore given by:

$$\phi_{PL} = \frac{P_{sample}}{P_{laser1} - P_{laser2}} \tag{4.5}$$

where P_{sample} is the integrated intensity of the photoluminescence spectrum, P_{laser1} is the intensity of the laser beam without a sample present and P_{laser2}

is the intensity of the laser beam with a sample present.

This method was successfully used for a range of samples and good agreement with the photodiode method was achieved. The CCD method has the advantage that no cut-off filter is required and that the absorption is measured directly without the need to measure the reflection and transmission separately. However, it has the disadvantage that the calibration of the CCD is more likely to change with time.

Using this method the PLQY of the samples used in this work are summarised in table 4.1.

Luminescent Material	Chapter	PLQY
MEH-PPV	4,7,8	30±4%
1,4OPPV	5	36±4%
DDO-PPV	5	12±3%
Lumogen Red	9	95±5%
Lumogen Orange	9	85±5%

Table 4.1: Table of Photoluminescence Quantum Yield Data

4.6 Spectral Line Narrowing

Under high energy pulsed excitation, polymer solutions and films exhibit a dramatic narrowing of the photoluminescence spectrum, characteristic of stimulated emission [11–16]. High pump excitation densities are required to achieve a population inversion.

The first observation of lasing from a conjugated polymer was made using a solution of MEH-PPV excited with high pulse energies from a frequency doubled Nd-YAG laser [11]. Since then there have been many reports of gain in conjugated polymer films. Some work has been on planar waveguides

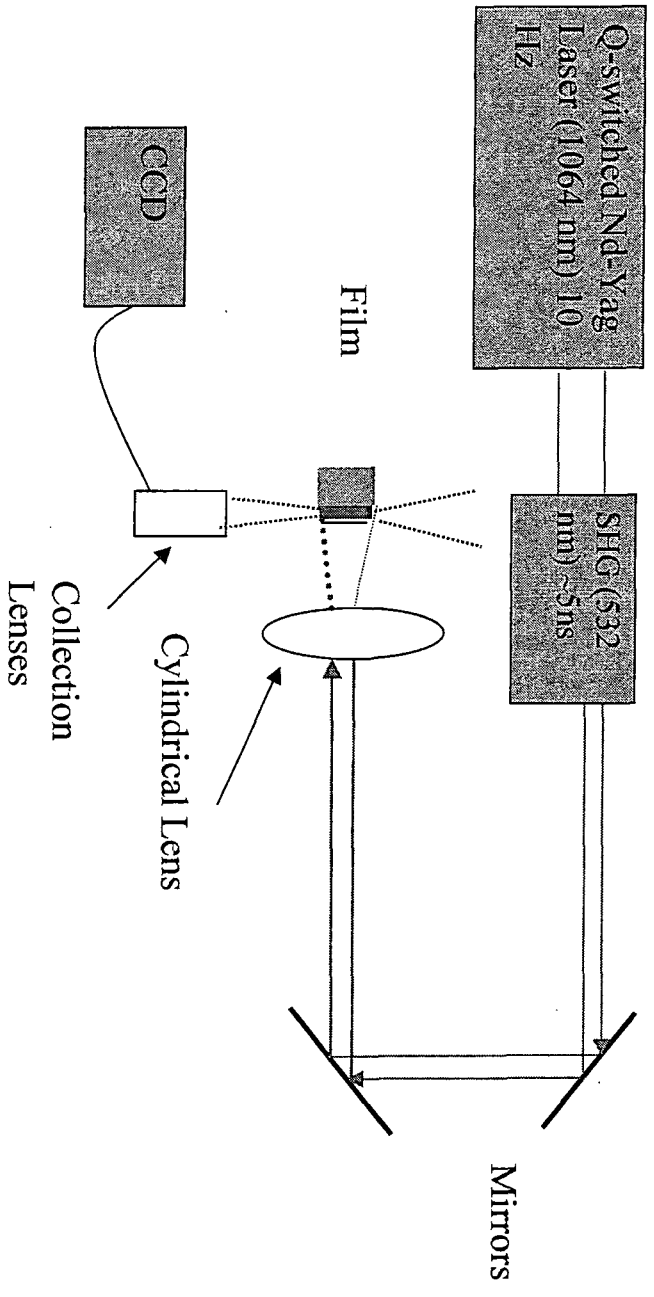

Figure 4.3: Experimental set-up of the spectral line narrowing experiment

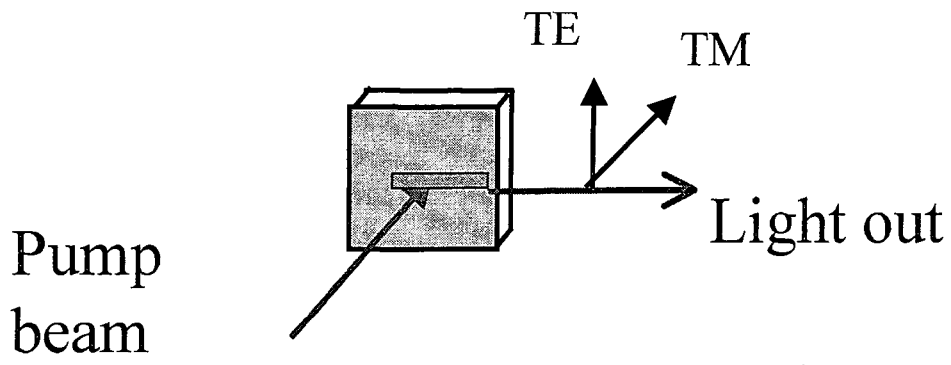

Figure 4.4: Excitation geometry used for the spectral line narrowing experiment. Arrows depict the direction of the electric field vectors.

where the emission is widely accepted to be due to amplified spontaneous emission (ASE) [13, 15, 16] and some on geometries which produce laser emission such as microcavities [12] or microstructured gratings which introduce feedback [17].

For most of the SLN experiments in this thesis a pulsed Q-switched Nd:YAG laser (Spectra-Physics Inc) was used. A diagram of the experimental set-up used for the spectral-line narrowing experiment is shown in figure 4.3. The fundamental emission at 1064 nm was either frequency doubled to produce green light (532 nm) or frequency tripled to produce UV excitation (355 nm). The appropriate wavelength was chosen in order to excite the polymer near to the absorption maximum. The second and third harmonic generation was achieved using KDP second and third harmonic generation crystals. These were kept in a temperature controlled environment as they are sensitive to thermal shock [18]. In order to produce second harmonic generation (SHG) the SHG crystal was moved into the path of the

fundamental beam. Third harmonic generation was achieved by summing the fundamental and the second harmonic using the third harmonic generation crystal. The SHG and THG laser emission had a pulse width of 5 ns and were run at a frequency of 10 Hz.

For some experiments a nitrogen pumped dye laser was used as the excitation source. The nitrogen laser, which produced pulsed emission at 337 nm, was used to pump the dye laser. The dye laser consists of two quartz cells containing dye solutions. A beam splitter is used to split the emission from the nitrogen laser into two parts. The first beam is used to pump the lasing cuvette. The dye laser emission and the second nitrogen laser beam are then used to pump the amplification cell. By using suitable laser dyes emission in the range 380 nm - 600 nm could be achieved. The laser produced 500 ps pulses at 5 Hz.

In order to produce the very high excitation densities needed to achieve stimulated emission, the beam was first expanded and then formed into a stripe (approximately 5 mm$\times$ 200 μm) using a cylindrical lens. Quartz prisms were used to direct the light into the sample chamber.

The sample was held in a specially designed vacuum chamber which could be evacuated with a turbo pump to pressures as low as 1×10^{-5} mbar. The chamber was anodised black in order to minimise problems due to reflected light. The sample was excited through the front window and emission spectra from the sample were collected through the glass cylinder, perpendicular to the excitation beam. In order to ensure no loss of intensity when using UV excitation, the front window was made of quartz.

The diagram in figure 4.4 shows the sample geometry used in this experiment. In order to build up a large enough population inversion to achieve stimulated emission, the light must travel a distance as large as possible. This is achieved through waveguiding in the polymer film as described in chapter 3. For this reason, the front face of the sample was excited and the

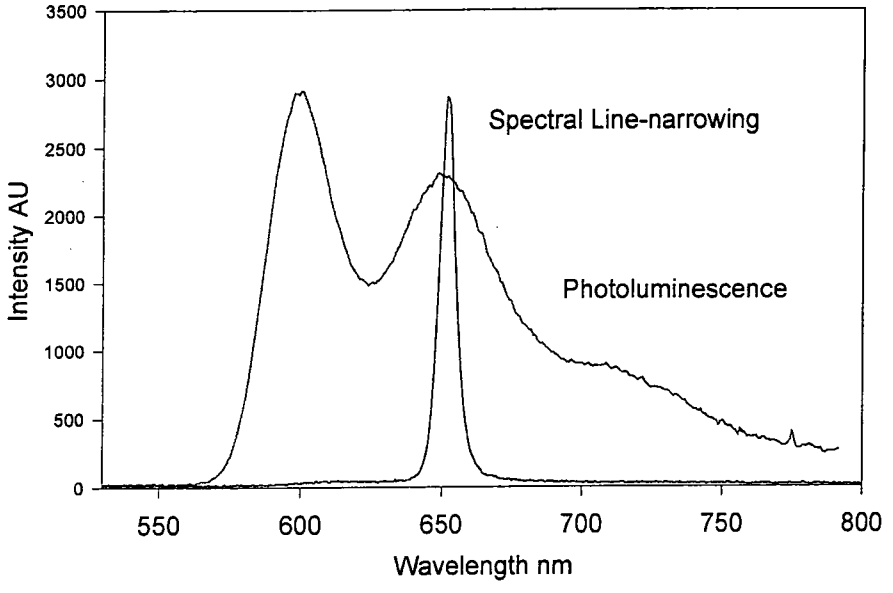

Figure 4.5: Photoluminescence and SLN spectra for MEH-PPV at 117K

waveguided emission was collected at 90^0 to the excitation light.

A CCD spectrograph was used to detect the emission spectrum. The slit width used was typically of the order of 0.1 mm giving a resolution of approximately 1 nm. The integration time was selected according to the intensity of the signal but was never less than 0.5 seconds so that at 10 Hz at least 5 pulses were recorded in each measurement. Integration times shorter than this led to low signal to noise ratios and unrepeatable measurements.

An example of the SLN and PL spectra measured in this work is shown in figure 4.5.

Bibliography

[1] I. D. W. Samuel, G. Rumbles, C. J. Collison, S. C. Moratti, and A. B. Holmes. *Chemical Physics*, 227(1-2):75–82, 1998.

[2] L. J. Rothberg, M. Yan, F. Papadimitrakopoulos, M. E. Galvin, E. W. Kwock, and T. M. Miller. *Synthetic Metals*, 80(1):41–58, 1996.

[3] A. Monkman, M. Halim, S. Dailey, I.D.W. Samuel, M. Sluch, and L.E. Horsburgh. *SPIE*, 3145:208–217, 1998.

[4] L. Magnani, G. Rumbles, I. D. W. Samuel, K. Murray, S. C. Moratti, A. B. Holmes, and R. H. Friend. *Synthetic Metals*, 84(1-3):899–900, 1997.

[5] A. K. Sheridan, I. D. W. Samuel, A. Bleyer, and D. D. C. Bradley. *Synthetic Metals*, 101(1-3):259–260, 1999.

[6] N. C. Greenham, I. D. W. Samuel, G. R. Hayes, R. T. Phillips, Yarr Kessener, S. C. Moratti, A.B. Holmesm, and R.H. Friend. *Chemical Physics Letters*, 241(1-2):89–96, 1995.

[7] N. C. Greenham, S. E. Burns, I. D. W. Samuel, R. H. Friend, S. C. Moratti, and A. B. Holmes. *Molecular Crystals and Liquid Crystals Science and Technology Section a-Molecular Crystals and Liquid Crystals*, 283:51–56, 1996.

[8] M. Atreya, S. Li, E. T. Kang, K. G. Neoh, Z. H. Ma, K. L. Tan, and W. Huang. *Polymer Degrdation and Stability*, 65:287, 1999.

[9] M. Halim, I. D. W. Samuel, E. Rebourt, and A. P. Monkman. *Synthetic Metals*, 84(1-3):951–952, 1997.

[10] J. C. deMello, H. F. Wittmann, and R. H. Friend. *Advanced Materials*, 9(3):230, 1997.

[11] D. Moses. *Applied Physics Letters*, 60(26):3215–3216, 1992.

[12] N. Tessler, G. J. Denton, and R. H. Friend. *Nature*, 382(6593):695–697, 1996.

[13] S. V. Frolov, M. Ozaki, W. Gellermann, Z. V. Vardeny, and K. Yoshino. *Japanese Journal Of Applied Physics Part 2-Letters*, 35(10B):L1371–L1373, 1996.

[14] X. Long, M. Grell, A. Malinowski, D. D. C. Bradley, M. Inbasekaran, and E. P. Woo. *Optical Materials*, 9(1-4):70–76, 1998.

[15] F. Hide, B. J. Schwartz, M. A. DiazGarcia, and A. J. Heeger. *Chemical Physics Letters*, 256(4-5):424–430, 1996.

[16] F. Hide, M. A. DiazGarcia, B. J. Schwartz, M. R. Andersson, Q. B. Pei, and A. J. Heeger. *Science*, 273(5283):1833–1836, 1996.

[17] C. Kallinger, M. Hilmer, A. Haugeneder, M. Perner, W. Spirkl, U. Lemmer, J. Feldmann, U. Scherf, K. Mullen, A. Gombert, and V. Wittwer. *Advanced Materials*, 10:920, 1998.

[18] Spectra Physics. *Manual for the Nd-YAG laser system.*

Chapter 5

Factors Controlling ASE

5.1 Introduction

The use of organic chromophores as the emissive materials in solid and thin film lasers was first demonstrated in the late 1960s [1, 2]. More recently, the first observation of lasing using conjugated polymer microcavities [3] and thin films doped with titania nanoparticles [4] has opened up the possibility of using these materials in devices such as lasers and optical amplifiers. Conjugated polymers have a number of attractive features for these applications. They are readily processible from solution to give uniform thin films and their broad spectra make them suitable for tuneable lasers. Materials with energy gaps across the visible region of the spectrum are available and in contrast to other organic chromophores they suffer little concentration quenching.

Gain in thin films of conjugated polymers has frequently been studied by the process of spectral line-narrowing: when a film is excited by short light pulses above a threshold intensity, a dramatic narrowing of the emission spectrum is observed. This process has been assigned to amplified spontaneous emission (ASE) [5–9] and is seen in films thick enough to support waveguide modes. It has been used to study gain in a wide range of polymers. c Con-

trol of the ASE is very important in the context of device fabrication. There have recently been a number of works investigating the way in which film morphology [10–12], and temperature [13, 14] control the gain.

This chapter is in two parts. In the first part the optical properties of two new PPV derivatives and of MEH-PPV are investigated. The absorption and photoluminescence are measured and they are assessed for their suitability as the amplification materials in laser/amplification devices. The role of waveguiding and aggregation in the results obtained from the spectral line narrowing experiment are discussed.

In the second part of this chapter, the ASE from thin films of MEH-PPV is characterised and some of the factors which affect the gain properties are investigated. The angular dependence, the effect of excitation wavelength and excitation energy on the ASE are explored. Measurements of the gain and the loss coefficients are made and are compared to similar work in the literature.

5.2 PPV Derivatives

Figures 5.1, 5.2, and 5.3 show the chemical structures of the PPV derivatives used in this chapter.

Much of the early work on conjugated polymers used the green emitting polymer PPV. However, PPV is not soluble and is therefore processed from a non-conjugated precursor. The precursor is used to spin films which are then baked in a vacuum oven at high temperatures. In this work PPV derivatives which have side chains joined to the phenylene ring have been used. These side chains increase the solubility of the polymer. Films can therefore be spun directly from the polymer solution, making them easier to process.

The structure of poly (p-phenylenevinylene-co(2,5-dioctyl)*p*-phenylene vinylene) (OPPV) is shown in figure 5.1. It is similar to PPV but has octyl side

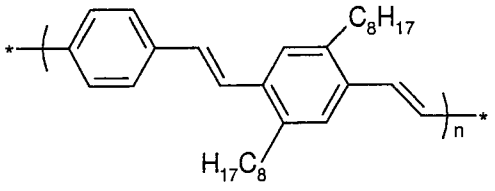

Figure 5.1: Chemical structure of OPPV.

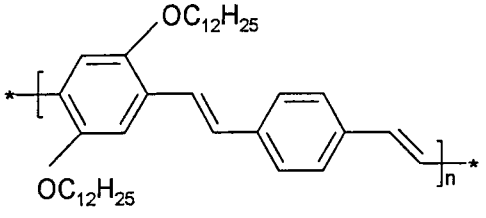

Figure 5.2: Chemical structure of DDO-PPV.

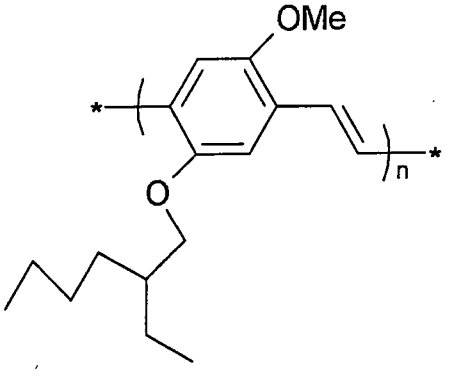

Figure 5.3: Chemical structure of MEH-PPV.

groups which confer solubility on every other phenylene unit. OPPV is soluble in a range of organic solvents including xylene and toluene. Thin films of OPPV were formed by dissolving 30 mg of polymer in 1 ml of toluene and spin coating onto quartz substrates. The polymer was synthesised by Andreas Bleyer at the University of Sheffield via a Wittig reaction. The weight average molecular weight is about 5000 which is quite low compared to some other conjugated polymers (see MEH-PPV below). The photoluminescence quantum yield was measured and found to be 36 % in thin films [15]. This is higher than most dialkoxy PPVs which tend to have lower quantum yields and is consistent with other work showing that polymers with dialkyl side groups tend to lead to higher quantum yields [16].

The structure of poly(2,5-didodecyloxy *p*-phenylenevinylene co p-phenylenevinylene) (DDO-PPV) shown in figure 5.2 is also similar to PPV but in this case the side chains are alkoxy groups and have 12 carbon atoms in each. The side groups are substituted on alternate phenylene unit. The result of adding alkoxy groups is to shift the luminescence to the red in comparison to PPV. This polymer was synthesised by Andreas Bacher at Sheffield University via a Heck reaction. The molecular weight of DDO-PPV is about 4800. Thin films of DDO-PPV were formed by dissolving 30 mg of polymer in 1 ml of toluene and spin coating onto quartz substrates. The quantum yield of thin films of this polymer was measured using the integrating sphere and found to be 13 %.

The chemical structure of poly(2-methoxy-5-(2'-ethylhexyloxy)-*p*-phenylenevinylene) (MEH-PPV) is shown in figure 5.3. MEH-PPV was supplied by Covion in Germany and has a molecular weight of 1.6×10^6. MEH-PPV has asymmetrically substituted alkoxy side groups on the phenylene ring. These groups confer solubility and also give the material a narrower energy gap which shifts the luminescence to the red in comparison to PPV. Thin films of MEH-PPV were formed by dissolving 5 mg of polymer in 1 ml of

chlorobenzene and spin coating onto quartz substrates. The photoluminescence quantum yield of a film of MEH-PPV spun from THF was measured to be 30 %.

The novel polymers DDO-PPV and OPPV both have very low molecular weights therefore very high quantities of polymer were required to form films. However, when such large amounts of polymer were used, there were problems with solubility. Despite the large concentration, the greatest film thickness that could be achieved was 60 nm. The solutions were filtered before they were used. In comparison, MEH-PPV formed films between 50 and 200 nm easily.

5.2.1 Absorption and Photoluminescence

The graph in figure 5.4 shows the absorption and photoluminescence (PL) spectrum for OPPV (bold line) and for comparison the absorption and photoluminescence of PPV (thin line). By comparison to PPV, the effect of the alkyl chains in PPV-co-DOctPV can be discussed. The absorption spectra are very similar with the peak close to 420 nm for both OPPV and PPV. The PPV PL has some vibronic structure with peaks at 550 and 510 nm. In comparison, the film PL of OPPV is broad, structureless and red shifted by 40 nm. Another alkyl substituted PPV derivative is poly(2-butyl-5-(2'-ethylhexyl)-1,4-phenylenevinylene) (BUEH-PPV). BUEH-PPV is asymmetrically substituted with a butyl group on one side and an eight member alkyl group on the other which gives more random packing. The PL of BUEH-PPV [17] has similar vibronic structure to PPV with peaks at 550 and 520 nm. The broad red-shifted PL spectrum of the film of OPPV compared with films of PPV and BUEH-PPV suggests that PL from films of OPPV is from an inter molecular excited state such as an aggregate or excimer. This possibility has been investigated by using poor solvent mixtures. The PL spectra

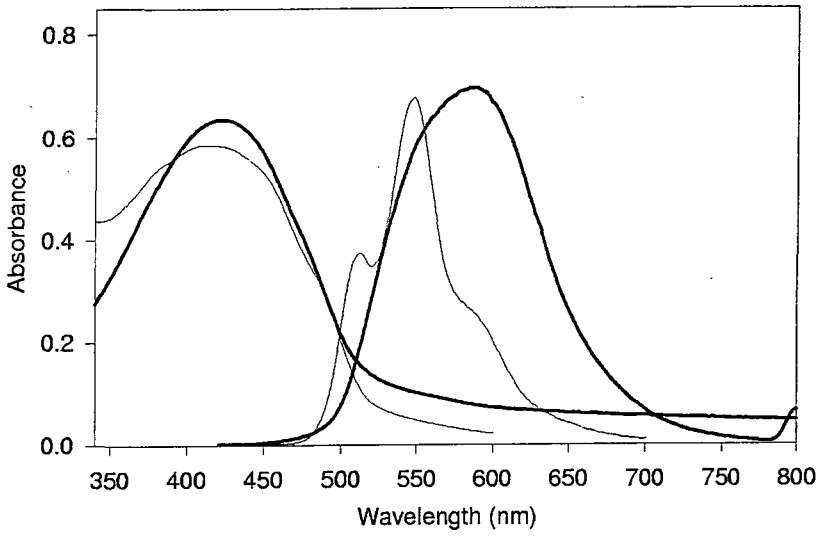

Figure 5.4: Photoluminescence and absorption spectra of OPPV (bold line) and PPV (thin line).

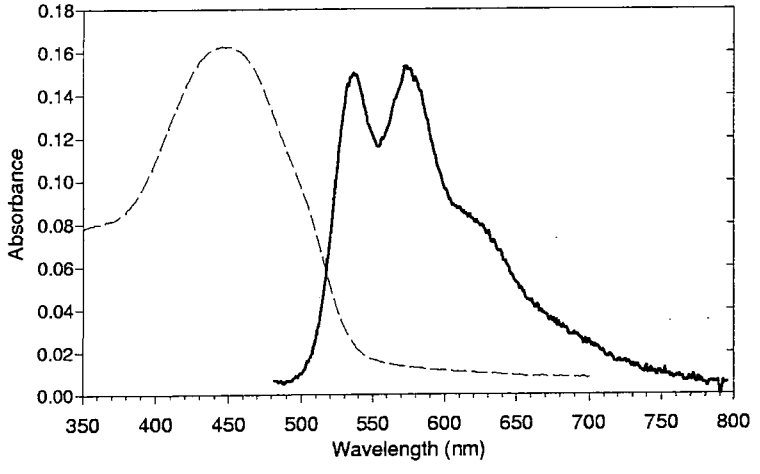

Figure 5.5: Photoluminescence and absorption spectra of DDO-PPV film.

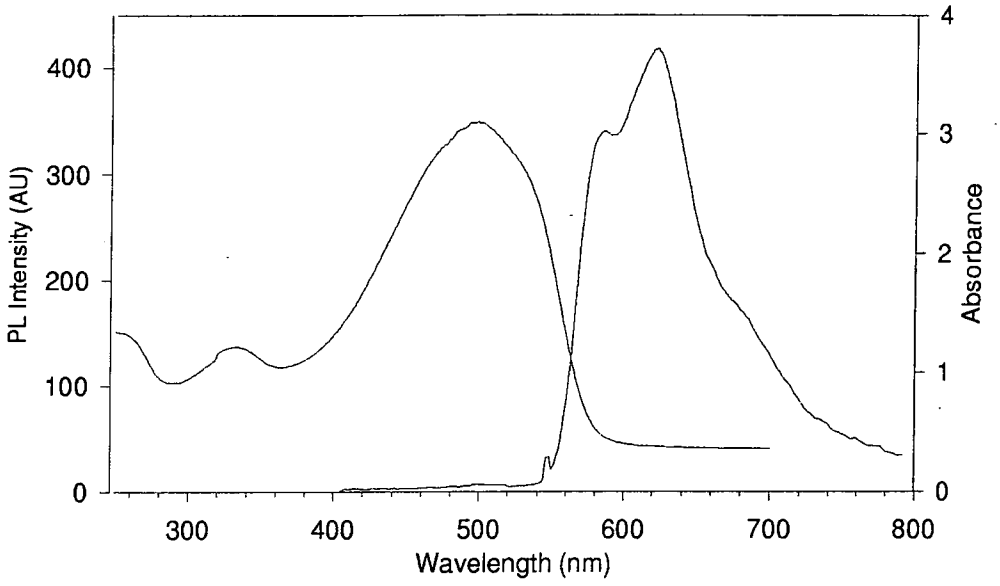

Figure 5.6: Photoluminescence and absorption spectra of MEH-PPV.

of films made from toluene, xylene (good solvents), cyclohexane (poorer solvent) and a mixture of methanol (poor solvent) and toluene in the ratio 6:5 have been measured [15]. It was found that the PL spectra were broadened and there was an increase in the red emission for bad solvents. This could be due to the formation of aggregates in poor solvents. This result will be important when discussing the SLN results.

The graph in figure 5.5 shows the absorption and photoluminescence spectrum for DDO-PPV. The absorption spectrum is similar to the absorption spectrum of OPPV. The peak is at 450 nm and it is broad and featureless. The PL spectrum however shows some vibronic structure with peaks at 540 and 590 nm. There is also a long photoluminescence tail.

The graph in figure 5.6 shows the absorption and photoluminescence

spectrum for MEH-PPV. Both the absorption spectrum and the photoluminescence spectrum are red shifted compared to the two PPV derivatives discussed above. The red shift is due to the side groups which give the material a narrower energy gap. Alkoxy side groups also lead to a bigger red shift than alkyl groups, due to their inductive effects. The PL shows some vibronic structure with peaks at 590 and 640 nm.

5.2.2 Spectral Line Narrowing

The graph in figure 5.7 below shows the result of exciting the OPPV film with high energy laser pulses. The excitation source was the third harmonic (355 nm) from the Nd-YAG laser described in chapter 4. A small peak is seen at 535 nm when the films were excited with 0.15 mJ, which indicates that this is close to the threshold for line-narrowing. However when the excitation energy was increased the film was photo-oxidised and only a PL background was seen. The peak is substantially shifted from the peak of the photoluminescence spectrum. No change in the emission spectrum of DDO-PPV was seen when films were excited under the same conditions.

The graph in figure 5.8 shows the emission spectra of a film of MEH-PPV measured at low (2 μJ) and high (20 μJ) excitation intensities. At low excitation intensities, the emission resembles that of the broad photoluminescence spectrum. As the excitation intensity is increased, the line-width of the spectrum collapses and at higher intensities a narrow line with a width of 6 nm is observed. The narrow peak is close to the peak of the PL spectrum.

5.2.3 Discussion

The peak seen in the OPPV spectrum is assigned to stimulated emission, however the narrowing is not complete and a substantial PL background can still be observed. It is now generally accepted in the literature that the mech-

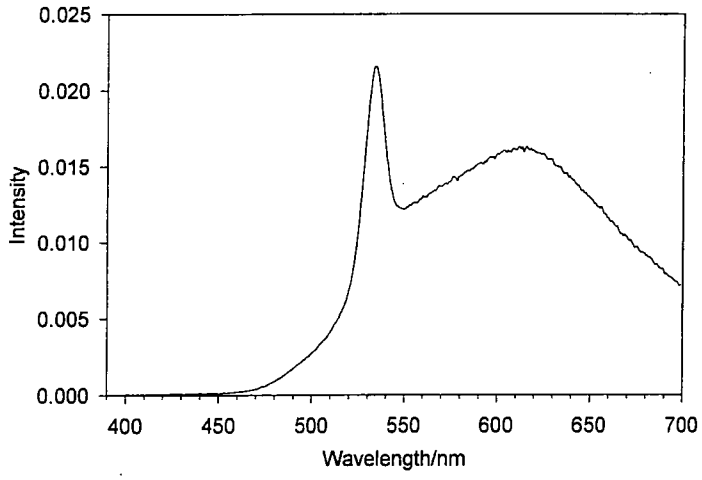

Figure 5.7: Emission spectrum excited with 0.15 mJ from a film of OPPV.

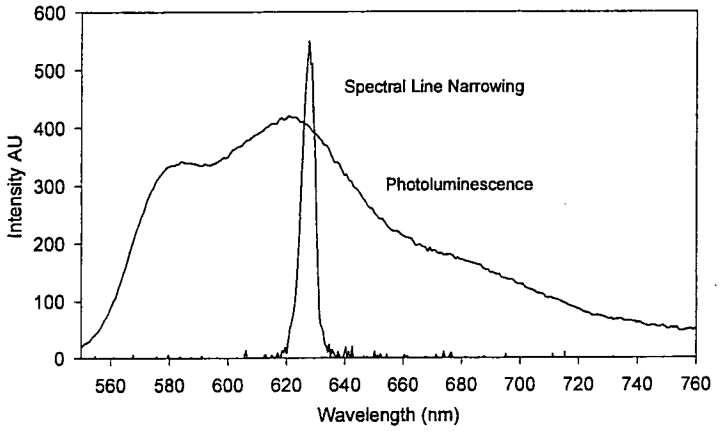

Figure 5.8: Photoluminescence and spectral line-narrowing spectra of MEH-PPV at 2 μJ and 20 μJ respectively.

anism of spectral line-narrowing is amplified spontaneous emission (ASE) as described in chapter 3 and references [5–9]. For ASE to be produced, waveguiding in the polymer film is necessary to confine the optical field over a long gain length [7]. If the gain exceeds the losses, then stimulated emission is produced. In order to form a waveguide, the refractive index of the polymer must be greater than that of both the substrate (quartz) and superstrate (air). However, for a given thickness of polymer film there will exist a cut-off wavelength, above which light will not be guided in the film. Equation 5.1 below shows how the cut-off thickness is related to the refractive indices of the substrate, air and polymer for a given wavelength [18].

$$h_{cutoff} = \frac{\lambda}{2\pi\sqrt{n_f^2 - n_s^2}} tan^{-1} \sqrt{\frac{n_s^2 - n_a^2}{n_f^2 - n_s^2}} \tag{5.1}$$

Here n_s is the refractive index of the substrate (for quartz n_s=1.46), n_f is the refractive index of the polymer film and n_a is the refractive index of the air (n_a=1). The polymer refractive index dispersion is not known but it is likely to be similar to that of MEH-PPV [19]. Conjugated polymers are highly birefringent, as the polymer chains tend to align along the plane of the film. This results in a high in-plane refractive index in comparison to the out of plane refractive index. For instance, in MEH-PPV the in-plane refractive index at 620 nm is 1.91 and the out of plane refractive index is 1.65. From these data, the in-plane refractive index is likely to be between 1.8 and 2.0 at the emission wavelengths. If these values are used in equation 5.1, a cut-off thickness of between 48 and 74 nm at 620 nm is calculated. The cut-off thickness at 620 nm is therefore very close to the measured thickness of the film. This shows that light at the peak of the gain spectrum (620 nm) may not be guided in the film and therefore no SLN is observed for the DDO-PPV film. Weak SLN is seen in the OPPV film, but shifted to 535 nm, below the cut-off for waveguiding. However, as this is not close to the peak

of the gain spectrum, the threshold is very high and such high excitation intensities tend to destroy the film. The effect of the thickness of the film and the cut-off thickness is discussed in more detail in chapter 7.

The calculations above show that the films were probably too thin to support waveguide modes at the peak of the net gain. This either totally suppressed the SLN as in DDO-PPV or made it extremely unstable as in OPPV. However, thicker films could not be made as the molecular weight of the materials is very low. Concentrations of approximately 30 mg/ml were required to form films 60 nm thick, however if larger concentrations were used the solutions would aggregate and very poor quality films were produced.

5.2.4 Aggregation

Another possible reason for the lack of SLN is that the polymer photophysics is modified by aggregation, which can quench the luminescence. In order to investigate the role of aggregation in OPPV, photoluminescence excitation spectra (PLE) were measured.

The broad red-shifted PL spectrum of the films of OPPV compared with the polymer in solution and films of PPV shown in figure 5.4 suggests that PL from films of OPPV is from an inter-chain molecular excited state such as an aggregate [15, 20].

PLE spectra have been measured in films of OPPV. The spectra measured at short detection wavelengths (corresponding to the short wavelength tail of the PL spectrum) are shown in figure 5.9. Differences in the spectra in the region of 350 nm and 450 nm indicate that the PL detected at longer wavelengths is more strongly excited by longer wavelength excitation. This is consistent with some emission from aggregates. No further change of excitation spectrum was observed for longer detection wavelengths up to 740 nm.

This is evidence that aggregation may play a role in quenching the luminescence and spectral line narrowing in OPPV films.

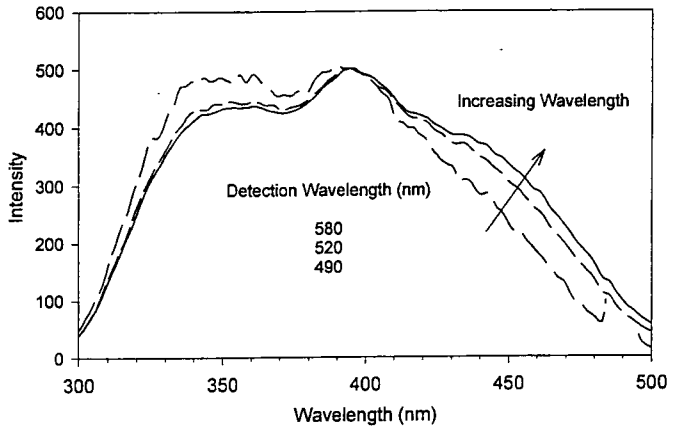

Figure 5.9: Photoluminescence excitation spectra for OPPV.

5.2.5 Summary

From the three PPV derivatives that have been investigated, only MEH-PPV is a suitable material for investigating the spectral line narrowing properties. The main problem with OPPV and DDO-PPV is their low molecular weight, which affects the ability to form good quality films which are thick enough to support waveguide modes at the peak of the gain. In addition to this the PLE measurements point to the formation of aggregates in OPPV. This leads to the formation of traps, which may quench the luminescence and hinder spectral-line-narrowing.

5.3 Factors which affect the ASE

In this section the factors which can affect the threshold for line-narrowing, the line-width and the spectral position are examined. MEH-PPV was chosen for these measurements as it is a well characterised polymer which exhibits good line-narrowing in films. The mechanism for line-narrowing in this work is assumed to be amplified spontaneous emission rather than a co-operative emission process, as good waveguiding in the polymer film is seen to be important for efficient line-narrowing and low thresholds. The importance of waveguiding in the behaviour of the device is discussed in more detail in chapter7. [7, 18].

5.3.1 Excitation Intensity

When assessing conjugated polymers for their use in amplification devices, one important parameter to measure is the threshold intensity for spectral line narrowing. This is defined as the power per unit area at which the line-narrowing begins. This has been measured for a variety of polymers.

In this work, the frequency doubled (532 nm) Nd:YAG laser with a pulse width of 5 ns and a stripe length of 5 mm$\times$200 μm as described in chapter 4 was used. The graph in figure 5.8 shows the spectra measured at high and low excitation intensities and the graph in figure 5.10 shows the full width at half maximum (FWHM) of the MEH-PPV luminescence spectrum as a function of excitation energy. The emission spectrum at low excitation intensity (2 μJ) resembles that of the photoluminescence spectrum with a FWHM of 60 nm. As the excitation intensity is increased, the FWHM decreases rapidly until a narrowed emission of 8 nm is observed at 8 μJ. From this graph the threshold for ASE is below 2 μJ. Figure 5.10 also shows how the position of the peak wavelength changes with excitation intensity. At low excitation intensities, the peak wavelength is constant at 616 nm, however at an energy

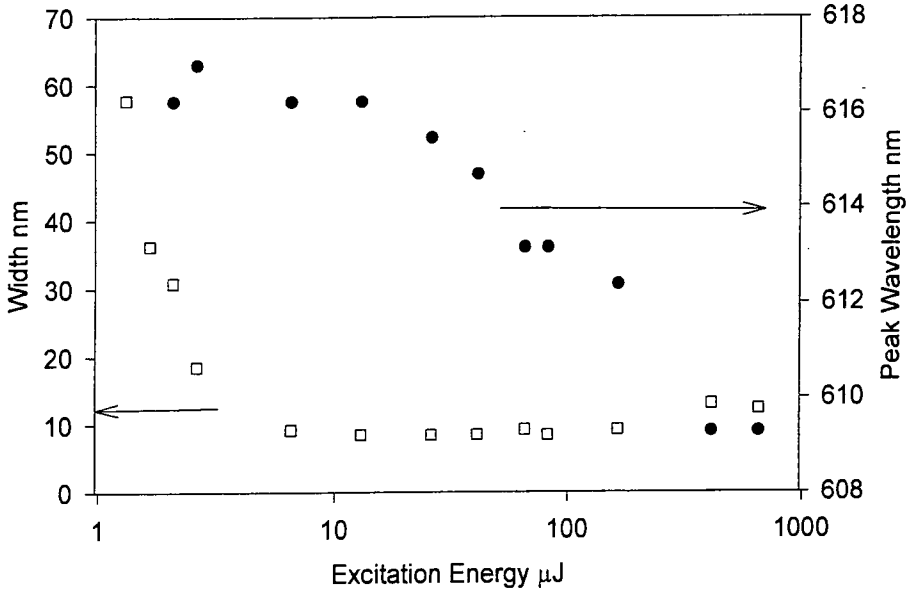

Figure 5.10: Width (squares) and peak wavelength (circles) as a function of excitation energy.

of 20 μJ the peak of the ASE shifts towards higher energies. In total the peak of the ASE moves by over 7 nm from 616 nm at low energies to 609 nm at high energies.

An interesting observation is that the peak position does not start to change until the incident energy is 20 μJ, well above the threshold for ASE. The observed shift may be due to the decrease in the decay time seen at high excitation densities [4, 21]. Ultrafast spectroscopy of MEH-PPV has shown that the emission spectrum immediately after excitation, shifts to the red over the first tens of picoseconds following excitation [5]. This is due to the energy

migration from excited polymer segments with shorter conjugation lengths to more ordered, longer segments. Above the ASE threshold, emission occurs before the energy migration can take place, resulting in gain from the early, blue emission.

It is also possible that photo-induced absorption, which has been assigned to the formation of polaron pairs, could cause the position of the ASE to move to higher energies. Yan et al. showed that there is competition between the stimulated emission and photoinduced absorption [22]. They also showed through time-resolved pump probe measurements that the stimulated emission and the photoinduced absorption are likely to by due to different species. Later work assigned the photoinduced absorption to interchain polaron pairs [23]. The position of the ASE is determined by the position of the maximum gain. This depends on factors such as the excited state and ground state absorptions. The formation of polaron pairs is a non-linear process and therefore as the excitation intensity is increased, the formation of polaron pairs could cause the position of the ASE to shift to higher energies.

Another possible explanation is that the observed blue shift on increasing excitation intensity can be accounted for by heating of the polymer. A number of works have shown that heating of the polymer film results in a blue shift of the photoluminescence spectrum [24–26]. Recent work, which is discussed in more detail in chapter 6 shows that the ASE position shifts by over 20 nm to the blue as the temperature of the film is increased from 98 K to 298 K. The effective change in the temperature of the polymer film due to the change of the excitation intensity, can be estimated from the specific heat capacity of the polymer. The specific heat capacity can be assumed to be similar to that of other organic polymers [27] and is taken here as 1.4 $Jg^{-1}K^{-1}$. The energy per pulse is about 500 μJ, however only about half of this light is absorbed and of the light absorbed only a maximum of 64% can be converted to heat as from the quantum yield measurements 36% of the ab-

sorbed light is re-emitted. The energy per pulse which contributes to heating is therefore approximately 160 μJ, the excited volume is 2×10^{-6}cm^3 and the density is 1 g cm^{-3}. This leads to a rise in temperature of the sample under these conditions of about 60 K. From the measurements in chapter 6 this would cause a change in the position of the ASE peak of about 6 nm. The actual change observed is 7 nm. This calculation shows that heating of the polymer film by increasing the excitation intensity could be an explanation for the blue shift of the ASE.

5.3.2 Angular Dependence of the Emission

In order to measure the angular dependence of the ASE, the sample was mounted in a specially designed vacuum chamber which allowed the detector to be rotated using a calibrated rotation scale. This measurement can be used to examine the emission profile of the light, particularly whether the emission is guided in the film or in the substrate.

ASE spectra were measured between $\pm20^{\ 0}$ perpendicular to the plane of the film as shown in figure 5.11. The spectra were measured at a distance of 10 mm from the edge of the film. This is the first measurement of the angular dependence of the emission from a planar film. The integrated intensity at each angle is plotted in the polar graph shown in figure 5.12. In order to model the data, the emission profile is assumed to be similar to the diffraction from a single slit of width a such that:

$$sin\theta = \frac{\lambda}{a} \tag{5.2}$$

where λ is the wavelength of light, a is the *effective* width of the slit and θ is the angle of the first minimum in the diffraction pattern. The intensity profile of the emission from a single slit is given by

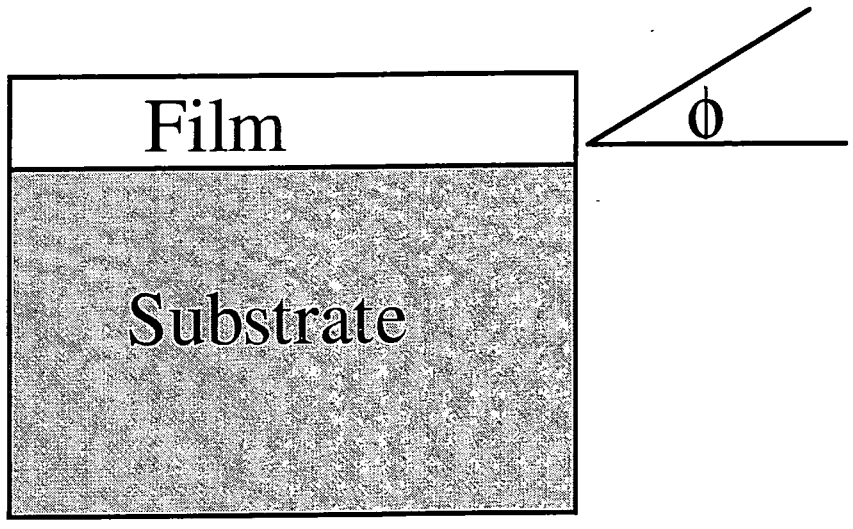

Figure 5.11: Schematic diagram showing how the ASE was investigated as a function of angle (θ).

$$I(\theta) = \left(\frac{sin(x)}{x}\right)^2 \tag{5.3}$$

where x is $a\pi sin(\theta)/\lambda$. The data in figure 5.12 has been fitted with the function described above and good agreement is achieved. The ASE was at 620 nm, and the thickness of the film was 100 nm, therefore it is clear from equation (5.2) that the slit width must be larger than the thickness of the film. From the fitting parameters, an effective slit width of 1.2 μm was obtained. This shows that the bound mode in the guide travels partly in the substrate and partly in the air as well as in the polymer film.

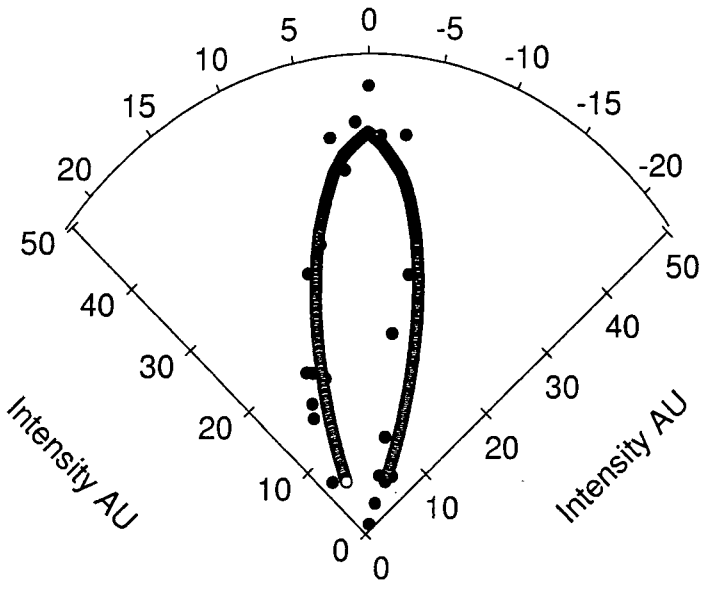

Figure 5.12: Integrated intensity of ASE spectra as a function of emission angle and fit to the data as described in the text.

5.3.3 Excitation Wavelength

The effect of excitation wavelength on the spectral position of the ASE has been investigated for excitations in the range 385-590 nm. This is the first measurement of the dependence of the ASE on the excitation wavelength in conjugated polymers. For this experiment the nitrogen pumped dye laser was used as described in chapter 4. Four dyes were used to span the range 385 nm to 590 nm. The dyes used were: PBBO (385-420 nm), coumarin 1 (436-486 nm), coumarin 307 (480-530 nm) and coumarin 153 (517-590 nm). All measurements were made at an excitation energy of 25 μJ as the excitation intensity can affect the position of the ASE as discussed in section 5.3.1. The excitation energy was controlled using neutral density filters.

The graph in figure 5.13 shows the peak positions as a function of exci-

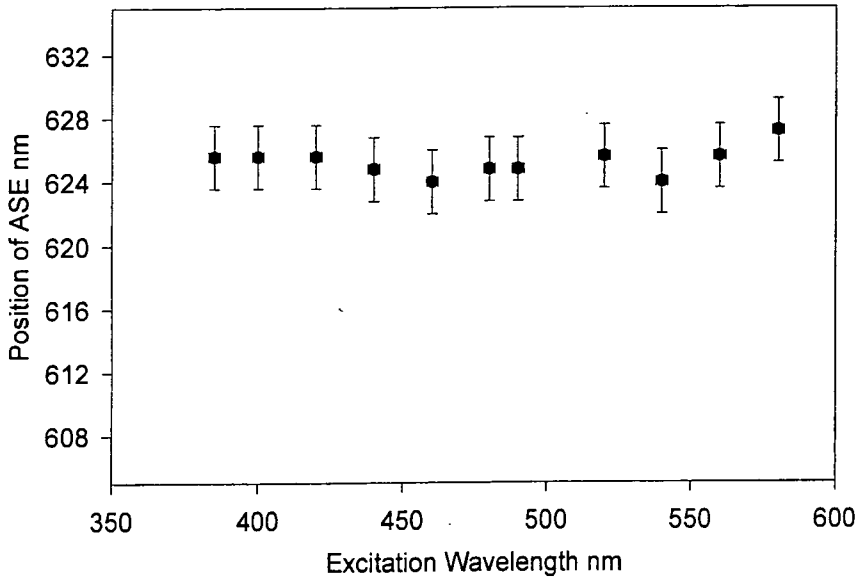

Figure 5.13: Position of the peak of the ASE as a function of excitation wavelength.

tation wavelength. The figure shows that within experimental errors, there is no change in the peak position with excitation wavelength.

It has been proposed that the mechanism for ASE is similar to that of a 4-level dye laser system [28, 29]. If this is the case then assuming that the polymer was pumped in the $\pi - \pi^{\star}$ band, excitation wavelength would not be expected to have an effect on the position of the ASE, which is determined solely by the energy of the vibronic states.

There has been some debate in the literature about whether the excitation wavelength affects the optical properties of the polymer and it has been shown that in cyano-substituted PPV the excitation and emission wavelength affect

the decay dynamics [20]. The authors concluded that the luminescence was from both inter and intra molecular excitations. In contrast, Vacar et al. [30] investigated the effect of the pump wavelength on the decay dynamics of the photo-induced absorption (PA) and stimulated emission of MEH-PPV and found that in pristine samples the decay dynamics were identical regardless of the pump wavelength. However, on an oxidised sample, they observed that the stimulated emission signal decreased, and the PA signal increased as the initial excitation intensity was increased. Other work by Harrison et al. [31] showed that the quantum efficiency of pristine PPV samples was constant with excitation wavelength, but for oxidised samples a decrease in the quantum efficiency and also in the decay time was observed.

5.4 Gain and Loss Measurements

5.4.1 Experimental

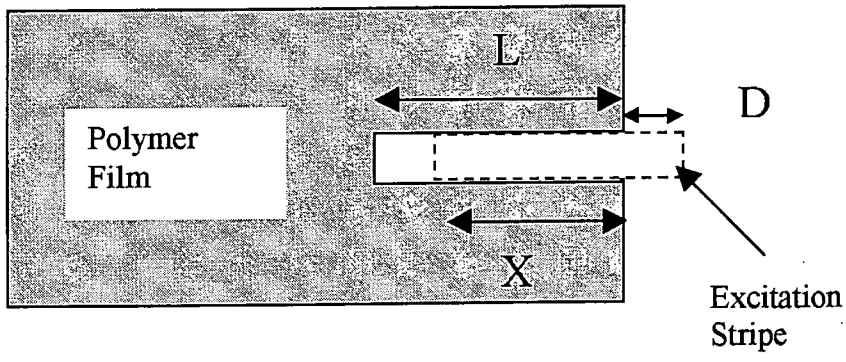

Figure 5.14: Schematic diagram of the gain measurement.

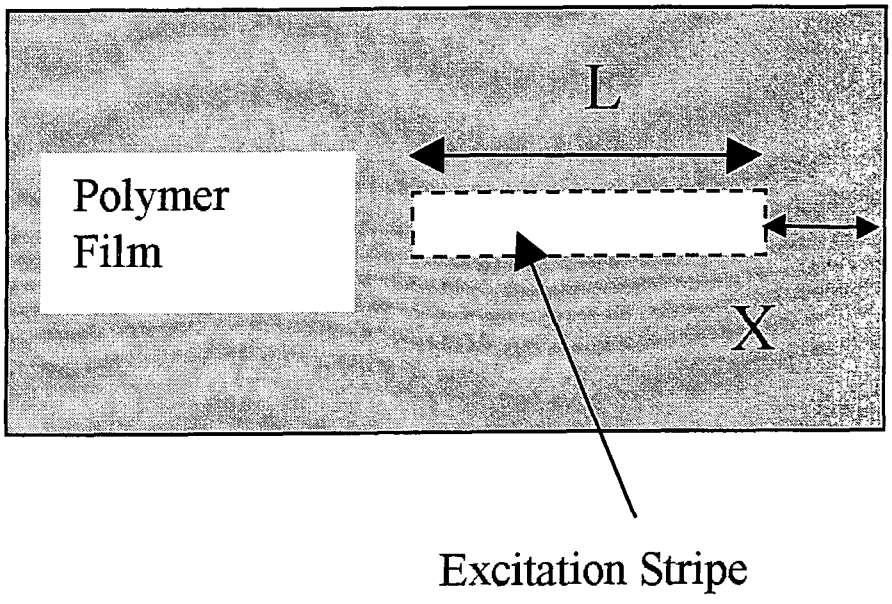

Figure 5.15: Schematic diagram of the loss measurement.

Gain and loss measurements were made by using a technique originally used for semiconductor lasers [32, 33] which has recently been applied to conjugated polymer films [6]. A good estimate of the gain coefficient at a given excitation intensity is essential for the characterisation of these materials and is very important for device fabrication. The method described also allows the loss, or the absorption coefficient at the emission wavelength (620 nm for MEH-PPV) to be measured. As discussed in chapter 4, the absorption coefficient of MEH-PPV at 550 nm was measured to be $1.1\times10^{5}\text{cm}^{-1}$. However this technique cannot be used to make an estimate of the absorption coefficient at 620 nm, as the errors on the absorption measurements in the absorption tail are too large due to scattering and reflection. The measurement of the loss, therefore provides a useful way of measuring the absorption coefficient at long wavelengths, where the absorption is very small.

The diagram in figure 5.14 shows a schematic diagram of the gain measurement. The excitation beam was expanded using a divergent lens and then formed into a stripe using a cylindrical lens. The intensity of the laser stripe has a gaussian-like profile, therefore to keep the excitation intensity as constant as possible only a small central region of the stripe was used to excite the polymer film. A slit with a width of 3 mm was placed in the beam to determine the stripe length. The sample chamber was mounted on a translation stage which was then moved perpendicular to the excitation beam, so that the excitation stripe was effectively translated across the film as shown in figure 5.14. The effective length of the stripe changed but was always kept flush with the edge of the film. The length of the stripe L was 3 mm and the pump intensity was 10 $kWcm^{-2}$. As the distance moved by the sample chamber (D) increased, the length of the excitation stripe (X) decreased.

The loss measurement was made using the same set-up, however this time the length of the excitation stripe was kept constant and by translating the sample chamber, the stripe was moved away from the edge of the film. This is shown in figure 5.15.

5.4.2 Theory

Assuming that the mechanism for spectral line narrowing is ASE, a relationship between the output intensity and the stripe length can be derived as shown by both Mcgehee and Berggren inthe literature [6, 36]. This is also a useful method for confirming that the emission is in fact ASE and not superfluorescence, as has been proposed [34], as the data would not fit the equation derived below if the emission was due to superfluorescence. The starting point for the derivation is the equations for spontaneous and for stimulated emission.

Spontaneous emission intensity I(x) emitted from a waveguide is given by:

$$I(x) = AI_P X \tag{5.4}$$

where A is given by $N_2 \frac{\omega}{4\pi}$ where N_2 is the population density of the excited state and $\omega/4\pi$ accounts for the proportion of photons emitted in directions for which amplification can occur. This can be approximated by A/L^2 where A is the cross-sectional area of the amplifier and L is its length. X is the excitation stripe length and I_P is the input power.

Similarly stimulated emission is given by:

$$\frac{\delta I(x)}{\delta x} = N\sigma I(x) = gI(x) \tag{5.5}$$

where N is the excited state population, σ is the cross section for stimulated emission and g is the net gain.

The sum of the intensities between a position x and δx along a stripe of length L is given by:

$$I_{tot}(x + dx) = I(x) + AI_P\delta x + gI\delta x \tag{5.6}$$

As $I_{tot}(x + dx) - I(x) = \delta I$, this leads to:

$$\frac{\delta I}{AI_P + gI} = \delta x \tag{5.7}$$

and

$$\int_0^I \frac{dI}{AI_P + gI} = \int_0^L dx \tag{5.8}$$

By integrating between the limits, the output intensity from one end of the stripe is then given by the following expression:

$$I(\lambda) = \frac{A(\lambda)I_p}{g(\lambda)}\left(e^{g(\lambda)L} - 1\right) \tag{5.9}$$

The gain coefficient was found by fitting equation 5.9 to the data. As the gain term gl is large this can be approximated to:

$$I(\lambda) = \frac{A(\lambda)I_p}{g(\lambda)}\left(e^{g(\lambda)L}\right) \tag{5.10}$$

The loss coefficient is simply the absorption coefficient at the emission wavelength. This is therefore related to the pump stripe length by:

$$I = I_0 e^{(-\alpha L)} \tag{5.11}$$

where α is the absorption coefficient.

5.4.3 Results

The graph in figure 5.16 shows the ASE spectra measured as the excitation stripe length is increased. The spectra increase in intensity as the stripe length is increased, as expected. It is also interesting to note that the spectra shift to shorter wavelengths at longer stripe lengths. The graph in figure 5.17 shows the integrated intensity of the ASE peaks as a function of stripe length. The line is a fit to equation 5.9. From this fit the parameter AI_P is found to be $1.4\times\ 10^4$ and the gain coefficient is 4 cm^{-1}. The pump intensity was 10 $kWcm^{-2}$. The graph shows that equation 5.9 fits well up to a stripe length of 1 mm. The deviation after this is caused by gain saturation. This occurs because the light travelling in the waveguide is so strongly amplified that a substantial fraction of the excitations are depleted. Any increase in the pump stripe length, does not then produce an increase in the amplification, in fact the gain coefficient is reduced when gain saturation takes place [35].

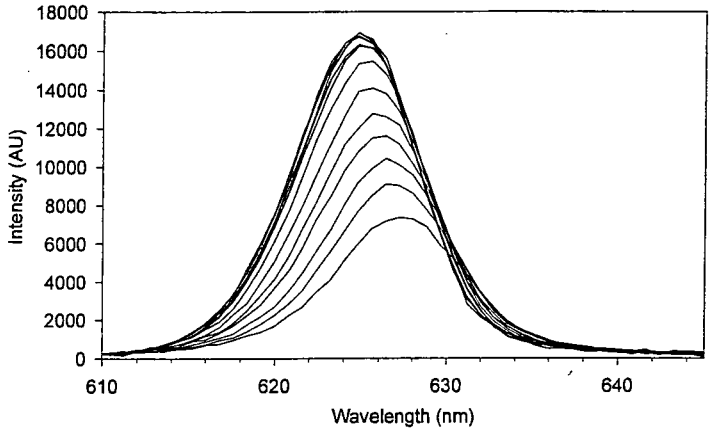

Figure 5.16: ASE spectra measured as a function of excitation stripe length.

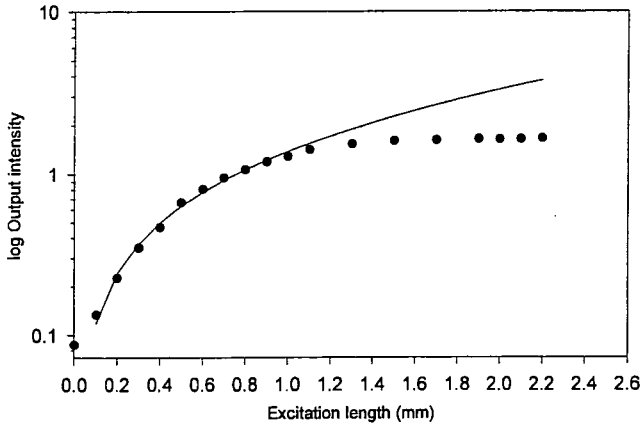

Figure 5.17: Intensity of ASE spectra as a function of excitation stripe length. The line is a fit to equation 5.9.

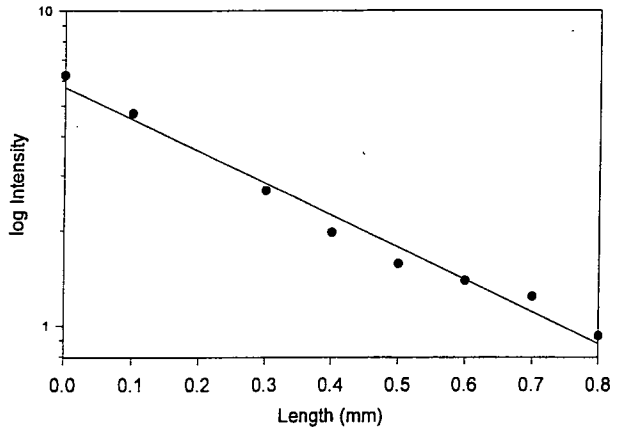

Figure 5.18: Integrated intensity of the ASE spectra as a function of distance from the pump stripe. The line is a fit to equation 5.11.

This result is similar to that measured by McGehee et al. [6] for the polymer poly[2-butyl-5-(2'-ethyl-hexyl)-1,4-phenylenevinylene] (BuEH-PPV) using the same method. For a pump intensity of 1.2 kWcm^{-2} they measured the gain to be 18 cm^{-1}. This polymer is similar in structure to MEH-PPV but has a higher photoluminescence quantum yield (62%) and is air stable. Bergren et al. [36] used a similar method to determine the gain and absorption coefficient in an alkyl substituted PPV doped into an oxidiazole compound. They measured a gain of 1 cm^{-1} at 0.7 kWcm^{-2}. These results show that MEH-PPV can demonstrate high gain comparable to that of other conjugated polymers.

The loss measurements are shown in figure 5.18. The graph shows the integrated intensity of the ASE spectra as the pump stripe is moved away from the edge of the film. The intensity decreases linearly as predicted by equation 5.11. From this graph, the loss coefficient, i.e. the absorption coef-

ficient at 620 nm is found to be 10 cm^{-1}. In comparison, McGehee measured a loss coefficient of 44 cm^{-1} at 562 nm and Berggren et al. measured a loss coefficient of 0.6 cm^{-1}. These measurements show that the loss coefficient can vary by over an order of magnitude, however the low loss coefficient coupled with the relatively high gain measured for MEH-PPV show that this polymer is suitable for laser and amplification applications.

5.5 Conclusions

In this chapter two novel PPV derivatives, OPPV and DDO-PPV have been investigated. The emission spectra at high excitation densities were measured and it was found that no spectral line narrowing was observed in DDO-PPV films. In films of OPPV, partial line-narrowing was observed at very high pump intensities, however this did not last more than a few seconds. The cut-off thickness was calculated for these films based on an estimate of the refractive index, and it was found that the measured thickness of the film was very close to the cut-off thickness. Thicker films could not be produced due to the low molecular weight of these polymers. It is therefore likely that light at the peak of the gain spectrum could not be waveguided in the film, and was therefore not confined over a gain length long enough for ASE to be produced. The possibility of aggregation formation, which could quench the excited state was also investigated. These materials have therefore not been used for further amplification studies.

Measurements on the PPV derivative MEH-PPV showed that stable, narrow emission was achieved at high excitation intensities. This polymer was therefore used to probe the angular dependence of the emission, the effect of excitation intensity and the effect of excitation wavelength. It was found that under high intensity excitation, the peak of the ASE moved to higher energies (i.e. blue shifted). The possible reasons for this are: 1) the decrease

in the decay time of the excited state causes emission to occur earlier in the migration process, 2) photoinduced absorption due to the formation of polaron pairs causes the peak of the ASE to shift to shorter wavelengths as the excitation intensity is increased, 3) heating of the polymer film leads to a blue shift of the emission spectrum.

The angular dependence of the emission was modelled as the diffraction from a single slit. An effective slit width of 1.2μm was calculated, showing that the bound mode is guided in both the substrate and the polymer layer. The measurements of the effect of excitation wavelength showed that there was no dependence on the excitation wavelength over the range 380-590 nm.

The gain and loss coefficients have been measured for thin films of MEH-PPV. The gain coefficient was found to be 4 cm^{-1} at 10 $kWcm^{-2}$ and the loss or absorption coefficient at 620 nm was found to be 10 cm^{-1}. These measurements show that MEH-PPV has the potential to be used in solid state diode lasers and for amplification devices.

Bibliography

[1] B.H. Soffer and B.B. McFarland. *Applied Physics Letters*, 10:266, 1967.

[2] H. Kogelnik and C.V. Shank. *Applied Physics Letters*, 18:152, 1971.

[3] N. Tessler, G.J. Denton, and R.H. Friend. *Nature*, 382:695, 1996.

[4] F. Hide, B. J. Schwartz, M. A. Diazgarcia, and A. J. Heeger. *Chemical Physics Letters*, 256(4-5):424–430, 1996.

[5] V. Doan, V. Tran, and B. J. Schwartz. *Chemical Physics Letters*, 288(2-4):576–584, 1998.

[6] M. D. McGehee, R. Gupta, S. Veenstra, E. K. Miller, M. A. DiazGarcia, and A. J. Heeger. *Physical Review B-Condensed Matter*, 58(11):7035–7039, 1998.

[7] F. Hide, M. A. Diazgarcia, B. J. Schwartz, M. R. Andersson, Q. B. Pei, and A. J. Heeger. *Science*, 273(5283):1833–1836, 1996.

[8] G. J. Denton, N. Tessler, M. A. Stevens, and R. H. Friend. *Advanced Materials*, 9(7):547, 1997.

[9] C. Zenz, W. Graupner, S. Tasch, G. Leising, K. Mullen, and U. Scherf. *Applied Physics Letters*, 71(18):2566–2568, 1997.

[10] T. Q. Nguyen, V. Doan, and B. J. Schwartz. *Journal of Chemical Physics*, 110(8):4068–4078, 1999.

[11] C. Y. Yang, F. Hide, M. A. DiazGarcia, A. J. Heeger, and Y. Cao. *Polymer*, 39(11):2299–2304, 1998.

[12] X. Long, M. Grell, A. Malinowski, D. D. C. Bradley, M. Inbasekaran, and E. P. Woo. *Optical Materials*, 9(1-4):70–76, 1998.

[13] C. Spiegelberg, N. Peyghambarian, and B. Kippelen. *Applied Physics Letters*, 75(6):748–750, 1999.

[14] A.K. Sheridan, J.M. Lupton, I.D.W. Samuel, and D.D.C. Bradley. *Chemical Physics Letters*, 322:51, 2000.

[15] A. K. Sheridan, I. D. W. Samuel, A. Bleyer, and D. D. C. Bradley. *Synthetic Metals*, 101(1-3):259–260, 1999.

[16] N. C. Greenham, I. D. W. Samuel, G. R. Hayes, R. T. Phillips, Yarr Kessener, S. C. Moratti, Holmesm A.B., and R.H. Friend. *Chemical Physics Letters*, 241(1-2):89–96, 1995.

[17] M.R. Anderson. *Synthetic Metals*, 85:1275, 1997.

[18] M. A. DiazGarcia, F. Hide, B. J. Schwartz, M. R. Andersson, Q. B. Pei, and A. J. Heeger. *Synthetic Metals*, 84(1-3):455–462, 1997.

[19] A. Boudrioua, P.A. Hobson, B.J. Matterson, W.L. Barnes, and I.D.W. Samuel. *Synthetic Metals*, 111:545, 2000.

[20] I. D. W. Samuel, G. Rumbles, C. J. Collison, S. C. Moratti, and A. B. Holmes. *Chemical Physics*, 227(1-2):75–82, 1998.

[21] G. R. Hayes, I. D. W. Samuel, and R. T. Phillips. *Physical Review B-Condensed Matter*, 52(16):11569–11572, 1995.

[22] M. Yan, L. J. Rothberg, F. Papadimitrakopoulos, M. E. Galvin, and T. M. Miller. *Physical Review Letters*, 72(7):1104–1107, 1994.

[23] M. Yan, L. J. Rothberg, E. W. Kwock, and T. M. Miller. *Physical Review Letters*, 75(10):1992–1995, 1995.

[24] T. W. Hagler, K. Pakbaz, K. F. Voss, and A. J. Heeger. *Physical Review B-Condensed Matter*, 44(16):8652–8666, 1991.

[25] K. Pichler, D. A. Halliday, D. D. C. Bradley, P. L. Burn, R. H. Friend, and A. B. Holmes. *Journal of Physics-Condensed Matter*, 5(38):7155–7172, 1993.

[26] J. W. Yu, M. Hayashi, S. H. Lin, K. K. Liang, J. H. Hsu, W. S. Fann, C. I. Chao, K. R. Chuang, and S. A. Chen. *Synthetic Metals*, 82(2):159–166, 1996.

[27] A. Skotheim, R.L. Elsenbaumer, and J.R. Reynolds. *Handbook of Conducting Polymers.* 2nd edition, 1986.

[28] B. Schweitzer, G. Wegmann, H. Giessen, D. Hertel, H. Bassler, R. F. Mahrt, U. Scherf, and K. Mullen. *Applied Physics Letters*, 72(23):2933–2935, 1998.

[29] X. A. Long, A. Malinowski, D. D. C. Bradley, M. Inbasekaran, and E. P. Woo. *Chemical Physics Letters*, 272(1-2):6–12, 1997.

[30] D. Vacar, A. Dogariu, and A. J. Heeger. *Chemical Physics Letters*, 290(1-3):58–62, 1998.

[31] N. T. Harrison, G. R. Hayes, R. T. Phillips, and R. H. Friend. *Physical Review Letters*, 77(9):1881–1884, 1996.

[32] S. Hess, R. A. Taylor, J. F. Ryan, B. Beaumont, and P. Gibart. *Applied Physics Letters*, 73(2):199–201, 1998.

[33] K.L. Shaklee and R.F. Leheny. *Applied Physics Letters*, 18:475, 1971.

[34] S. V. Frolov, M. Ozaki, W. Gellermann, M. Shkunov, Z. V. Vardeny, and K. Yoshino. *Synthetic Metals*, 84(1-3):473–474, 1997.

[35] A. Yariv. *Optical Electronics.* Saunders College Publishing, 1991.

[36] M. Berggren, A. Dodabalapur, Z. N. Bao, and R. E. Slusher. *Advanced Materials*, 9(12):968, 1997.

Chapter 6

Effect of Temperature and Film Morphology on the Spectral Line-Narrowing in MEH-PPV

6.1 Introduction

The temperature dependence of the absorption and photoluminescence of conjugated polymers was first studied in MEH-PPV in 1991 [1] in MEH-PPV polyethylene blends. Since then many studies, both theoretical and experimental have investigated the temperature dependence of the optical properties of conjugated materials [2–6]. These measurements lead to a good understanding of some of the fundamental properties of these materials such as the Huang-Rhys factor associated with different chain lengths [2] as well as the effect of disorder on the system [1, 6]. In the context of controlling the gain in conjugated polymers, a knowledge of how the materials behave under changes of temperature is vital for device fabrication, as it leads to an understanding of the gain mechanism. The ASE of thin films and the factors affecting it have been widely studied [7–11]. In particular factors such as the

threshold for stimulated emission [7, 8, 12], the spectral position of the line-narrowing [13], the film morphology [4, 12] and the film thickness [13] have all been recently investigated. Spiegelberg et al. recently investigated the effect of temperature on the threshold intensity for SLN in a PPV derivative [14]. Their work shows that the threshold for SLN has only a slight temperature dependence.

There has also been some evidence in the literature that the morphology can affect the optical properties of the polymers. The effect of the spinning solvent on the SLN for a range of polymers and solvents was investigated by Hide et al. [12]. Their results showed that in MEH-PPV the threshold for SLN was a factor of five times higher for films spin-coated from chlorobenzene (CB-films) than for films spin-coated from tetrahydrofuran (THF-films). They also found that the narrowed linewidth was only 50 nm with the CB-films compared to 17 nm with the THF-films. This was the first indication that film morphology is a critical factor which determines the behaviour of the SLN. Other work by Yang et al. [15] has shown that THF-films have a higher degree of crystallinity than CB-films, and Nguyen et al. showed that the degree of order in polymer films can depend on the spinning solvent used.

This chapter presents a detailed study of the temperature dependence of the spectral line narrowing, absorption and photoluminescence in films of MEH-PPV. These are the first temperature dependent measurements of SLN in MEH-PPV. The effect of film morphology was also investigated by fabricating films spun from two spinning solvents (THF and CB) and comparing the temperature dependent absorption, PL and spectral line narrowing results. The temperature dependence of the SLN was measured at the University of Sheffield and I am grateful to Michael Redecker for his advice on the equipment. All the absorption measurements were made by John Lupton of Durham University.

The first part of this chapter presents the absorption, photoluminescence

and SLN temperature dependence data. In the second part, the SLN data is compared to the absorption and photoluminescence data for the films spun from CB and THF and the results are discussed in the light of previous work in the literature. Finally, a comparison between the absorption and photoluminescence data is made which leads to interesting conclusions concerning exciton migration.

6.2 Experimental

Thin films approximately 100 nm thick were prepared by spin-coating concentrated solutions (5 mg/ml) of MEH-PPV in either tetrahydrofuran (THF) or chlorobenzene (CB) onto spectrosil substrates. All temperature dependent measurements were carried out using an Oxford Instruments liquid nitrogen cooled cryostat.

The diagram in figure 4.3 shows the experimental set-up used for the temperature dependent SLN measurements. For these measurements the films were excited using a dye laser pumped by a pulsed nitrogen laser (337 nm) operating at 10 Hz. The laser dye coumarin 153 was used to give an excitation wavelength of 523 nm. The energy incident on the sample was up to 10 mJ per pulse. The beam was focused using a cylindrical lens into a stripe of dimensions 200 *mu*m x 5 mm. Emission was collected perpendicular to the incident light.

Absorption spectra were measured by John Lupton in a Lambda 19 dual beam spectrometer. For the photoluminescence measurements the 514 nm line of an argon-ion laser was used to excite the samples. PL emission was measured from the far side of the sample at close to normal incidence. The positions of the 0-1 PL peaks (which are unaffected by self absorption) were determined using a peak fitting programme by modelling the peaks as a Gaussian convoluted with a Lorentzian. The absorption spectrum was fitted

by using a superposition of peaks using the following form where a, b,c and d are fitting parameters. This equation has been used in the literature to fit the absorption spectra of conjugated polymers [16]:

$$y = aexp\left(\frac{ln2ln\left(\frac{(x-b)(c^2-1)}{dc}+1\right)^2}{lnc^2}\right) \tag{6.1}$$

6.3 Results

In this section the results for the temperature dependent absorption, photoluminescence and spectral line-narrowing will be presented, followed by a comparison of the THF-film and CB-film data.

6.3.1 Photoluminescence

Film	Temperature	Position of 0-0 peak (eV)	Position of 0-1 peak (eV)
CB-film	77K	2.067	1.901
THF-film	77K	2.064	1.899
CB-film	298K	2.124	1.988
THF-film	298K	1.980	2.127

Table 6.1: Table of photoluminescence data

The graphs in figure 6.1 and figure 6.2 show the PL spectra measured for a CB-film and a THF-film respectively. The spectra have been normalised to the low energy tail of the PL spectra. A red shift of the spectra is clearly seen as the temperature is decreased from room temperature to 81 K. The vibronic structure can be seen clearly in all four graphs, however as the

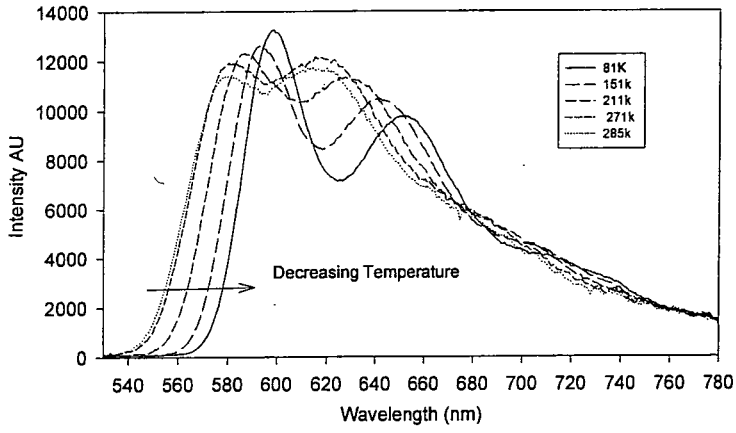

Figure 6.1: Photoluminescence spectra from a CB-film from 81K to 285 K

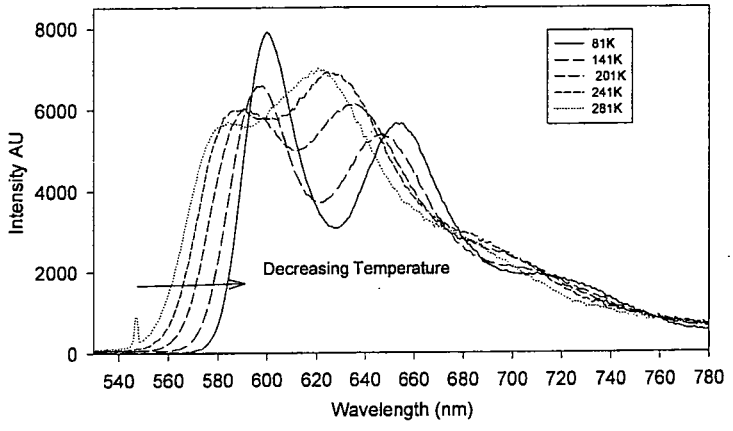

Figure 6.2: Photoluminescence spectra from a THF-film from 81 K to 281 K

temperature is decreased, the vibronic structure becomes more pronounced. The high energy peaks are assigned to the 0-0 transition, and the second peak is assigned to the 0-1 peak of the π to $\pi^{\star}$ transition. The peak positions are summarised in table 6.1. In both films the relative intensity of the peaks changes. At room temperature the high energy 0-0 peak is less intense than the 0-1 peak, however as the temperature is decreased the 0-0 peak becomes stronger than the 0-1 peak.

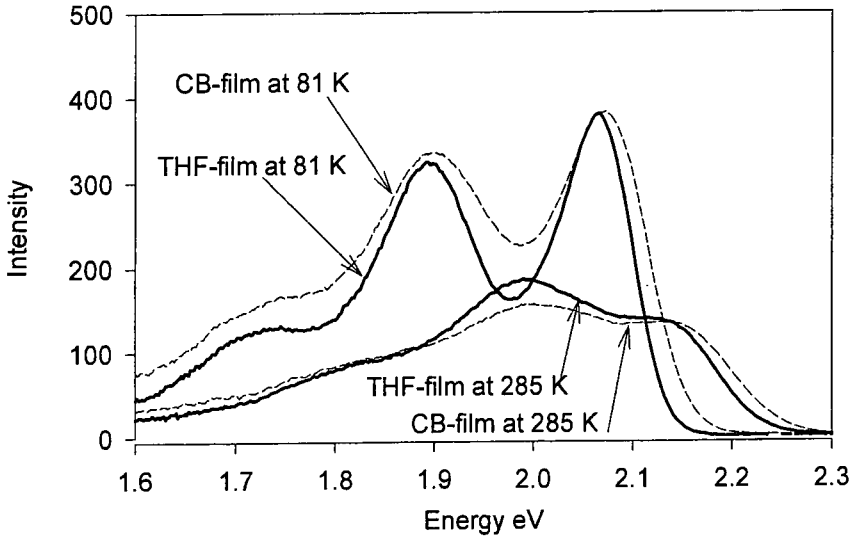

Figure 6.3: Photoluminescence from a CB-film and a THF-film at 81 K and 285 K

The graph in figure 6.3 shows the PL spectra at 285 K and at 81 K for films spun from both THF and CB. In order to compare the magnitude of the shift of the absorption with temperature, PL and SLN spectra, all graphs

have been converted to an energy scale and all shifts are quoted in meV. The red shift as the temperature is decreased and the increase in the vibronic structure discussed earlier can be seen clearly.

Although the peak positions are similar, there are significant differences in the shape of the spectra for the two solvents. The spectra from the CB-film are broader and show less vibronic structure than the spectra from the THF-film. It should also be noted that the integrated intensity of the spectra at 81 K is greater than that of the spectra at room temperature. For further analysis of this data the peak positions of the 0-1 transition are used for comparison with the SLN and absorption data so as to avoid any possible effect of self-absorption on the 0-0 peak. The overall shift with temperature of the 0-1 peak is 79 meV for THF-films and 88 meV from CB-films.

6.3.2 Absorption

The data in figure 6.4 and figure 6.5 show the absorption spectra for a CB-film and a THF-film respectively. The graphs show clearly that as the temperature is decreased the spectra shift to longer wavelengths, as was observed for the PL spectra. The overall shift of the spectra with temperature is slightly larger for the CB-film than for the THF-film. This will be discussed in more detail later.

6.3.3 Spectral Line Narrowing

The graphs in figures 6.6 and 6.7 show the spectral line narrowing spectra as a function of temperature for a CB-film and a THF-film respectively. These spectra are narrow with a full width at half maximum (FWHM) of 19 meV (7 nm) at room temperature. As the sample is cooled a red shift of the peak position is observed. The small FWHM of 19 meV observed for the CB-film is much smaller than the value of about 159 meV previously reported by Hide

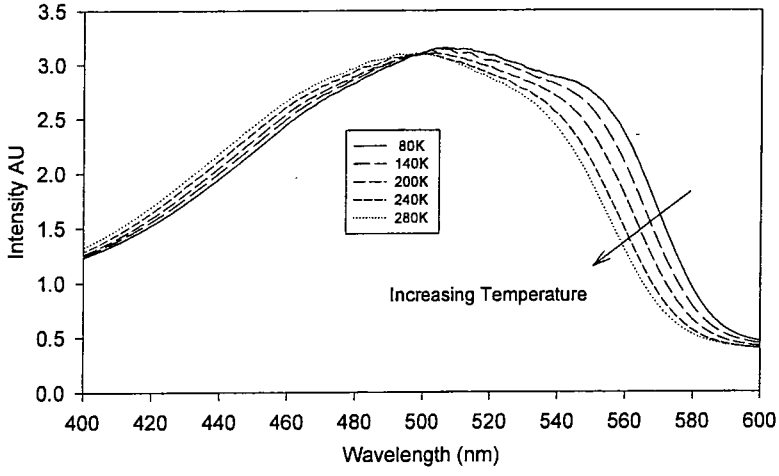

Figure 6.4: Absorption data for a CB-film as a function of temperature (from John Lupton).

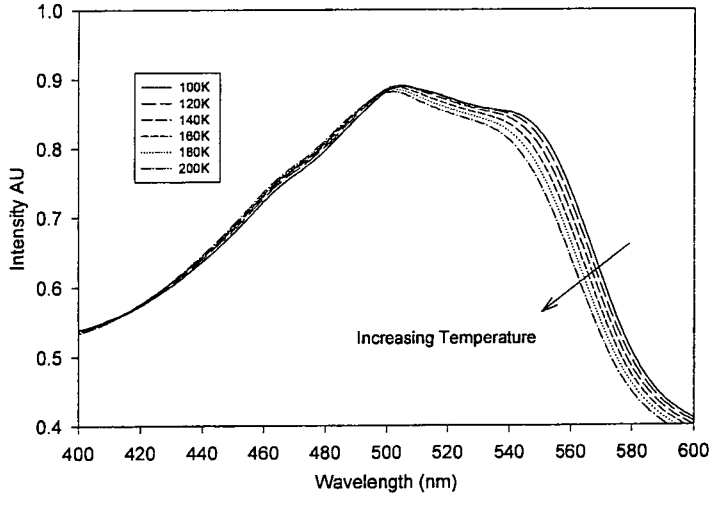

Figure 6.5: Absorption data for a THF-film as a function of temperature (from John Lupton).

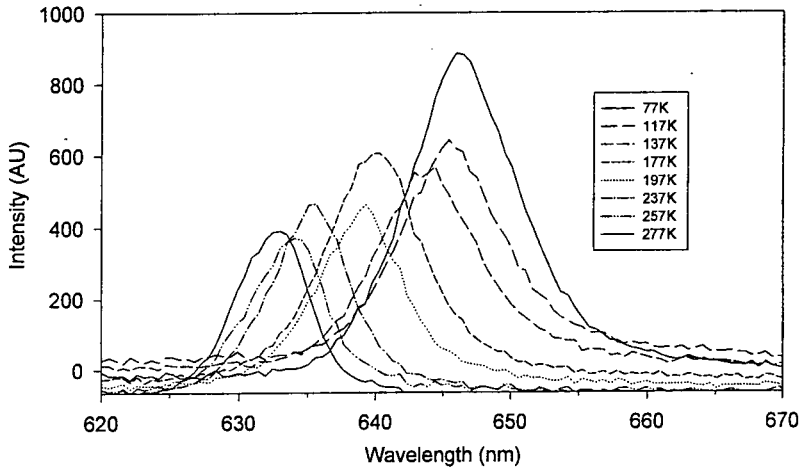

Figure 6.6: ASE spectra as a function of temperature for a CB-film.

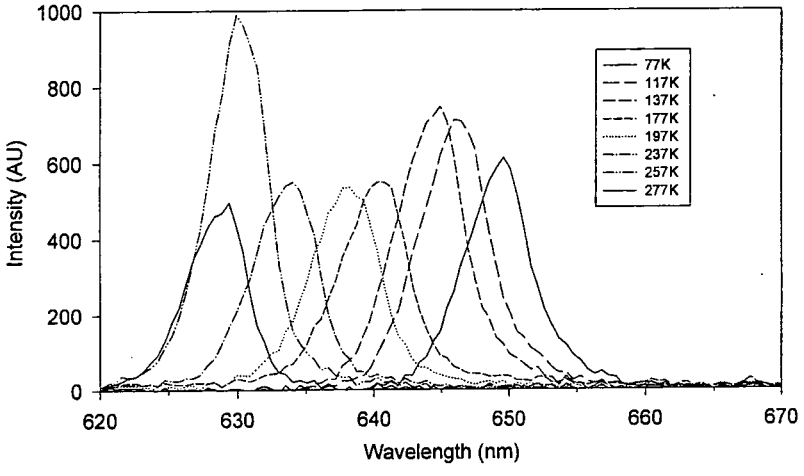

Figure 6.7: ASE spectra as a function of temperature for a THF-film.

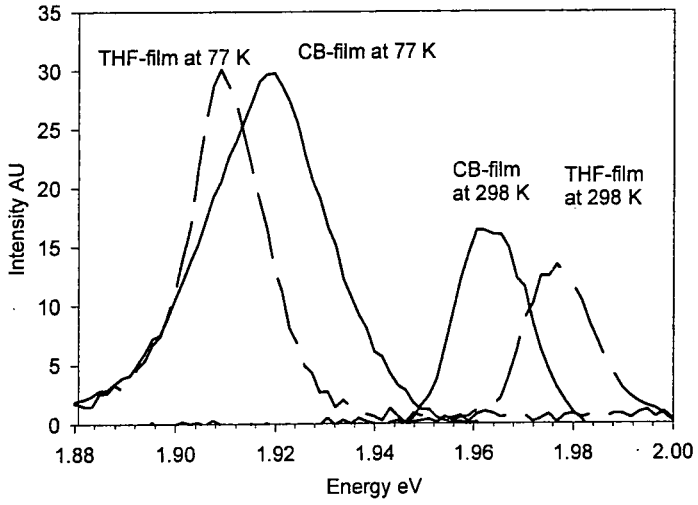

Figure 6.8: ASE spectra for a THF-film and a CB-film at 77K and 297K.

et al. [9]. This may be due to the improved quality of the polymer.

Figure 6.8 compares the SLN spectra measured for the CB-film and THF-film spectra at 77 and 298 K. This graph is plotted on an energy scale so that the shift of the spectra can be easily compared with shifts of the absorption and PL spectra. The peak positions of the SLN spectra for the CB-film shift from 1.959 at 298 K to 1.918 at 77 K, giving a total shift of 41 meV. The THF-film peaks shift from 1.976 eV at 298 K to 1.908 eV at 77 K, giving a total shift of 68 meV. It is interesting point to note is that the overall shift of the CB-film is smaller (41 meV) compared to the shift of the THF-film spectra (68 meV). The figure also shows that the spectra from each film do not coincide at either high or low temperatures. This is probably simply due to the slight sample to sample variation in the peak position of the SLN. However, this is small compared to the overall shift of the peak positions. It is also interesting to note that as with the PL spectra seen in figure 6.3, there is

an increase in the integrated intensity as the temperature is decreased. This effect is much more pronounced in the CB-film data. This figure also shows that while the FWHM of the THF-film SLN spectra is constant at 19 meV across the temperature range studied, the CB-film spectra decrease from a FWHM of 28 meV at room temperature to 19 meV at 298 K. This decrease in the FWHM of the spectra is contrary to the disorder induced broadening seen in absorption and PL as the temperature is increased [3].

6.3.4 CB-film data

The graph in figure 6.9 shows the peak positions of the SLN compared with the 0-1 peak of the absorption spectra and the 0-1 peak of the PL spectra. The absorption data has been shifted to lower energies by 0.355 eV to facilitate comparison with the SLN data. No shift has been applied to the PL data. This figure shows clearly that the temperature dependence of the SLN is different from that of both the absorption and the PL. The total change in the absorption peak position across the temperature range is 86 meV which is more than double the change of the SLN peak position (41 meV). A similar behaviour is seen in the lower panel where the SLN data is plotted against the PL data. Here the change in the PL peak position is 88 meV which is again much larger than the change in the SLN peak position. The figure also shows that the peak positions of the SLN and PL only coincide at 220 K. At lower temperatures the SLN is blue-shifted from the PL and at higher temperatures it is red-shifted.

6.3.5 THF-data

The data for the THF-film SLN, absorption and photoluminescence are shown in figure 6.10. The temperature dependence is somewhat different for the THF-film than that which was observed for the CB-film discussed above.

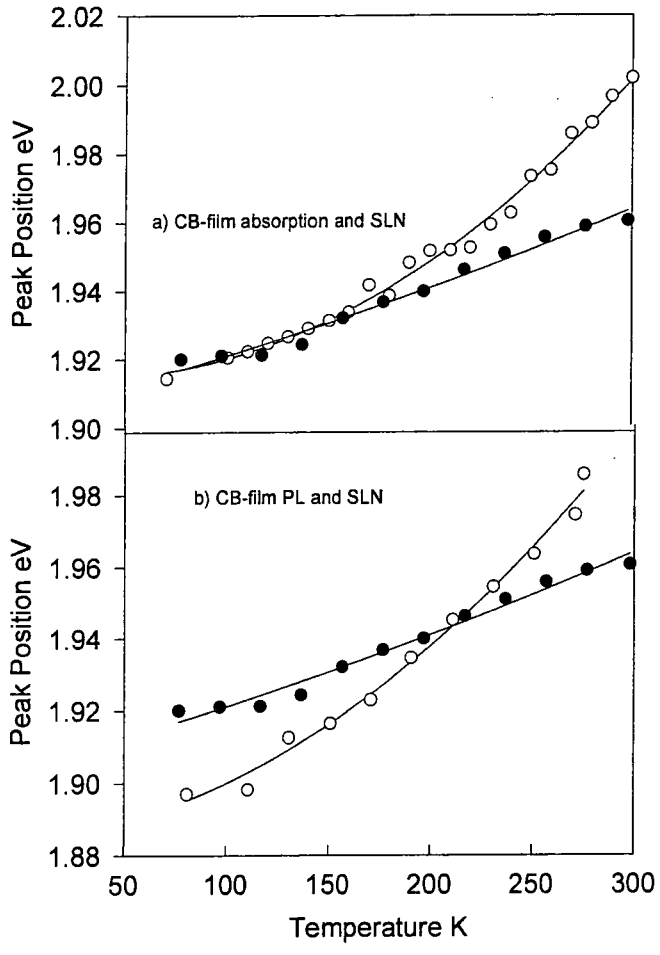

Figure 6.9: MEH-PPV films spun from CB. Top panel: absorption (white circles) and SLN (black circles. Bottom panel: photoluminescence (white circles) and SLN (black circles).

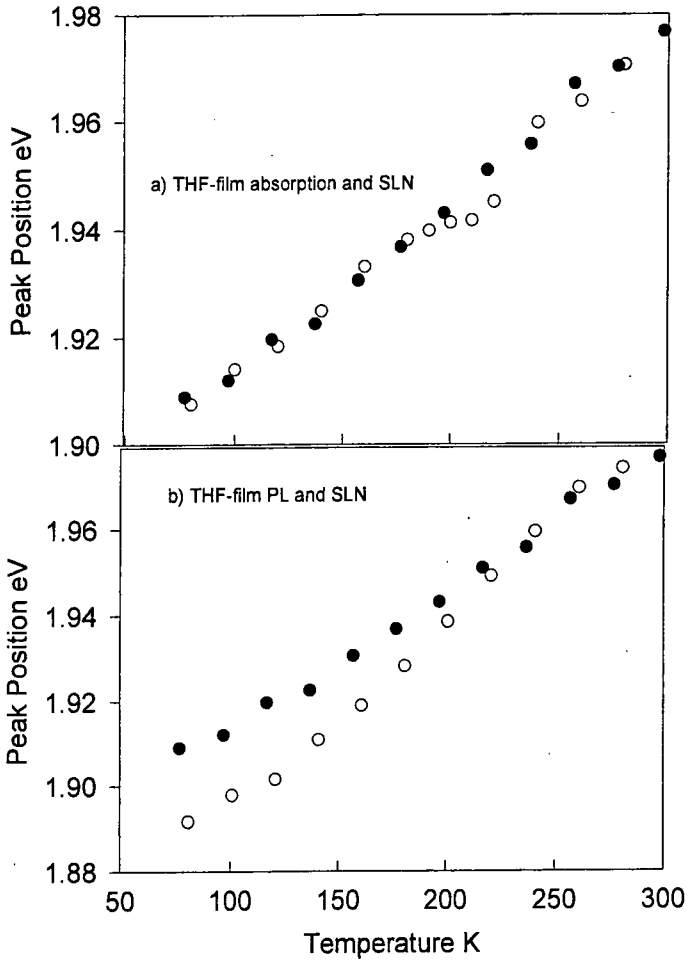

Figure 6.10: MEH-PPV films spun from THF. Top panel: absorption (white circles) and SLN (black circles. Bottom panel: photoluminescence (white circles) and SLN (black circles).

Here the absorption and SLN show identical behaviour, both showing a shift of 72 meV. The change in the peak positions of the PL and SLN data is slightly different - the shift of the SLN is slightly smaller (68 meV) than the shift of the PL peak (79 meV). However no distinct cross-over is seen as with the CB-data, instead the peak positions coincide over the temperature range 250-300 K.

Table 6.2 summarises the overall shifts observed for the THF-film and the CB-film.

	CB-film (meV)	THF-film (meV)
SLN	41	68
PL	88	79
Absorption	86	72

Table 6.2: Shift of peak positions with temperature.

6.4 Comparison of PL and Absorption

It is interesting to compare the absorption and PL data for each of the films. It was found that the magnitude of the difference in the temperature dependencies is kT. In order to demonstrate this the PL data has been shifted to lower energies by an amount kT and plotted with the absorption data. The absorption data has been shifted a constant amount so the two data sets can be easily compared. The data in figure 6.11 and figure 6.12 shows the temperature dependence of the (PL-kT) and the absorption data for the CB-film and the THF-film respectively. The graphs show that for both the CB-film and the THF-film, good agreement between the absorption and the PL-kT data is observed.

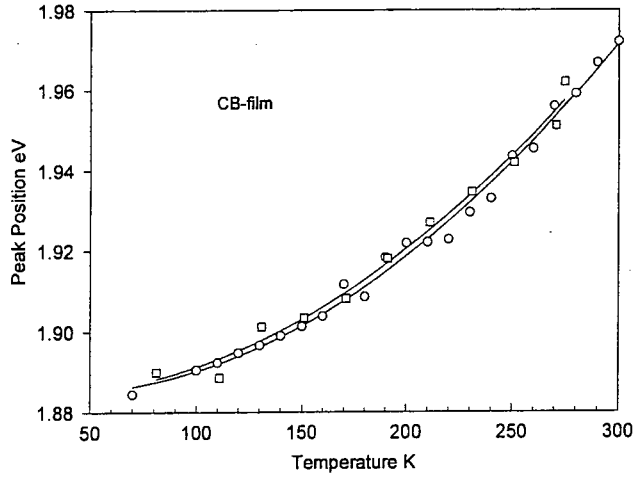

Figure 6.11: Position of the 0-1 peak of the PL (squares) (with kT subtracted and absorption (circles) for a CB film.

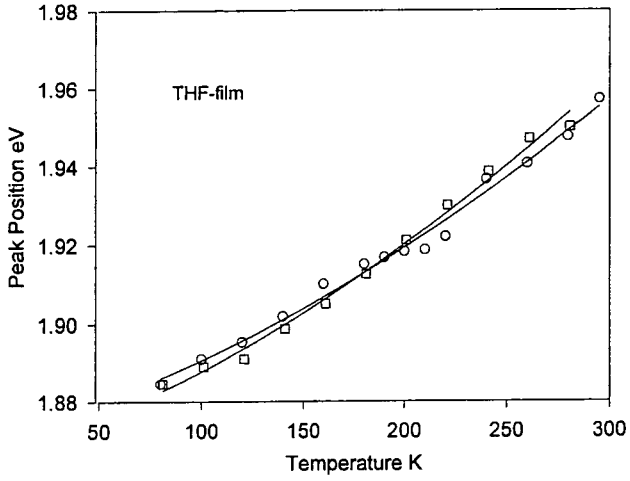

Figure 6.12: Position of the 0-1 peak of the PL (squares) (with kT subtracted and absorption (circles) for a THF film.

6.5 Discussion

6.5.1 Film Morphology

The observation of a red-shift of SLN as temperature is decreased can be understood to arise for the same reasons as the red-shift of absorption and PL that has been studied in detail for PPV and MEH-PPV [1–5]. The decrease in temperature freezes out torsions along the polymer backbone, increasing the planarity of the polymer chains. This increases the extent of electron delocalisation and reduces the energy of the $\pi - \pi^\star$ transition. The position of the SLN is determined by the gain and absorption in the sample. As both the gain and absorption move to longer wavelengths at lower temperature, so does the SLN.

There are a number of important observations from the data presented here. The first is that the SLN peak positions for the THF-film show a different temperature dependence than that of the CB-film, while the absorption and PL temperature dependencies for each film are very similar.

This is due to the differences in the conformation of the polymer molecules and film morphology. Work by Hide et al. [9] has shown that the SLN properties were strongly dependent on the solvent used for spin casting the films. They showed that the threshold for spectral line-narrowing was a factor of 5 higher for MEH-PPV films, if the spinning solvent chlorobenzene was used, compared with THF. Many factors affect the morphology of the films. The boiling point of THF is only 65°C whereas that of CB is 132°C. This means that the solvent evaporates more quickly from THF solution as the film is being formed. The morphology of the polymer in solution is therefore more easily transferred to the film. Experiments carried out by Nguyen et al [17] confirmed this by showing that films keep some degree of 'memory' of their conformation in solution when they are spin-coated to form films. CB is said to be a 'better' solvent for MEH-PPV as there is more interaction

between the solvent and the polymer [18, 19]. X-ray diffraction studies of MEH-PPV have compared films spin-coated from both THF and CB [15]. The results indicate that the morphology of the films is strongly dependent on the spinning solvent. Analysis of the results showed that films cast from THF were about 40% crystalline compared to 20% for CB-films.

Light scattering experiments [17] have shown that the hydrodynamic radius (R_H), which is a measure of the size of the polymer chains, was half the size for solution of MEH-PPV in THF than it was for solutions in CB. In addition to these measurements the spectra in figure 6.3 show that the PL spectra from the CB-film are broader and less structured than those from the THF-film. This indicates that the THF-film is more highly ordered than the CB-film. Given this evidence it is likely that the difference in the morphology and therefore the interchain photophysics, will depend upon the spinning solvent used to cast the films.

6.5.2 PLQY

The decrease in the intensity of the SLN and PL spectra with increasing temperature, for example as seen in figures 6.1 and 6.6 is due to a decrease in the photoluminescence quantum yield (PLQY). It has previously been shown that at low temperatures there is an increase in the intensity of the PL in PPV [20, 21]. This was also seen in recent work by Spiegelberg et al. [14] in which it was suggested that the increase in quantum yield at lower temperatures accounts for the observed decrease in threshold intensity for SLN in a PPV derivative. This is because the PLQY depends on the relative rates of radiative and non-radiative decay [22]. At low temperatures the rate of non-radiative decay is reduced, which increases the lifetime of the excited state responsible for stimulated emission. This in turn causes an increase in the gain. Although the absorption spectrum shifts with temperature, the

films were excited just below the absorption peak, so that the total shift of the absorption spectra (around 30 nm) had very little effect on the optical density of the sample.

6.5.3 SLN Behaviour

The effect of the morphology on the films explains why the general temperature dependence may be different in THF-films from that in CB-films. However the results also show that the shift of the SLN peak positions is smaller than the shift of the PL peaks in both the films studied. There are two possible explanations for these differences. The first is that the PL and SLN occur from different sites or regions in the polymer film. The results of Hide and Yang et al. [9, 15] have shown that SLN is more effective in more crystalline films. This suggests that amplification may be particularly associated with crystalline regions of the films. In contrast the PL may be due to the entire film including amorphous regions, which will have a different temperature-dependence.

It is also possible that other factors, such as the absorption of the sample may have a different temperature dependence than that of the PL and SLN. The peak of the SLN is determined by the net gain which is the difference between the gain of the material and the loss. The loss is due to processes such as ground state absorption, excited state absorption and scattering. It has been shown by pump probe measurements on PPV that the spectral shape and position of the stimulated emission band depends on the overlap of the gain spectrum and the photo-induced absorption band (due to excited state absorption) [20, 23, 24]. These processes may have a different temperature dependence from the PL, and hence the temperature dependence of the SLN peak can differ from that of the PL. This will affect the SLN much more strongly than the PL, as the measurement geometry is different. In the case

of the SLN, the light is waveguided a few millimetres through the film before it is emitted. In contrast, in PL the light travels a maximum distance of the thickness of the polymer film (100 nm). Therefore absorption will affect the SLN spectrum more than the PL spectrum. However, the red-shift of ground state absorption observed as the temperature is decreased would be expected to cause a larger red-shift of SLN than of PL. In fact a smaller shift of the SLN than the PL is observed, which may be due to a counteracting effect from excited state absorption. In addition, temperature will affect the waveguiding properties of the polymer film as the refractive index and thickness of the polymer film changes.

6.5.4 PL and Absorption Data

The observation that PL-kT and the absorption data have the same temperature dependence in each of the solvents is extremely interesting. This is probably due to the effect of thermal energy on exciton migration. Excitons migrate from the polymer chain segments where they are created, to longer chain segments on a range of timescales from femtoseconds to nanoseconds [25–27]. The excitons will migrate until they are within an energy of order kT of the lowest energy sites in the sample. This gives an additional contribution to the temperature-dependence of the PL.

6.6 Conclusion

The temperature dependence of the photoluminescence, absorption and spectral line-narrowing have been investigated for films of MEH-PPV spin coated from both THF and CB. The results obtained are important both for a theoretical analysis of the SLN but also for device fabrication. A red shift of the SLN is observed when the temperature is reduced and the shift of the

peak position is found to be smaller than the PL shift for both CB-films and THF-films. The differences in the behaviour of the films spun from different spinning solvents are due to the different morphology of the films.

There are two possible explanations for the smaller shift of the SLN peak positions, compared to the absorption and PL. The first is that the SLN originates from ordered sites whereas the PL is due to all sites, and the second is that the position of the net gain is influenced by other processes such as excited state absorption. These measurements show that the morphology of the films is a very important factor which can determine the SLN characteristics. This understanding can be used to improve performance and will be useful for the production of devices in the future.

Bibliography

[1] T. W. Hagler, K. Pakbaz, K. F. Voss, and A. J. Heeger. *Physical Review B-Condensed Matter*, 44(16):8652–8666, 1991.

[2] J. W. Yu, M. Hayashi, S. H. Lin, K. K. Liang, J. H. Hsu, W. S. Fann, C. I. Chao, K. R. Chuang, and S. A. Chen. *Synthetic Metals*, 82(2):159–166, 1996.

[3] K. Pichler, D. A. Halliday, D. D. C. Bradley, P. L. Burn, R. H. Friend, and A. B. Holmes. *Journal Of Physics-Condensed Matter*, 5(38):7155–7172, 1993.

[4] A.K. Sheridan, J.M. Lupton, I.D.W. Samuel, and D.D.C. Bradley. *Synthetic Metals*, 111-112:531, 2000.

[5] J.M. Lupton and I.D.W. Samuel. *Synthetic Metals*, 111:381–384, 2000.

[6] M. Severin and O. Inganas. *Journal of Chemical Physics*, 105:8446, 1996.

[7] V. Doan, V. Tran, and B. J. Schwartz. *Chemical Physics Letters*, 288(2-4):576–584, 1998.

[8] M. D. McGehee, R. Gupta, S. Veenstra, E. K. Miller, M. A. DiazGarcia, and A. J. Heeger. *Physical Review B-Condensed Matter*, 58(11):7035–7039, 1998.

[9] F. Hide, M. A. Diazgarcia, B. J. Schwartz, M. R. Andersson, Q. B. Pei, and A. J. Heeger. *Science*, 273(5283):1833–1836, 1996.

[10] G. J. Denton, N. Tessler, M. A. Stevens, and R. H. Friend. *Advanced Materials*, 9(7):547, 1997.

[11] C. Zenz, W. Graupner, S. Tasch, G. Leising, K. Mullen, and U. Scherf. *Applied Physics Letters*, 71(18):2566–2568, 1997.

[12] F. Hide, B. J. Schwartz, M. A. Diazgarcia, and A. J. Heeger. *Chemical Physics Letters*, 256(4-5):424–430, 1996.

[13] A.K. Sheridan, G.A. Turnbull, A.N. Safonov, and I.D.W. Samuel. *Physical Review B*, 62(18), 2000.

[14] C. Spiegelberg, N. Peyghambarian, and B. Kippelen. *Applied Physics Letters*, 75(6):748–750, 1999.

[15] C. Y. Yang, F. Hide, M. A. DiazGarcia, A. J. Heeger, and Y. Cao. *Polymer*, 39(11):2299–2304, 1998.

[16] M. Liess, S. Jeglinski, Z. V. Vardeny, M. Ozaki, K. Yoshino, Y. Ding, and T. Barton. *Physical Review B-Condensed Matter*, 56(24):15712–15724, 1997.

[17] T. Q. Nguyen, V. Doan, and B. J. Schwartz. *Journal of Chemical Physics*, 110(8):4068–4078, 1999.

[18] L.E. Horsburgh. Private communication.

[19] J. McMurry. *Organic Chemistry.* Brooks/Cole Publishing, 1984.

[20] M. Yan, L. J. Rothberg, F. Papadimitrakopoulos, M. E. Galvin, and T. M. Miller. *Physical Review Letters*, 72(7):1104–1107, 1994.

[21] D.D.C. Bradley, R.H. Friend, and W.J. Feast. *Synthetic Metals*, 17:645, 1987.

[22] N.S. Sariciftci, editor. *Primary Photoexcitation in conjugated polymers: Molecular Exciton versus Semiconductor Band Model.* World Scientific Co., 1997.

[23] W. Holzer, A. Penzkofer, S. H. Gong, A. Bleyer, and D. D. C. Bradley. *Advanced Materials*, 8(12):974–978, 1996.

[24] G. J. Denton, N. Tessler, N. T. Harrison, and R. H. Friend. *Physical Review Letters*, 78(4):733–736, 1997.

[25] G. R. Hayes, I. D. W. Samuel, and R. T. Phillips. *Physical Review B*, 52(16):11569–11572, 1995.

[26] I. D. W. Samuel, B. Crystall, G. Rumbles, P. L. Burn, A. B. Holmes, and R. H. Friend. *Synthetic Metals*, 54(1-3):281–288, 1993.

[27] B. Mollay, U. Lemmer, R. Kersting, R.F. Mahrt, H. Kurz, H.F. Kuffman, and H. Bässler. *Physical Review B*, 50:10769, 1994.

Chapter 7

Tuneability of Amplified Spontaneous Emission

7.1 Introduction

The observation of stimulated emission in conjugated polymers using techniques such as transient absorption measurements [1–4] opened up the possibility of using these materials in devices such as lasers. For this reason a lot of work has been directed towards studying the gain process in order to understand the mechanism behind it and the factors which affect it. As discussed earlier, the dramatic narrowing of the emission spectrum is commonly assigned to ASE. This process is seen in films which are thick enough to support waveguide modes.

Control of the ASE is very important in the context of device fabrication. There have recently been a number of works investigating the way in which film morphology [5–7], excitation intensity (chapter 5) and temperature [8, 9] control the gain. However, the factors which determine the spectral position of the emission are not well understood.

In this chapter the way in which the film thickness affects the peak posi-

tion of the ASE is investigated. Through controlling the film thickness it is shown that the spectral position of the peak of the ASE can be controlled, demonstrating that gain can be tuned over a broad bandwidth. A theoretical analysis is used to model the thin films as asymmetric waveguides. Through this modelling of the waveguide modes the theoretical cut-off wavelengths for guides of varying thicknesses are obtained. This information is used to understand how film thickness affects the peak position of the ASE in these experiments.

In addition a simple technique has been used to measure the waveguide cut-off wavelength for the thin films and the results are found to compare well with the theoretical calculations.

7.2 Theory

7.2.1 Spectral Location of the ASE

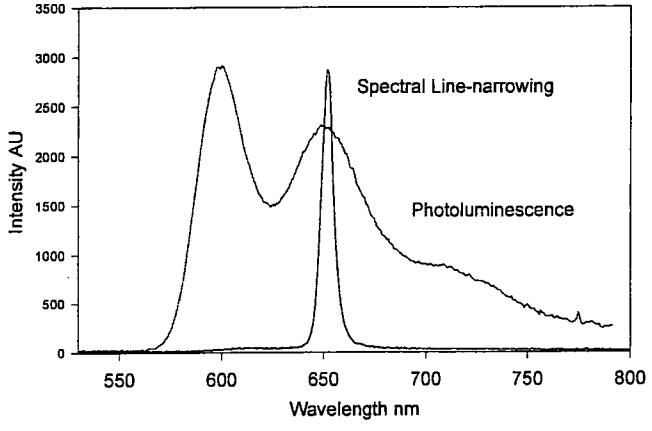

Figure 7.1: PL and spectral line-narrowing for MEH-PPV at 117 K.

The main factor that determines the position of the ASE is the position of the peak of the net gain spectrum. The net gain is determined by both the material gain and the excited state and ground state absorption losses and to a first order approximation is similar to the PL spectrum. However, the peak of the ASE is generally located close to the 0-1 peak of the PL [10] as shown in figure 7.1, indicating that the peak of the gain is not at the peak of the PL spectrum, but is shifted to lower energies by ground state absorption.

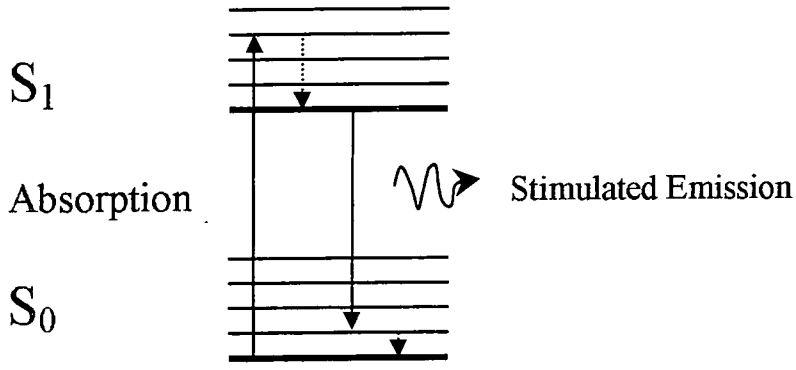

Figure 7.2: 4-level laser system.

Another way to approach this is to consider the polymer system to be analogous to a 4-level dye laser system (figure 7.2) [10, 11]. In this approach absorbed pump radiation excites the molecule from the ground state levels S_0 to a higher vibrational level of the first singlet state S_{1vib}. The relaxation from S_{1vib} to S_1 is very fast (in the order of ps or faster) and radiationless. Stimulated emission then occurs from the lowest level of the first singlet state S_1 to a vibrational level in the ground state S_{0vib}. This transition is to an

unoccupied vibrational level rather than the populated ground state so that a population inversion can be achieved between the two states. This is a necessary condition for amplification to occur. The transition from the S_1 state to the S_{0vib} state corresponds to the 0-1 peak in the PL spectrum. Again the molecule quickly relaxes from the S_{0vib} to S_0 state [12].

7.2.2 ASE and Waveguiding

As discussed in chapter 3, the mechanism for spectral-line narrowing has been assigned to ASE. In this process, the length over which amplified light can build up must be large enough for the light to be macroscopically amplified. This process is helped by waveguiding in the film and it has been found that if the film is too thin to support waveguide modes, no ASE is observed [13]. Hide et al. calculated a cut-off thickness (for light at 620 nm), below which no ASE is seen [13]. However, as conjugated polymers have a broad spectral emission and large material dispersion over the emission region, the cut-off thickness is highly wavelength dependent. In order to investigate this further, the ASE from six films of different thicknesses, close to the cut-off, have been investigated.

As previously discussed, the structure used in these experiments make simple one layer waveguides in which the substrate is the quartz or glass on to which the polymer is spun, and the superstrate is air. The diagram in figure 7.4 shows the structure of these waveguides. A guided mode can be thought of as a beam of photons being totally internally reflected at both interfaces and hence propagating down the waveguide.

7.2.3 Modelling

Using the theory described in chapter 3 the guided modes in a glass/MEH-PPV/air waveguide were modelled. In order to account for the refractive

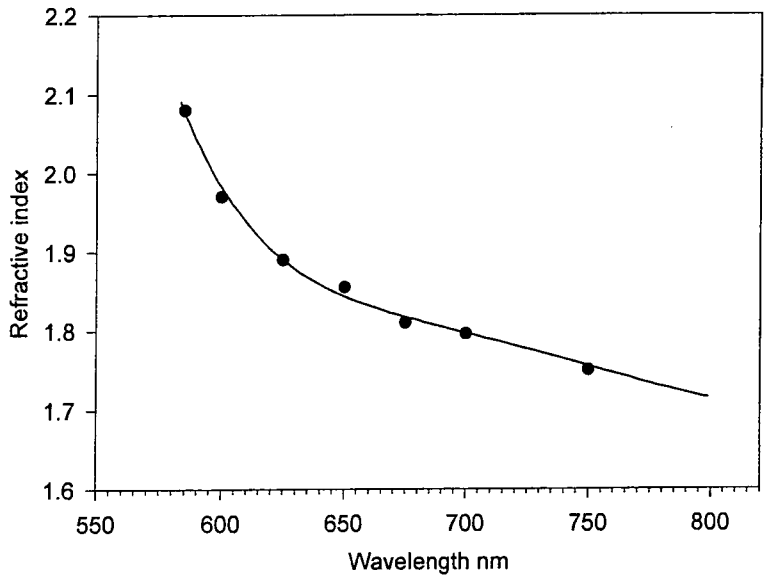

Figure 7.3: In-Plane Refractive Index Dispersion of MEH-PPV. The line is a fit to the data as described in the text.

index dispersion of MEH-PPV, measurements made by Safonov et al. [14] were used. Their results can be used with confidence as they used the same batch of MEH-PPV as that used in this work, and the same spinning solvent to form films. In their work thin films were formed by spin-coating on to a microstructured diffraction grating with a period of 400 nm. The grating acts as an ordered array of scattering centres, which results in constructive interference of the light at an angle θ to the normal to the plane of the guide. This is the Bragg condition. The scattering angle θ, is wavelength dependent and so the emission spectrum measured at a particular angle exhibits sharp

peaks at the Bragg scattered wavelengths that satisfy the relation:

$$n_g sin\alpha - n_a sin\theta = \frac{\lambda N}{\Delta} \tag{7.1}$$

where N is the diffraction order (N=0 corresponds to Snell's law), Δ is the grating period, α is the angle of the light in the guide to the normal to the plane of the guide, n_g is the refractive index of the glass and n_a is the refractive index of the air. The positions of these peaks were recorded at different angles and these data were used to calculate the in-plane refractive index between 580 nm and 800 nm. These data were fitted with the following Sellmeier equation which is a standard way of fitting refractive index data:

$$n_0 = \sqrt{3.3 + \frac{0.148}{\left[1 - \left[\frac{552}{\lambda}\right]^2\right]}} \tag{7.2}$$

The refractive index data is shown in figure 7.3. As conjugated polymers are highly birefringent materials, the out of plane refractive index is also required to model the TM modes. Out-of plane refractive index data was measured by Barnes et al. [15] using prism coupling.

7.3 Experimental Details

Six films of varying thickness of MEH-PPV were fabricated by spin-coating a solution consisting of 5 mg of polymer dissolved in 1 ml of chlorobenzene. Changing the spin speed between 1200 and 3000 rpm controlled the thickness of the polymer layer. Films of thickness between 46 nm and 154 nm were obtained and were used in spectral-line narrowing experiments. For these experiments the substrate used was glass microscope slides cut to 12 x 12 mm squares. Glass was used rather than fused silica which is used in

other experiments as it was found that the quality of the waveguide at the substrate edges, was better and therefore less scattering of the emitted light was observed. This was particularly important for the measurement of the cut-off wavelength described in section 7.3.1.

The ASE spectra were obtained by exciting the front of the films with the second harmonic of the Nd:YAG laser (532 nm) at 10 Hz. The energy per pulse was about 10 μJ. All spectra were measured very close to threshold.

7.3.1 Measurement of Cut-off Wavelength

In order to measure the cut-off wavelength a simple technique was used. The films were painted black on the back of the substrate to suppress reflections from the substrate/air interface. The film was held in a vacuum and excited with a spot close to the edge of the film with the 488 nm line of an argon ion laser. At detection angles greater than 20^o to the plane of the film, the usual MEH-PPV spectrum was measured. However when the detector was held close to the plane of the film , shown by an angle δ in figure 7.4, a narrow feature was seen with a width of approximately 30 nm.

In the simple ray model of optical waveguiding there are two conditions that need to be fulfilled in order for a guided mode to propagate in the film. The first is that in order for light to be totally internally reflected the angle of propagation must exceed the critical angle, θ_c for the interface. The second is that light of a certain wavelength can only propagate as a guided mode at one angle. This angle decreases with wavelength. The equation for waveguide modes is given as:

$$2ndk_0cos(\theta) = \phi_1 + \phi_2 + 2N\pi \tag{7.3}$$

Where n = refractive index of polymer, d= polymer film thickness, θ =

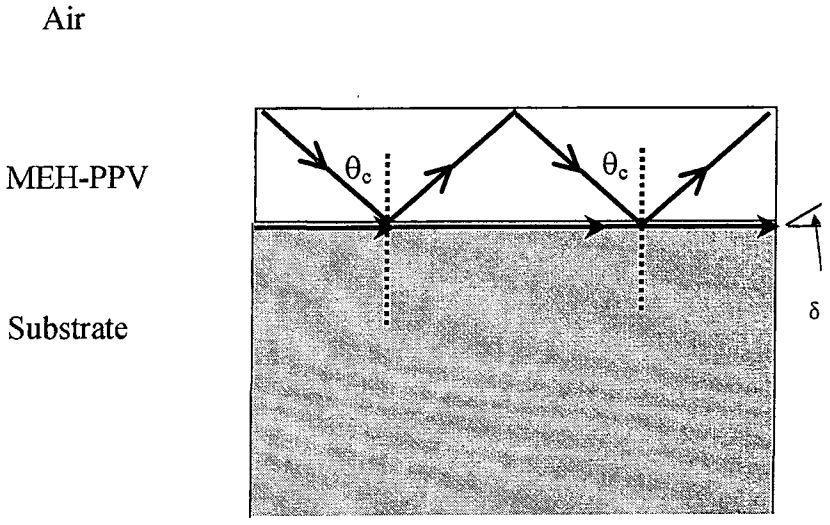

Figure 7.4: The waveguide structure showing light that is totally internally reflected and light travelling in the substrate parallel to the plane of the film.

angle of propagation, ϕ_1 and ϕ_2 are the phase change on reflection from the polymer/air interface and polymer/glass interface respectively. N is an integer and k_0 is the free space wave vector.

At the cut-off wavelength for the waveguide the angle for propagation will be equal to the critical angle for the polymer/glass interface and therefore no total internal reflection will occur. Instead some of the light will be lost from the guided mode and will propagate in the substrate parallel to the plane of the film as shown in figure 7.4 by the arrow running parallel to the polymer/substrate interface. Successive partial reflections from the polymer-glass boundary will also contribute as sources to this substrate wave. For most wavelengths emitted at the critical angle, these sources interfere destructively and the accumulated substrate wave will be weak. However, for the cut-off wavelength of the guide, the sources are correctly phased to interfere constructively and so an enhancement is seen around this wavelength. For

emission angles less than the critical angle the leaky modes will spread out into the substrate, and similar interference effects are seen for longer wavelengths. However the cut-off wavelength for the waveguide is that at which the peak is observed parallel to the plane of the film.

A similar technique has been used by the Cambridge group to determine the refractive index dispersion of a polyflourene derivative [16].

7.4 Results

7.4.1 Experimental Results

Figure 7.5 shows the ASE spectra obtained for six films of different thickness. The spectra vary slightly in width as they were measured at incident energies a little above the threshold for spectral line-narrowing.

The figure shows that the peak of the ASE spectrum is blue shifted as the thickness of the film is decreased. For the thickest film (154 nm) the peak of the ASE is at 623 nm and for the thinnest film (46 nm), the peak of the ASE is at 592 nm. This shows that the peak of the ASE depends on the film thickness. The interesting feature of this graph is the separation between the three thickest and the three thinnest films. The peaks of the ASE for the three thickest films are very similar, all positioned between 618 nm and 623 nm. However as the film thickness is reduced below this a large blue shift of the ASE spectra is seen. This demonstrates that a broadband tuneability of the ASE of 31 nm (25 THz) has been achieved. These results are explained in section 7.4.2 through modelling of the waveguide modes.

7.4.2 Modelling Results

Figures 7.6 and 7.7 show the mode intensity for a 100 nm thick film at 590 nm and a 50 nm thick film at 590 nm. In figure 7.6 the sinusoidal distribution

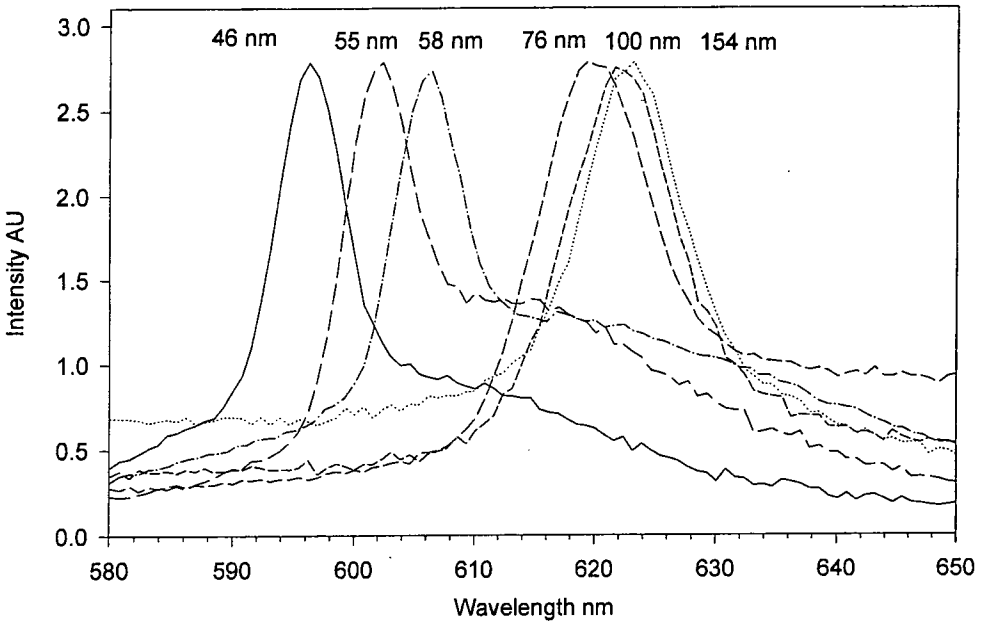

Figure 7.5: ASE spectra as a function of film thickness.

in the polymer and the exponential decay in the sub and superstrates can be clearly seen. For this waveguide much of the mode intensity which corresponds to energy carried by the mode is in the polymer layer. Figure 7.7 has the same mode relations but in this case the thickness of the polymer layer is very close to the cut-off thickness for the waveguide at this wavelength. Here very little of the mode is confined to the polymer and a lot of the energy is in the substrate. The asymmetric nature of the graph is due to the different refractive indices of the air and glass layers. The two figures show how the proportion of the mode energy in the polymer layer changes as the cut-off thickness is approached. For a polymer film well above the cut-off thickness the mode is nearly symmetrical and mostly confined to the polymer layer.

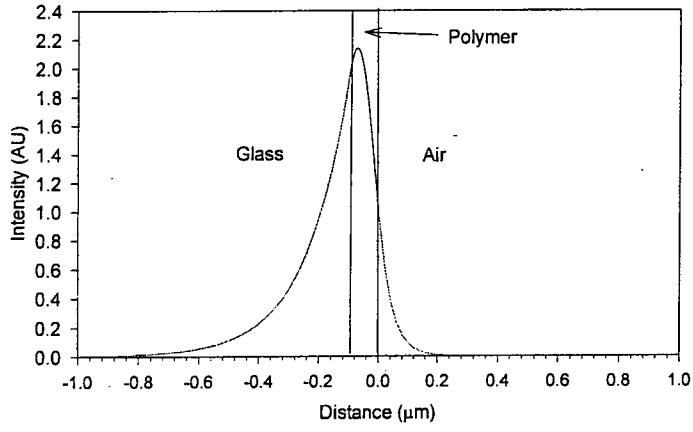

Figure 7.6: Mode structure for 620 nm light in an MEH-PPV film 100nm thick.

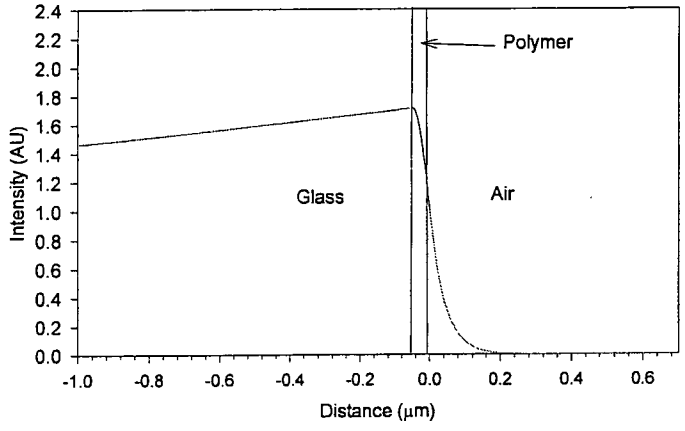

Figure 7.7: Mode structure for 620 nm light in an MEH-PPV film 50 nm thick.

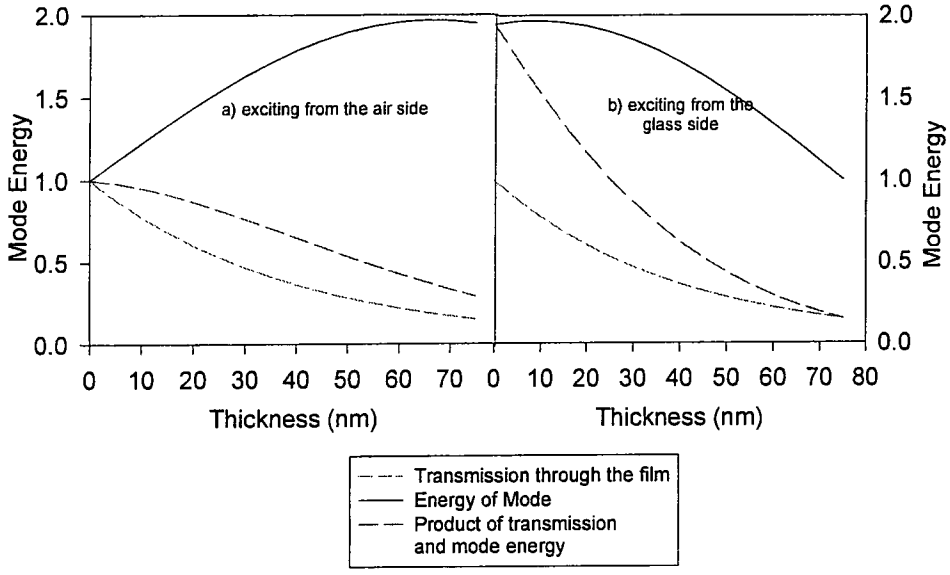

Figure 7.8: Confinement factor for excitation from the air (a) and from the glass side (b). For each graph the glass interface is at 0 nm and the air interface is at 75 nm

As the polymer film thickness approaches the cut-off thickness for light of a given wavelength, more of the mode energy is in the glass and the mode becomes highly asymmetrical. At the cut-off thickness no light of this wavelength will propagate in the polymer film as a bound mode. The relative amount of energy can be evaluated using the confinement factor. Here this is defined as the integral of the mode energy multiplied by the transmission in the film. As the mode is asymmetric close to the cut off thickness, the confinement factor should depend on which side of the waveguide is excited with incident radiation. Figure 7.8 shows the mode energy in the film, the transmission through the film and the product of these two quantities for

samples excited both from the air side (a) and from the glass side (b). The area under the product of the transmission and the mode energy gives the confinement factor. This is found to be 50 for figure 7.8a and 60 for figure 7.8b. In order to calculate how the confinement factor affects the threshold for ASE, it is important to first calculate how the Fresnel reflections affect the intensity of the incident light . The Fresnel equation for unpolarized light at normal incidence is:

$$T = \frac{4n_i n_t}{(n_t + n_i)^2} \tag{7.4}$$

where T is the amount of light transmitted from the first medium of refractive index n_i to the second medium of refractive index n_t. For excitation from the glass side, the calculation must be done in two steps to account for the reflections from the air/glass interface and the glass/polymer interface.

Using the refractive index of the glass as 1.51, of the air as 1.0 and of the polymer as 2.3 gives $I_{glass} = 0.91$ and $I_{air} = 0.84$. The Fresnel reflections are very similar in each case.

The threshold for ASE has been measured for excitation from both the glass and the air side. For excitation from the air side the threshold is $3 \pm 0.1 \times 10^{-7}$ J and from the glass side it is $2.5 \pm 0.1 \times 10^{-7}$ J. The important observation is that the threshold for the glass side is slightly lower than for excitation from the air side. This is predicted by the confinement factor calculation.

Figure 7.9 shows the cut-off wavelength calculated as a function of thickness from equation 3.16 as described in chapter 3 for the first order TE and TM modes. For a given thickness, only light of a wavelength shorter than the cut-off wavelength can guide in the polymer layer. The figure shows that light of 590 nm will be guided in films thicker than 50 nm whereas light of 620 nm will only be guided if the polymer layer is thicker than 76 nm. These results will be compared to the measured positions of the ASE peaks, and are used to explain the observed blue shift in peak position as the thickness

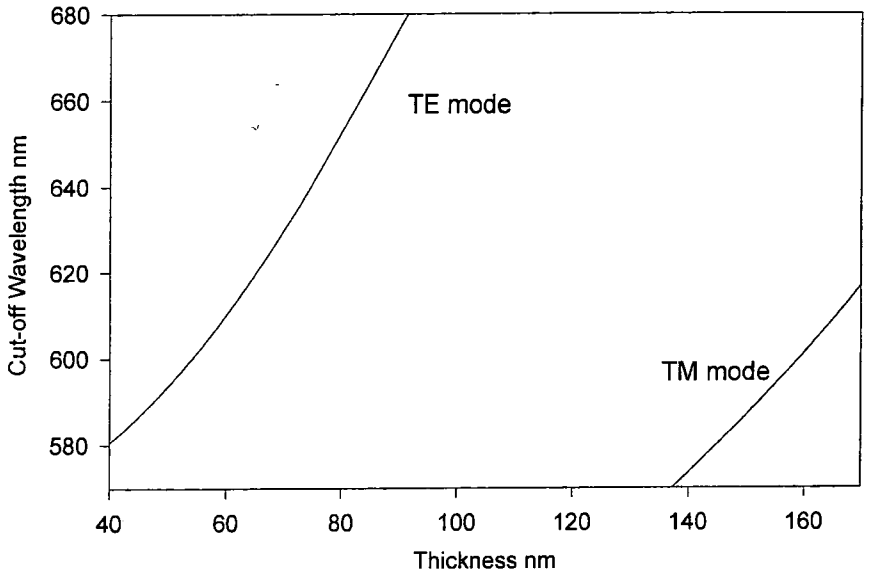

Figure 7.9: Calculated cut-off wavelengths

is decreased.

7.4.3 Comparison of Experimental and Theoretical Data

Figure 7.10 shows the peak positions of the ASE spectra taken from figure 7.5 as a function of film thickness and the theoretically calculated cut-off wavelengths from figure 7.9. The figure shows that for the three thickest films the position of the ASE is very similar (618 nm-623 nm) as described earlier. However, the position of the ASE for the three thinnest films is very close to the cut-off wavelength calculated by the model. Hence the position of the ASE for thin films (< 76 nm) is determined by the cut-off wavelength

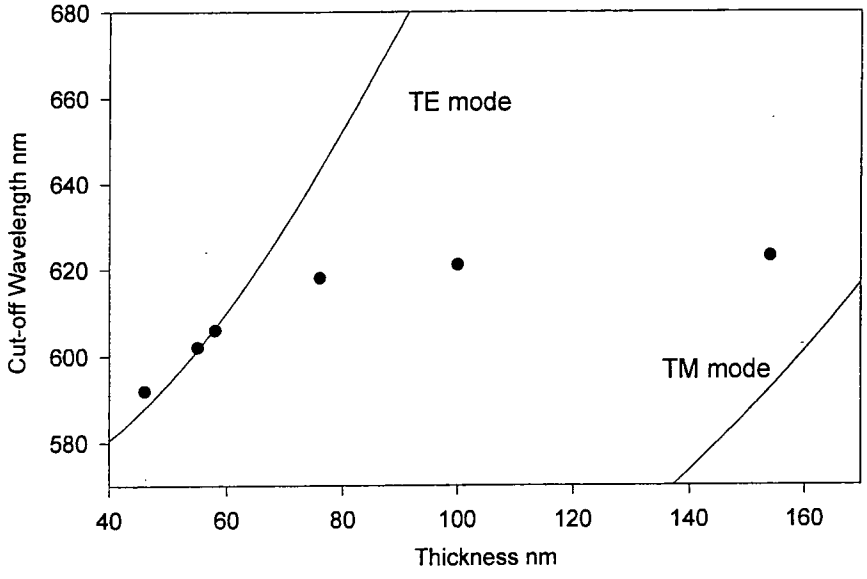

Figure 7.10: Calculated cut-off wavelengths

for the guide whereas for thick films it is determined by the position of the maximum gain density. Therefore by controlling the thickness of the film it is possible to tune the emission wavelength of the ASE. In this work the ASE has been tuned by 31 nm which corresponds to a bandwidth of 25 THz.

Tuning of the stimulated emission in conjugated polymer films has previously been demonstrated in a laser cavity for example in the work of Kumar [18] in which tuning was achieved in a blend of a PPV derivative using an external cavity resonator by the rotation of a grating . Another approach has been to use wavelength scale microstructure as in DFB lasers [19]. In this work the emission was tuned by 43 nm by adjusting the period of the gratings. Here we achieve tuning without an external cavity or microstructure

simply by changing the film thickness.

The polarisation ratio of the ASE for thick and for thin films has been measured. A calibrated linear polariser was placed between the film and the CCD collection fibre. Emission spectra were measured for different angles of the polariser and a sine function was fitted to the points. The polarisation ratio is defined as the ratio of in-plane (TE) to out-of plane (TM) emission intensity. For thin films (<76 nm) this ratio was found to be 98±2% and for thick films (>140 nm) this was 75±2%. This shows that for thin films the ASE is completely TE polarised and that all the light is guided in the zero order TE mode. The lower polarisation ratio measured for thick films may be due to both TE and TM modes being allowed to guide at the emission wavelengths. Although figure implies that TM modes should not be guided, it should be noted that there is a significant uncertainty of ±0.05 in the out-of plane index data [15]. This results in an upper limit of 620 nm for the cut-off wavelength for the TM mode in a 150 nm thick film.

7.5 Measurement of Cut-off Wavelength

The cut-off wavelength for each of the six films used in the line-narrowing experiments was measured using a simple technique [16] described in section 7.3.1. The spectra obtained by this method are shown in figure 7.11.

When the emission was collected at 90 ± 5^0, narrow spectra with a width of approximately 30 nm were obtained. The usual photoluminescence spectrum was observed when light was collected from the front face. The wavelength of the peak of these spectra determines the cut-off wavelength for the guide as explained in section 7.3.1. However, data could only be obtained for the five thinnest films as the cut-off wavelength for the 154 nm film occurred at a wavelength beyond the photoluminescence emission. As predicted by figure 7.11 the position of the peak moves to longer wavelengths as the thickness

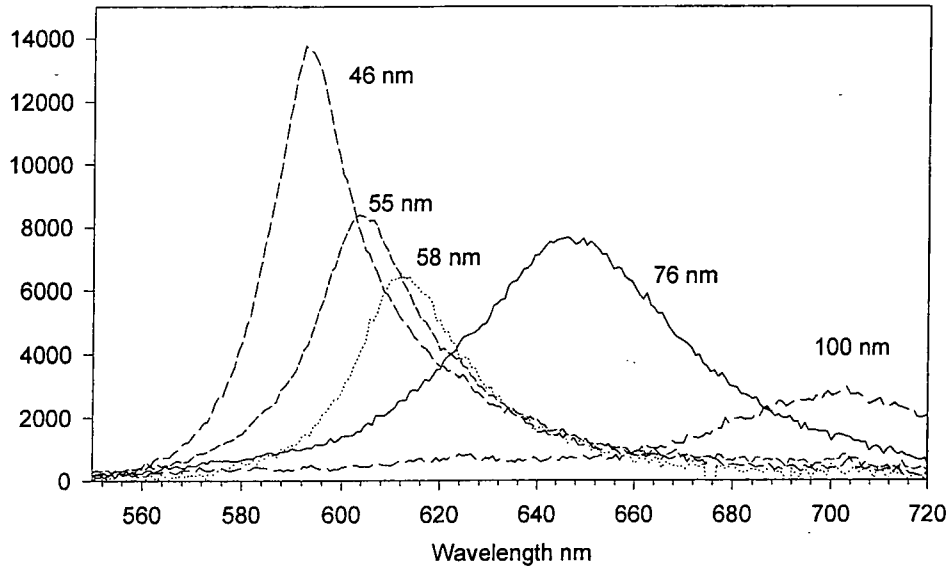

Figure 7.11: Spectra measured using the cut-off wavelength technique.

of the film is increased. The spectra also get broader as the thickness of the films is increased. This broadening is due to the shape of the refractive index dispersion curve. Narrow spectra are only obtained when the change in the refractive index is large with respect to wavelength (i.e. the gradient is large). For light at angles less than the critical angle in the waveguide, light will spread into the substrate as a leaky mode. The angle at which the light is emitted into the substrate depends on the refractive index of the MEH-PPV for that particular wavelength. Therefore, for large changes in refractive index as a function of wavelength, light will be dispersed at greater angles in the substrate and a narrow band emission spectrum will be measured. As figure 7.3 shows, the gradient of the refractive index curve

decreases with increasing wavelength, therefore spectra observed at longer wavelengths are broader than those at shorter wavelengths.

7.5.1 Comparison of Theoretical and Experimental Cut-off Data

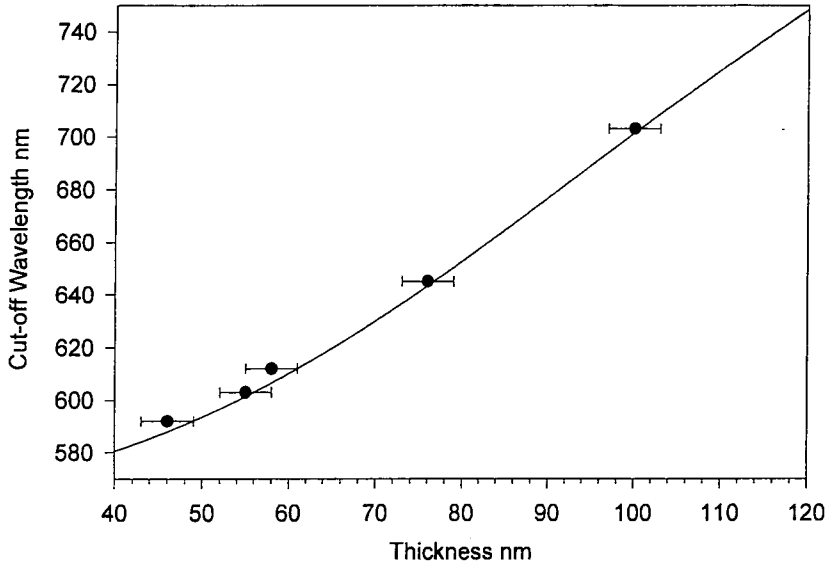

Figure 7.12: Calculated cut-off wavelengths with measured wavelengths

Figure 7.12 shows the measured cut-off wavelengths (circles) and the calculated cut-off wavelength as a function of film thickness. All 5 points show good agreement with the calculated values. This method for measuring the cut-off wavelength has been used to calculate the refractive index dispersion for a polyfluorene [16].

Film	Film Thickness (nm)	Position of ASE (nm)	Measured Cut-off λ (nm)	Calculated Cut-off λ (nm)
1	46	592	592	588
2	55	602	603	602
3	58	606	612	607
4	76	618	645	644
5	100	621	703	702
6	154	623	NA	816

Table 7.1: Table of Results

A summary of the results in this chapter is shown in table 7.1.

7.6 Conclusions

In this chapter the effect of changing the thickness of the polymer layer on the position of the ASE has been investigated.

The experiments show that by controlling the film thickness the position of the ASE can be tuned by 31 nm which corresponds to a bandwidth of 25 THz. This is an extremely important result in the context of device fabrication. By tuning the position of the ASE, the results show that gain can be achieved over a broad range. This shows that conjugated polymers have the potential to be used as broad-band optical amplifiers or as tuneable solid state lasers.

By modelling the waveguide modes in the polymer film as simple asymmetric waveguides, a good understanding of how the thickness of the film affects the position of the ASE, has been achieved. The waveguide modes for two films, one with a thickness greater than the cut-off thickness and one very close to the cut-off thickness were calculated. The cut-off wavelength as a function of film thickness was also calculated. The results show that for thick films (> 76 nm) the position of the ASE is determined only by the position of the maximum gain, which depends on the ground and excited state absorption losses. However for thin films, the position of the ASE is determined by the cut-off wavelength for the waveguide, and is therefore highly dependent on the thickness of the film. Hence the position of the ASE can be tuned by controlling the thickness of the film.

In addition the cut-off wavelength has been measured for these films. Good agreement with the calculated values was achieved, showing that modelling these structures as asymmetric waveguides is a reliable way of investigating the propagation of waveguide modes in the polymer waveguides.

Bibliography

[1] G.J. Denton, N. Tessler, N.T. Harrison, and R.H. Friend. *Physics Review Letters*, 78:733, (1997).

[2] E.S. Maniloff, A.V. Klimov, and D.W. McBranch. *Physical Review B*, 56:1876, 1997.

[3] A. Dogariu, D. Vacar, and A.J Heeger. *Physical Review B*, 58:10218, 1998.

[4] S.V. Frolov, M. Liess, P.A. Lane, W. Gellerman, Z.V. Vardeny, M. Ozaki, and Yoshino K. *Physics Review Letters*, 78:4285, 1997.

[5] T. Q. Nguyen, V. Doan, and B. J. Schwartz. *Journal Of Chemical Physics*, 110(8):4068–4078, 1999.

[6] C. Y. Yang, F. Hide, M. A. DiazGarcia, A. J. Heeger, and Y. Cao. *Polymer*, 39(11):2299–2304, 1998.

[7] X. Long, M. Grell, A. Malinowski, D. D. C. Bradley, M. Inbasekaran, and E. P. Woo. *Optical Materials*, 9(1-4):70–76, 1998.

[8] C. Spiegelberg, N. Peyghambarian, and B. Kippelen. *Applied Physics Letters*, 75(6):748–750, 1999.

[9] A.K. Sheridan, J.M. Lupton, I.D.W. Samuel, and D.D.C. Bradley. *Chemical Physics Letters*, 322:51, 2000.

[10] B. Schweitzer, G. Wegmann, H. Giessen, D. Hertel, H. Bassler, R. F. Mahrt, U. Scherf, and K. Mullen. *Applied Physics Letters*, 72(23):2933–2935, 1998.

[11] X. A. Long, A. Malinowski, D. D. C. Bradley, M. Inbasekaran, and E. P. Woo. *Chemical Physics Letters*, 272(1-2):6–12, 1997.

[12] F.P. Schaefer. *Topics in Applied Physics.* Springer-Verlag, 1973.

[13] F. Hide, M. A. Diazgarcia, B. J. Schwartz, M. R. Andersson, Q. B. Pei, and A. J. Heeger. *Science*, 273(5283):1833, 1996.

[14] A.N. Safonov, M. Jory, B.J. Matterson, J.M. Lupton, M.G. Salt, J.A.E. Wasey, W.L. Barnes, and I.D.W. Samuel. *Synthetic Metals*, in press.

[15] A. Boudrioua, P.A. Hobson, B.J. Matterson, W.L. Barnes, and I.D.W. Samuel. *Synthetic Metals*, 111:545, 2000.

[16] T. Kawase, D.J. Pinner, and R.H. Friend. *Synthetic Metals*, 111:583, 2000.

[17] A. Yariv. *Optical Electronics.* Saunders College Publishing, 1991.

[18] N.D. Kumar, J.D. Bhawalkar, P.N. Prasad, F.E. Karasz, and B Hu. *Applied Physics Letters*, 71:1999, 10997.

[19] M. D. McGehee, M.A. Diaz-Garcia, F. Hide, R. Gupta, E.K. Miller, D. Moses, and Heeger A.J. *Applied Physics Letters*, 72:1536, 1998.

Chapter 8

Efficient Energy Transfer in Perylene Dyes

8.1 Introduction

Amplification was first observed in organic systems in the 1960s [1, 2]. More recently the first observations of simulated emission in conjugated polymer systems using transient absorption measurements [3–6], has lead to research directed towards understanding the mechanism for the stimulated emission and the factors which control the emission properties [7–10]. One goal of this research is to fabricate an amplifier for the polymer optical fibre networks. Polymer optical fibres are transparent at 650 nm therefore an amplifier in a polymer optical fibre would ideally emit around 650 nm. However, it is essential to make the amplifiers compatible with suitable pump lasers. This can be achieved by using energy transfer, for instance a red emitting molecule which has an absorption in the green can be doped into a system which absorbs in the blue. This system could then be pumped using the commercially available GaN (gallium nitride) laser. Energy would be transferred from the blue absorbing host to the red emitting chromophore.

Energy transfer was first observed in 1922 by Cario and Franck [11] using mercury and thalium vapour. More recent work has investigated the process in a range of organic systems relevant to electro-luminescence [12–18]. Using energy transfer in lasers has been shown to reduce the threshold for lasing, as the emission region is shifted away from the absorption region [17]. Work by Mattoussi has shown that by using a highly efficient acceptor material it is also possible for the quantum efficiency of the system compared to that of the pure host to be improved dramatically [13]. Energy transfer can also be useful in organic light emitting diodes to achieve white light emission [19].

Energy transfer can be used to control the emission wavelength and other properties of the emission and it is therefore very important for the fabrication of lasers, amplifiers, and light emitting diodes, that a detailed understanding of the energy transfer mechanism is gained.

In this chapter the energy transfer properties of two conjugated organic chromophores, lumogen orange and lumogen red, supplied by BASF, in Ludwigshafen, Germany were investigated. Thin films are made by doping the chromophores into a host matrix of poly methyl methacralate (PMMA). These dilute films can be treated as if they are solutions. These materials are perylene derivatives and their chemical structures are shown in figure 8.1 and figure 8.2. They were first made as part of a series of perylene dyes by Seybold and Wagonblast in the late 1980's [20]. At this time there was great interest in synthesising perylene dyes for the fabrication of solid state tuneable lasers [21, 22]. The high photostabilities and high quantum yields of these materials makes them ideal for laser applications [23]. These materials have also attracted interest for their use in tuneable dye lasers [24] and in optically pumped solid state lasers in PMMA, sol-gel and a composite glass [25]. Laser emission of these dyes in a PMMA host has also been observed [25] with laser emission at 578 nm for lumogen orange and 613 nm for lumogen red. They are often referred to as perylene orange and perylene

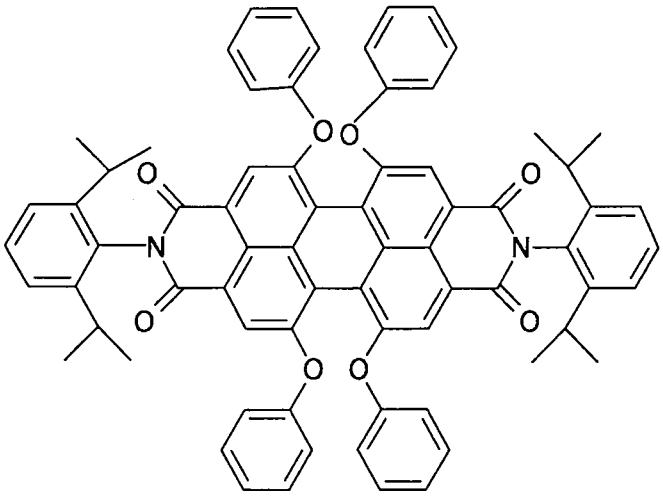

Figure 8.1: Lumogen Red

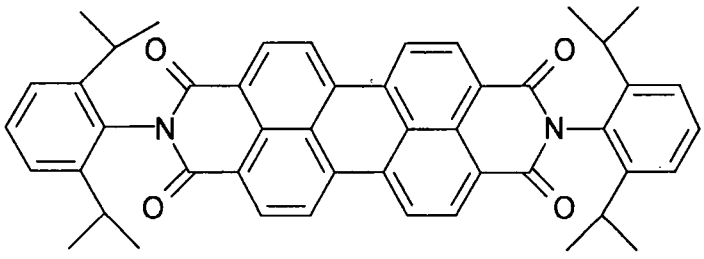

Figure 8.2: Lumogen Orange

red in the literature.

In this chapter the energy transfer dynamics in thin film blends of lumogen orange and lumogen red, in the host matrix PMMA have been investigated. In these blends, lumogen orange acts as the donor and lumogen red as the acceptor. Measurements of the amplified spontaneous emission (ASE) are made for blends of lumogen orange and lumogen red at different concentrations. In order to understand these results two different methods are used to determine the rate of energy transfer between the dyes. The first method involves measuring the photoluminescence quantum yield of the luminescence from the donor and the second uses time-resolved luminescence measurements which were carried out at Sheffield University. Results obtained using these two methods are compared. The results of the measurement of the rate of energy transfer are used to make an estimate of the excited state lifetime of lumogen orange and hence to understand the concentration dependence of the ASE results.

8.2 Theory

8.2.1 Energy transfer mechanisms

The term energy transfer simply means the transfer of energy from a donor system to an acceptor system and can be achieved through vibrational, rotational, translational or electronic energy. However, it is more convenient to limit this to electronic energy transfer where an acceptor is promoted to a higher electronic state. This can be described by equation 8.1 [26]:

$$D^* + A \rightarrow D + A^* \tag{8.1}$$

Initially the donor D is in an excited state. This excitation is then passed to the acceptor A and the donor is demoted to a lower electronic state.

One common type of energy transfer is radiative transfer, which is also referred to as trivial energy transfer [27]. In this process there is no direct interaction between the donor and acceptor. It is a two stage process in which the donor, initially in an excited state, decays to a lower energy state with the emission of a photon. The photon is then absorbed by the acceptor, as shown below:

$$D^* \rightarrow D + h\nu \tag{8.2}$$

$$h\nu + A \rightarrow A^* \tag{8.3}$$

This type of energy transfer differs from non-radiative transfer discussed in the next section, in that there is no change in the donor emission lifetime and the change in the emission spectrum can be fully accounted for in the absorption spectrum of the acceptor.

8.2.2 Non-radiative Energy Transfer

Non-radiative energy transfer is more complicated than the 'trivial' energy transfer described above. This is a one step process in which there is some direct interaction between the donor and the acceptor, without a photon being produced. The process can only occur if the initial and final states are degenerate and if they are coupled by a donor-acceptor interaction.

An overlap integral (J) which defines the strength of the coupling between the donor and the acceptor can be defined as:

$$J = \int P_D(\nu)\epsilon_A(\nu)\frac{1}{\nu^4}d\nu \tag{8.4}$$

Here, $P_D(\nu)$ is the photoluminescence of the donor and $\epsilon_A(\nu)$ is the extinction

spectrum of the acceptor. Both of these quantities are normalised to one on a wavenumber scale.

8.2.3 Förster (Long-range) Energy Transfer

Förster developed a formalism for energy transfer in which he only considered transfer via dipole-dipole interactions [28, 29]. His theory assumes that the energy transfer is much slower than the vibrational relaxation in the donor and acceptor and applies only to systems in which the donor and acceptor molecules are separated by at least 2 nm. He showed that the rate constant for excitation transfer in which the initial and final states are coupled through a dipole-dipole interaction is given by:

$$k = \frac{9000 f^2 ln10 \phi_D}{\tau_D R^6 128 \pi^5 N_A n^4} J \tag{8.5}$$

where f^2 is an orientation factor, which for a solid solution with random orientation of the donor and acceptor dipole moments is $\frac{2}{3}$, ϕ_D is the photoluminescence quantum yield of the donor which accounts for competition for the energy transfer by other non radiative pathways. N_A is Avagadro's number, n is the refractive index of the system and J is the overlap integral. τ_D is the natural radiative decay time of the pure donor, R is the average distance between the donor and acceptor molecules and R_0 is the characteristic Förster radius, which is linked to the rate of energy transfer by:

$$k = \frac{1}{\tau_D}\left(\frac{R_0}{R}\right)^6 \tag{8.6}$$

R_0 is the separation of the donor and acceptor at which the rate of intermolecular energy transfer is equal to the sum of the rates for all other de-excitation processes.

As equation 8.5 shows, the rate of energy transfer depends on the overlap integral J. In order to get efficient energy transfer, it is therefore necessary to have good overlap between the donor emission spectrum and the acceptor absorption spectrum. Figure 8.3 below shows the absorption and photoluminescence spectra for lumogen red and lumogen orange. In these experiments the lumogen orange is the donor and lumogen red is the acceptor. This graph shows clearly that there is good overlap between the donor emission spectrum and the acceptor absorption spectrum and that this system is therefore an interesting one to investigate in terms of energy transfer.

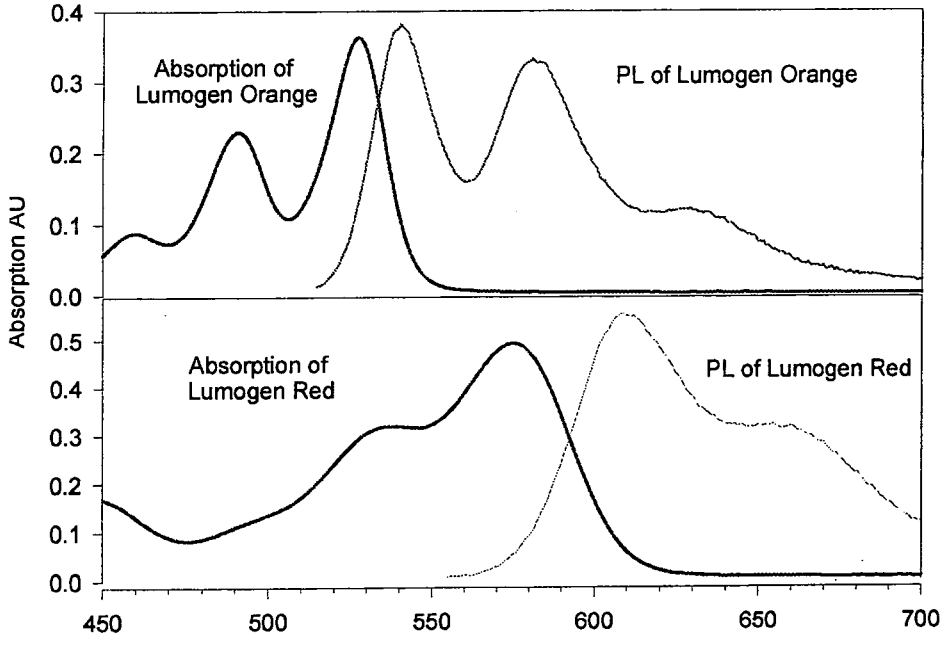

Figure 8.3: Absorption (bold line) and photoluminescence (thin line) spectra of films of lumogen orange (upper panel) and lumogen red, both doped in PMMA (lower panel).

A critical concentration C_A^0 is defined as the concentration at which the energy transfer is 50% efficient. This is related to R_0 through:

$$R_0 = \frac{7.35}{C_A^{0\,\frac{1}{3}}} \tag{8.7}$$

The diagram in figure 8.4 shows the energy transfer process between lumogen orange and lumogen red. The pump energy is absorbed by the lumogen orange donor molecule, and is subsequently transferred to a lumogen red acceptor molecule where the exciton radiatively recombines, emitting a photon. The Förster energy transfer is shown by the dashed arrows between the molecules. The solid arrows show the Franck-Condon shift in each molecule.

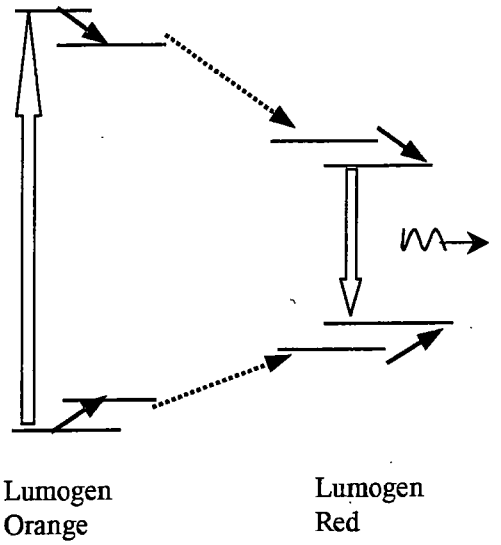

Figure 8.4: Förster transfer from lumogen orange to lumogen red molecules.

As equation 8.6 shows, the rate of energy transfer is a strong function of the acceptor and donor separation (R^6). In this chapter the rate of energy

transfer is investigated by controlling the concentration of the donor and the acceptor in the films and hence the intermolecular distance between them.

8.2.4 Least Squares Fitting

In order to quantify the energy transfer from donor to acceptor, it is useful to model the absorption and photoluminescence as a sum of the spectra of the pure materials. In order to do this accurately, a least squares fitting procedure was used. A least squares fit or linear regression is commonly used to find the best fit line through a series of experimental points. A function $F(x)$ is assumed to be linearly related to $G(x)$ through: $F(x) = aG(x) + b$ where a and b are constants [30]. In order to find the best way of describing a spectrum as the linear combination of two other spectra, this form has to be adapted to: $F(x) = aG(x) + bH(x)$ where $G(x)$ and $H(x)$ are the two spectra to be summed. By taking derivatives of this equation and setting it equal to zero to minimize it, the following relation is obtained:

$$b = \frac{[gf][hg] - [gg][hf]}{[hg]^2 - [gg][hh]} \tag{8.8}$$

$$a = \frac{[hf][hg] - [gf][hh]}{[hg]^2 - [gg][hh]} \tag{8.9}$$

where the formalism [gf] is used to denote $\Sigma_0^n G(x)F(x)$ where n is the number of points to be summed.

8.3 Experimental

8.3.1 Film Preparation

Blends of lumogen red and lumogen orange were formed in the host matrix poly methylmethacralate (PMMA). 250 mg of PMMA was dissolved in 1 ml of toluene. Lumogen red and lumogen orange were then added in the quantities shown in table 8.1. The total quantity of lumogen orange and lumogen red added was kept constant at 2.5 mg. Films approximately 3 μm were formed by spin coating onto fused silica substrates at 1500 rpm. In the measurements described later, the concentration of the dye molecules in the PMMA host i.e. the number of moles per unit volume was required. This was calculated by using the following relation:

$$C = \frac{\rho N_a}{M_m} \tag{8.10}$$

where C is the concentration in moldm^{-3}, ρ is the density of the PMMA (1.1 gcm^{-3}), M_m is the molar mass (700 g for lumogen orange and 1102 g for lumogen red) and N_A is Avagadro's number.

Film	Mass of red (mg)	Mass of orange (mg)	% Red by weight	% Orange by weight	Mass of PMMA (mg)
A	0.15	2.35	6	94	250
B	0.25	2.25	10	90	250
C	0.375	2.125	15	75	250
D	0.75	1.75	30	70	250
E	1.0	1.5	40	60	250

Table 8.1: Film composition

8.3.2 Quantum Yield Measurements

The photoluminescence quantum yield (PLQY) was measured using an integrating sphere [31]. The PLQY is defined as:

$$\phi = \frac{k_r}{k} = \frac{\tau}{\tau_r} = \frac{No.photons emitted}{No.photons absorbed} \tag{8.11}$$

where k is the total rate of decay, k_r is the rate of radiative decay and τ and τ_r are the corresponding lifetimes. The rate of radiative decay is the decay rate which is measured in the absence of any non-radiative decay. In practice non radiative decay competes with radiative decay, therefore the measured rate is the sum of radiative and non-radiative decay rates i.e. k=k_R+k_{NR}. In order to measure the PLQY, the method described by de Mello [32] was employed which was described in more detail in chapter 4. A CCD spectrograph was used to collect the excitation and photoluminescence light. Two spectra were recorded. The first was taken without a sample in the integrating sphere, to measure the intensity of the laser light. The sample was then placed in the integrating sphere in the path of the laser beam and the resulting spectrum measured. This method avoids the need to measure the absorption of the sample independently as the absorption is given by the drop in integrated laser intensity of the spectrum with a sample compared to the integrated intensity measured without a sample. The quantum yield of the sample is then calculated by integrating under the PL spectrum to give the number of photons emitted by the sample.

In order to calculate the rate coefficient for energy transfer, both the PLQY for a lumogen orange film and the PLQY for the orange component of the emission in the blends are required. The orange component of the emission was calculated by measuring the PL from the blend in the integrating sphere. The red and orange component of the spectrum were then

calculated by using a least squares fitting routine described in section 8.2.4. The quantum yield of the orange component could then be calculated.

8.3.3 Time-resolved Luminescence Measurements

The picosecond time resolved luminescence measurements were carried out on the same set of samples using the streak camera set-up at Sheffield University. The experimental set-up is shown in figure 8.5. The excitation source was the second harmonic (490 nm) of a mode-locked Ti-sapphire laser which produced 100 fs pulses. The luminescence was collected with an achromatic lens system and a double subtractive spectrometer (for spectral filtering of the emission with 10 nm FWHM resolution) and detected with a 2 ps resolution streak camera from DRS Hadland. Excitation light of 490 nm was used as the lumogen red is nearly transparent at this wavelength, therefore most of the pump radiation was absorbed by the lumogen orange.

8.4 Results - Evidence for Energy Transfer

In this investigation, it is first important to establish whether efficient energy transfer is taking place. In order to do this, the absorption and photoluminescence spectra for films with varying ratios of lumogen red to lumogen orange were measured. The graph in figure 8.6 shows the absorption for films doped with between 6% and 40% lumogen red. The graphs have been normalised to the peaks of the absorption as there was a slight variation in film thickness due to slightly varying viscosities of the spinning solutions. The figure shows strong vibronic features with peaks at 460 nm, 490 nm and 525 nm. These peaks are identical to the vibronic structure in lumogen orange in figure 8.3. The graph however shows an additional peak at 570 nm which changes in strength with doping concentration. By comparison to the lumogen orange

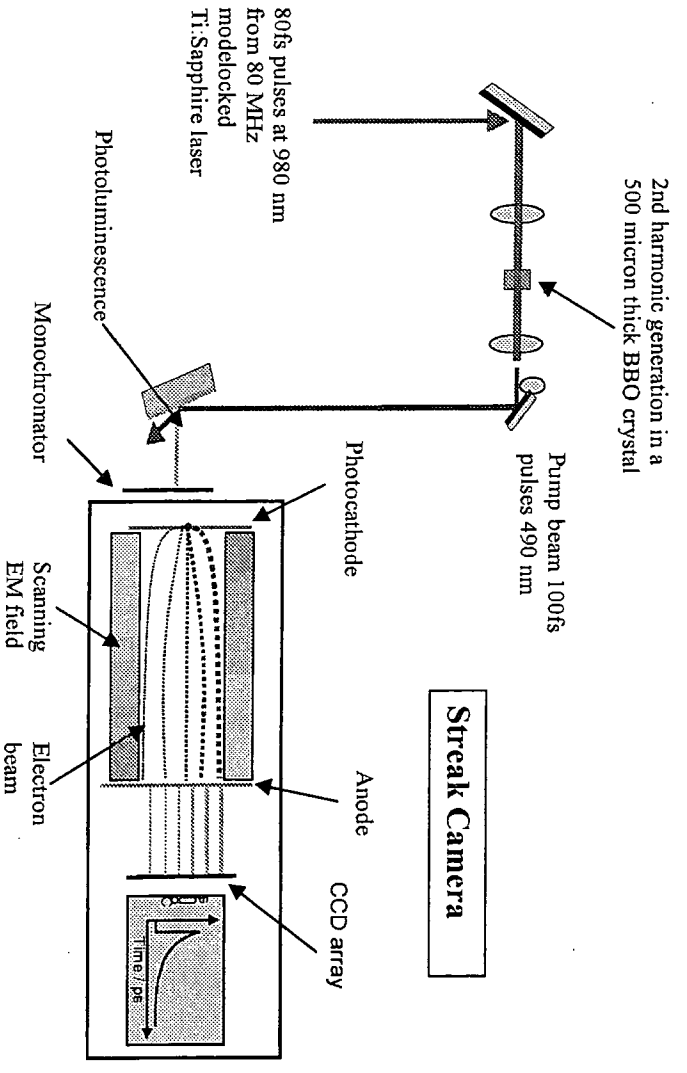

Figure 8.5: Schematic diagram of the streak camera set-up at Sheffield University

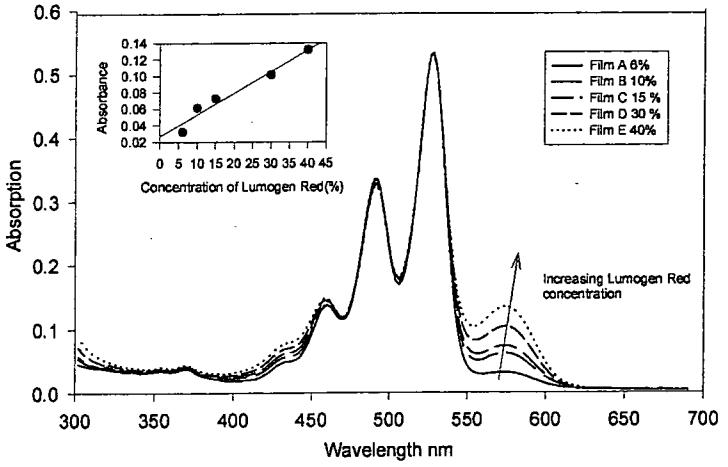

Figure 8.6: Absorption spectra of blends of lumogen orange doped with lumogen red. The insert shows the absorption at 570 nm as a function of concentration.

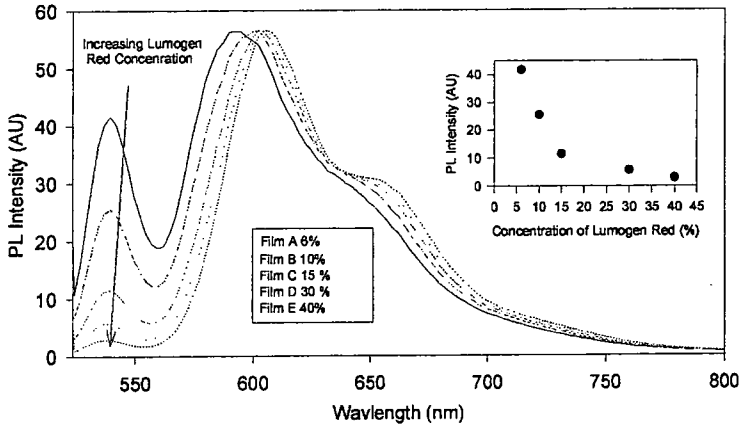

Figure 8.7: PL spectra of blends of lumogen orange doped with lumogen red. The insert shows the PL intensity at 540 nm as a function of concentration.

and lumogen red absorption spectra seen in figure 8.3, this peak is clearly due to the lumogen red absorption as the lumogen orange is transparent at this wavelength. As the concentration of the lumogen red is increased, the height of the peak at 570 nm also increases. The inset shows the absorbance at 570 nm against concentration of the lumogen red. A linear relationship is obtained as expected from the relation:

$$A = \epsilon CL \tag{8.12}$$

where A is the absorption of the sample, ϵ is the extinction coefficient, C is the concentration and L is the path length through the sample.

The photoluminescence spectra shown in figure 8.7 for the same films were measured using a flourimeter and exciting at a wavelength of 490 nm. The graphs have again been normalised to the peak of the PL spectrum. Some vibronic structure can be seen with peaks at 540 nm, 600 nm and 650 nm clearly visible. By comparison to the pure lumogen red and pure lumogen orange PL spectra in figure 8.3 the peak at 540 nm is assigned to the pure lumogen orange emission. As the concentration of the lumogen red in the blend increases the intensity of the peak at 540 nm decreases. The spectra also shift slightly to longer wavelengths as the concentration is increased. This is partly due to self-absorption. An increase in the absorption peak at 570 nm as the lumogen red concentration is increased is shown in figure 8.6. This affects the PL spectra by shifting them to the red with increasing concentration. However, a small shift is still seen at 650 nm, which is beyond the absorption tail. This is likely to be due to aggregation of the lumogen red. As the concentration is increased, the lumogen red molecules pack closer together, increasing the interaction between them.

The absorption spectra have been fitted using the least squares fitting routine described in section 8.2.4. Figures 8.8 and 8.9 show the results for

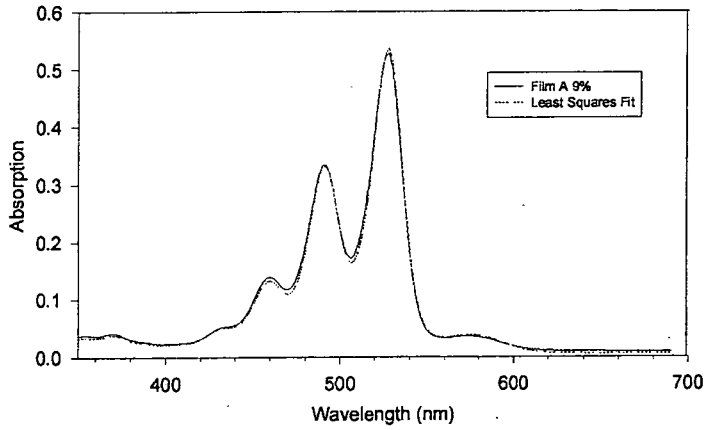

Figure 8.8: Absorption spectrum for film A (6%) (solid lines) and the results of the least squares fitting routine (dotted line).

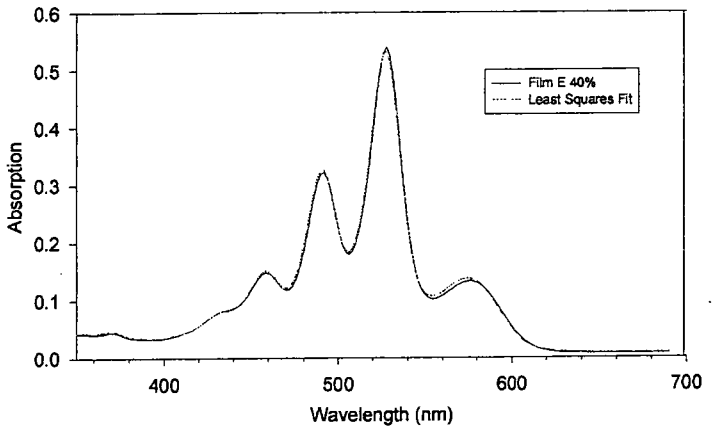

Figure 8.9: Absorption spectrum for film E (40%) (solid lines) and the results of the least squares fitting routine (dotted line).

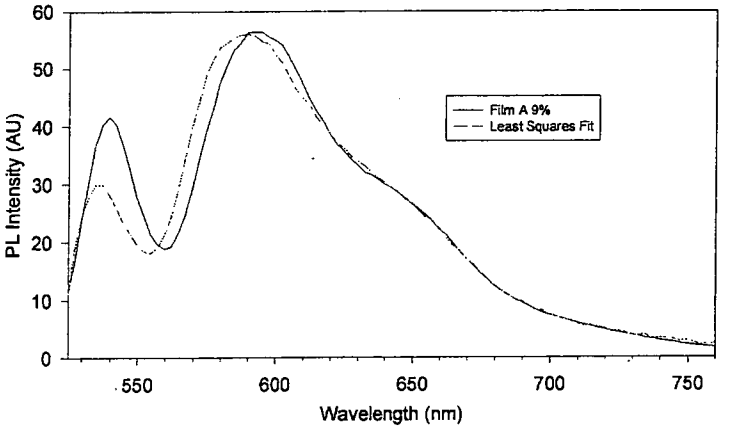

Figure 8.10: Photoluminescence spectrum for Film A (6%) (solid line) and the results of the least squares fitting routine (dotted line).

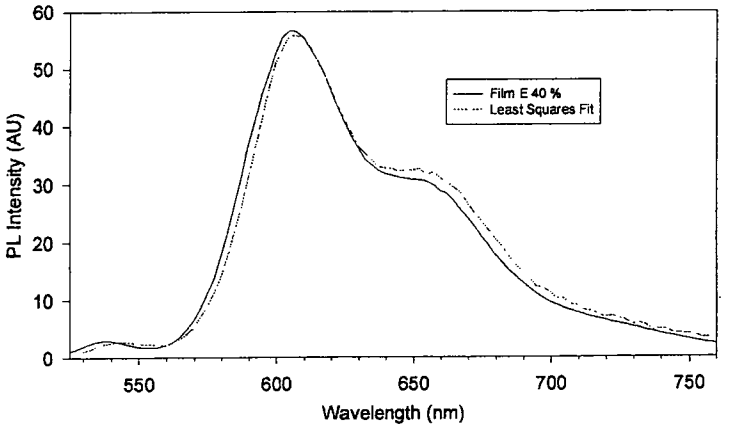

Figure 8.11: Photoluminescence spectrum for Film E (40%) (solid line) and the results of the least squares fitting routine (dotted line).

fitting the 6% and 40% doped film. These fits give very good agreement with the measured spectra. The ratio of lumogen orange to lumogen red is 16:1 for film A (6%) and 3:2 for film E (40%). These are the expected values for these films given the mass of material used. All the least squares fitting results are summarised in table 8.2.

Film	% Red by weight	%Absorption (red)	%Absorption (orange)	%PL (red)	%PL (orange)
A	6	6	94	25	75
B	10	10	90	58	42
C	15	15	85	78	22
D	30	30	70	84	16
E	40	40	60	94	6

Table 8.2: Table of data

Figures 8.10 and 8.11 show the photoluminescence spectra for film A and film E and the least squares fit obtained. The fit for film A is very good for wavelengths longer than 580 nm. Below 580 nm the general shape of the spectra are similar, but the intensity of the peak at 540 nm is not correctly represented. This could be due to slight differences in the thickness of the pure film compared to the thickness of the doped film. As there is a substantial overlap between the absorption and the emission for lumogen orange, self absorption can affect the relative ratios of the 0-0 peak at 540 nm and the 0-1 peak at 580 nm. However, at higher concentrations of lumogen red, the least squares fitted spectrum and the measured spectrum are very close, as shown in figure 8.11 for film E. The values for the ratios of lumogen red and lumogen orange obtained from the least squares fitting routine are shown in table 8.2 for both absorption and photoluminescence. These data show that the absorption spectra can be written as a linear sum of the absorptions of the pure materials and that the ratios are similar to the ratio by weight of

each material. In contrast, the photoluminescence data show that there is more emission from the lumogen red, than would be expected if there were no interaction between the two chromophores. This is clear evidence that efficient energy transfer occurs in this system. Figure 8.12 shows the absorption and PL spectra for film E (40% lumogen red) compared to the pure lumogen orange absorption and the pure lumogen red PL. The spectral characteristics of the film are very closely matched to the pure absorption and PL spectra, which is further evidence that efficient energy transfer is occurring in this system.

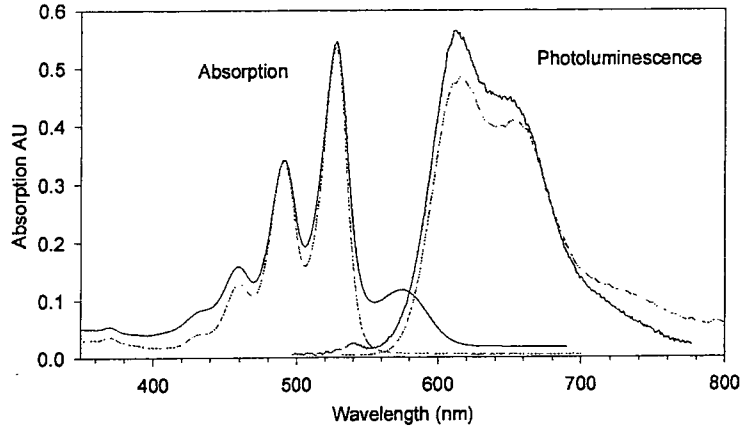

Figure 8.12: Absorption and photoluminescence of film E (40%) (solid lines) and absorption of pure lumogen orange and photoluminescence of pure lumogen red (dotted lines).

8.4.1 Determination of Ro from the Overlap Integral

The Förster radius R_0 can be determined from the overlap integral. As equation (8.5) shows, the rate of energy transfer is proportional to the overlap

integral which is given by equation (8.4).

Therefore a necessary condition for efficient energy transfer is good overlap between the donor (lumogen orange) emission and the acceptor (lumogen red) absorption. Figure 8.3 shows the absorption and photoluminescence for both lumogen orange and lumogen red, offset for clarity. This figure shows clearly that there is good overlap between the lumogen orange emission and the lumogen red absorption. In order to calculate the overlap integral and hence R_0, the extinction coefficient of the acceptor is required. The extinction coefficient for lumogen red was measured by making a set of five films of different optical densities. The absorption of these samples was then measured in pairs (one in the sample and one in the reference beam of the lambda 19 absorption spectrometer), so as to minimise the reflection from the front of the samples. The thickness of the samples was measured using the dektak profileometer. A graph of change in absorption against change in thickness for each pair of samples was then plotted and, using equation 8.12 an average extinction coefficient of $5\times10^4 \mathrm{cm}^{-1}$ was calculated. This technique has been used to calculate the absorption coefficient in conjugated polymer films and is described in more detail in chapter 4.

By integrating under the product of the photoluminescence spectrum of the donor and the extinction spectrum of the acceptor, the value of the overlap integral was calculated to be $7.3\times10^{-13}\mathrm{cm}^{-3}$. Equation (8.5) and (8.6) can be re-arranged to give the following relation:

$$R^6 = \frac{9000 f^2 ln10 \phi_D}{128\pi^5 N_A n^4} J \tag{8.13}$$

Values of the 1.47 for the refractive index (n) and 0.95 for the PLQY of the lumogen red (ϕ_D) were used in this equation to calculate the Förster radius. The value of the Förster radius was found to be 7.0 $\pm$1.0 nm. This compares well with the work of Sharma [34] who measured a Förester radius of 6.5 nm.

8.5 Results

8.5.1 ASE Results

The ASE spectra of blends with different lumogen red concentrations have been measured. The spectra were measured at excitation intensities a little above the threshold for ASE as shown in figure 8.13. This figure shows that the peaks of the ASE spectra are in two groups. The spectra of the film doped with the lowest concentration of lumogen red (6%) and the pure lumogen orange film are observed at 580 nm, whereas the spectra of the films with a higher concentration of lumogen red (10-40 %) are around 620 nm.

In order to show this data more clearly, the peak positions of the ASE have been plotted as a function of lumogen red concentration (figure 8.14). This graph shows clearly that there is a discontinuity in the spectral location of the peak of the ASE which occurs at a lumogen red concentration of about 10%. At high doping levels the position of the ASE is constant at 620 nm, whereas at low doping levels the ASE peak is observed at close to 580 nm. An important point to note is that the peak of the ASE spectrum from an undoped lumogen orange film is at 580 nm and the peak of the ASE spectrum for an undoped lumogen red film is observed at 620 nm. This shows that for films doped with less than 10% lumogen red the ASE is due to the lumogen orange molecules, whereas for higher concentrations energy transfer to the lumogen red takes place and the ASE is therefore due to the lumogen red molecules.

8.5.2 Determination of the Rate Coefficient

The absorption and photoluminescence measurements in this work have shown that efficient energy transfer can take place between lumogen orange and lumogen red. The ASE results presented above show that when the position

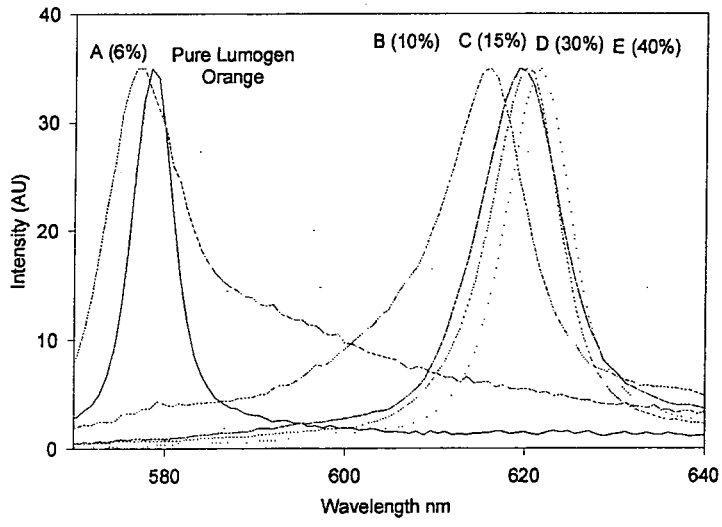

Figure 8.13: ASE spectra as a function of lumogen red concentration.

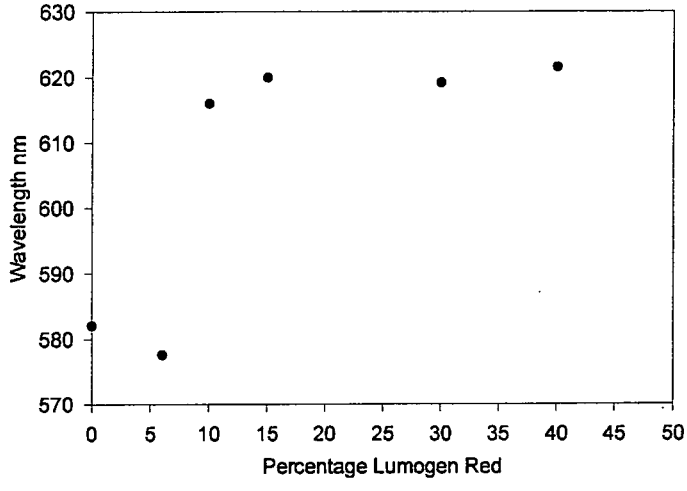

Figure 8.14: Peak position of the ASE spectra as a function of lumogen red concentration.

of the ASE peak is studied as a function of concentration, a discontinuity at about 10% is observed. In order to understand why the position of the ASE peak depends on the concentration of the lumogen red in the blend, the rate of energy transfer has been measured between these two dyes using two different methods.

The first method involves measuring how the photoluminescence quantum yield (PLQY) of the donor (lumogen orange) changes as the lumogen red concentration is increased. The second method uses the time-resolved luminescence technique to measure the radiative lifetime of the lumogen orange as a function of lumogen red concentration. Both of these methods give a measurement of the energy transfer coefficient (k_q). The energy transfer coefficient is the rate of energy transfer k_{ET} per unit mole dm^{-3} and is therefore related to the energy transfer rate through: $k_{ET} = [Q]k_q$ where [Q] is the concentration in mol dm^{-3} of the acceptor. This relation shows that as the concentration of the acceptor is increased, the distance between the acceptor and donor molecules decreases leading to an increase in the rate of energy transfer.

8.5.3 Method 1- Quantum Yield

Quantum yield measurements were made on films of lumogen red and lumogen orange using an integrating sphere as described in section 8.3.2. The quantum yield for a pure lumogen orange film was found to be 85±5% and the quantum yield for a pure lumogen red film was found to be 95±5%. The values in the literature are 0.96 and 0.99 respectively [25]. The measured quantum yield value for lumogen orange may be lower than the literature value as it shows a tendency to form crystals due to its planar structure [23, 33].

The quantum yield of a film is defined as in equation 8.11. In a blend of lumogen orange and lumogen red, the lumogen red quenches the lumogen

orange luminescence. The rate of quenching is equivalent to the rate of energy transfer from lumogen orange to lumogen red. It is therefore possible to derive an equation for the rate of quenching in terms of the quantum yield of the lumogen orange and lumogen red and the concentration of the lumogen red in the blend.

From equation 8.11 the quantum yield of a pure lumogen orange film can be written as:

$$\phi^0_{orange} = \frac{k_{orange}}{k} \tag{8.14}$$

where k_{orange} is the radiative decay rate of the lumogen orange and k is the total decay rate of the lumogen orange. The quantum yield of the lumogen orange component of the emission from the blend can be written as:

$$\phi_{orange} = \frac{k_{orange}}{k + k_q[Q]} \tag{8.15}$$

where k_q is the rate of quenching and $[Q]$ is the concentration of the acceptor (lumogen red in this case). By dividing equation 8.14 by equation 8.15 the following relation is reached:

$$\frac{\phi^0_{orange}}{\phi_{orange}} = 1 + \frac{k_q}{k}[Q] \tag{8.16}$$

This equation shows that the energy transfer coefficient is directly related to the quantum yield of the orange component of the emission in the blend, the quantum yield of a pure orange film and the concentration of the lumogen red in the film. These are all measurable parameters. The quantum yield of the lumogen red and lumogen orange components of the photoluminescence of the blends was measured. Figure 8.15 shows a plot of the ratio of the lumogen orange quantum yield of a pure film to the lumogen orange quantum yield

in a blend as a function of the lumogen red concentration (often referred to as a Stern Volmer plot).

Equation (8.16) shows that a plot of the ratio of the quantum yield of the pure orange to the quantum yield of the lumogen orange in the blends, as a function of concentration will give a straight line graph with an intercept of 1 and a gradient of k_q/k. This is believed to be the first demonstration of this relation using thin solid films of small organics.

The figure shows that a straight line is observed as expected from equation (8.16). The intercept of the graph is 0.7±0.2, close to the expected value of 1. The gradient of the graph is $1.93 \pm 0.02 \times 10^3 \text{mol}^{-1}\text{dm}^3$. In order to calculate k_q the measured decay rate is required. Sharma has made time-resolved luminescence measurements on blends of lumogen red and lumogen orange [34]. He measured a value of 3.6 ns for the decay time of lumogen orange. This corresponds to a decay rate of $2.8 \times 10^8 \text{s}^{-1}$. By using this value in equation (8.13), the energy transfer coefficient was found to be $5.4 \pm 0.2 \times 10^{11} \text{s}^{-1}\text{mol}^{-1}$ dm^3.

8.5.4 Method 2-Decay Rate

The second method for calculating the energy transfer coefficient involves measuring the decay rate of the lumogen orange component of the blend. When energy transfer occurs between a donor and an acceptor, the rate of decay of the donor increases i.e. the lifetime decreases. This increase in the rate is proportional to the rate of energy transfer. A similar method was employed to measure the rate of energy transfer in lumogens by Sharma [34].

The raw decay rate data is shown in figure 8.16. The data shows that as the concentration of lumogen red in the blend is increased, the decay time decreases, hence the decay rate increases. This data has been modelled using a bi-exponential fit of the form:

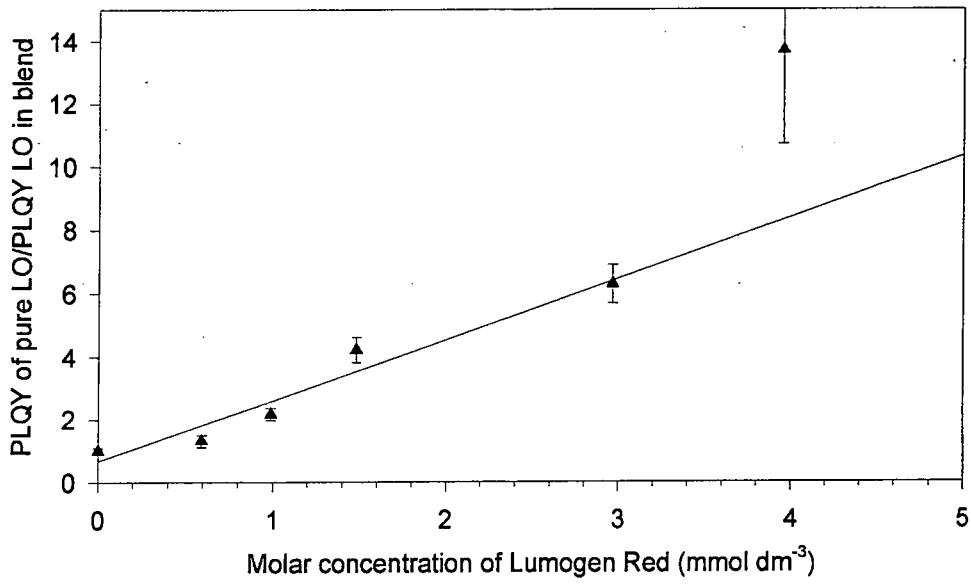

Figure 8.15: Quantum Yield Measurements as a function of concentration.

$$A + B_1 e^{-t/\tau_1} + B_2 e^{-t/\tau_2} \tag{8.17}$$

Where τ_1 and τ_2 represent the lifetimes to be fitted and B_1 and B_2 are the relative contributions of the individual lifetimes. The value of τ_1 corresponds to the decay time of the sample, however a second exponential was required to achieve a good fit and is due to defects in the sample such as inhomogeneity. The fits for film A and film E are shown in figure 8.17.

In order to express the energy transfer coefficient in terms of measurable quantities, equation 8.14 for the PLQY of a pure lumogen orange film can be rewritten to give an expression for the quantum yield of the lumogen orange

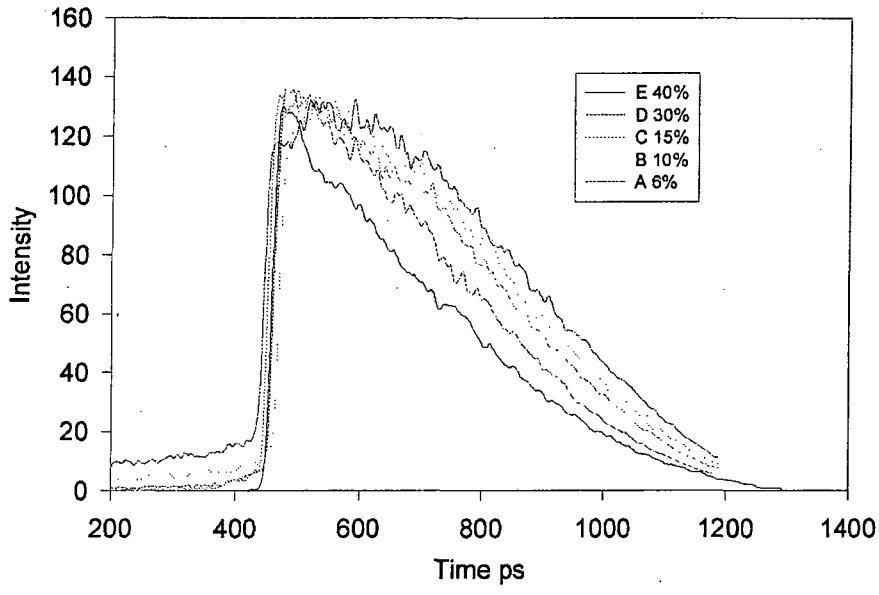

Figure 8.16: Raw time-resolved luminescence data for 5 films with different doping levels.

component of the blend. This is given by:

$$\phi_{orange} = \frac{k_{orange}}{k_b} \tag{8.18}$$

where k_b is the total decay rate of the blend. In the time-resolved luminescence measurements described above, the decay rate of the luminescence of the blend k_b is measured.

Equation 8.14 and equation 8.18 can then be substituted into the equation 8.16 which was derived for the quantum yield method in section 8.5.3. This

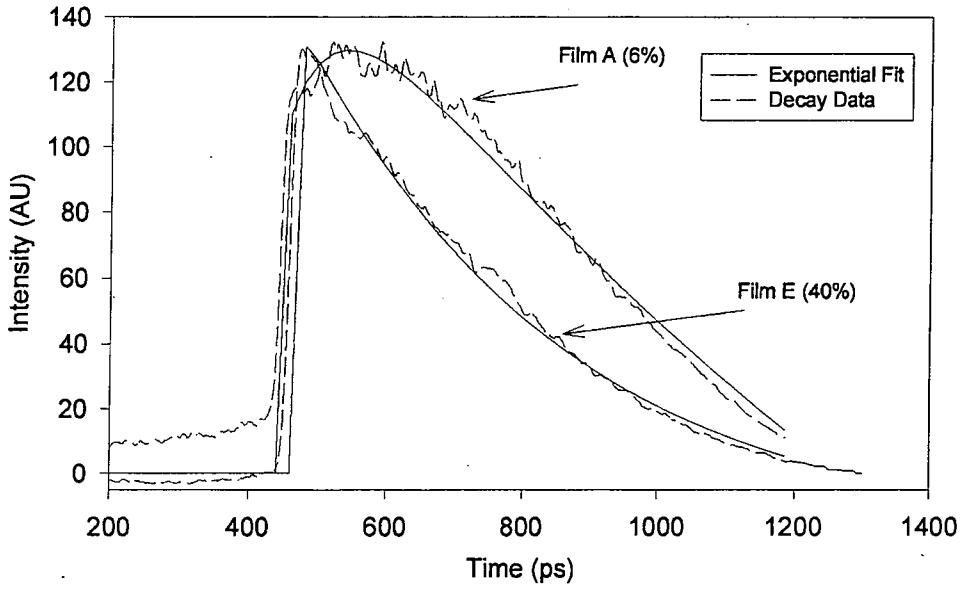

Figure 8.17: Exponential fits to time-resolved data for films A (6%) and E (40%).

gives a relation for the energy transfer coefficient in terms of measurable parameters:

$$k_b = k + k_q [Q] \tag{8.19}$$

This equation shows that by measuring the decay rate of the luminescence of the blend as a function of concentration, both the decay rate of the pure lumogen orange (k) and the energy transfer coefficient (k_q) can be derived.

The graph in figure 8.18 shows how the decay rate varies with concen-

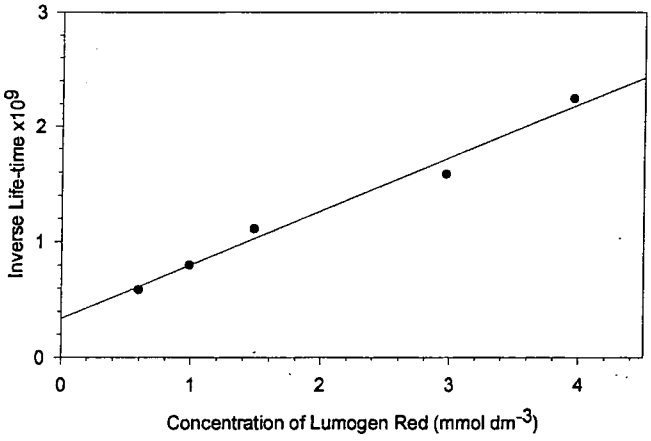

Figure 8.18: Decay rates measurements as a function of concentration.

tration of the lumogen red in the blend. The graph shows a linear relationship between the decay rate and the concentration. The gradient of the graph also gives the coefficient of energy transfer, k_q. From figure 8.18 k_q $= 4.6 \pm 0.2 \times 10^{11} s^{-1} mol^{-1} dm^3$. From the intercept k is $3.4 \times 10^8 s^{-1}$. This leads to a value of 2.9 ns for the radiative lifetime. This is close to the value of 3.6 ns obtained by Sharma on a similar system [34].

8.6 Comparison of Method 1 and Method 2

The absorption and photoluminescence data show that there is efficient dipole-dipole energy transfer between lumogen orange and lumogen red. The PLQY measurements and the time-resolved measurements of the blends of lumogen orange and lumogen red show that the rate coefficient is between $4.6 \pm 0.2 \times 10^{11}$ and $5.4 \pm 0.2 \times 10^{11} s^{-1} mol^{-1} dm^3$. It is possible to compare the data obtained using the two methods in one graph by translating the

time-resolved data into PLQY data as described below:

The ratio of the PLQY of the pure lumogen orange to the PLQY of the lumogen orange component in a blend can be related to the rate of decay of the pure lumogen orange and the rate of decay of the lumogen orange in the blend by dividing equations (8.14) and (8.18). This gives:

$$\frac{\phi^0_{orange}}{\phi_{orange}} = \frac{k_b}{k} \tag{8.20}$$

Using this equation, the decay rates measured using method 2 were translated into equivalent PLQY values. These values were plotted in figure 8.19 together with the PlQY values measured using method 1, so that the two methods could be compared.

The graph in figure 8.19 shows that there is very good agreement between the two sets of points and therefore the methods are both good ways of determining the rate of energy transfer.

From these measurements the critical concentration and hence the Förster radius can be calculated. The critical concentration is defined as the concentration at which the energy transfer is 50% efficient i.e when $2k_{rb} = k_r$ where k is the decay rate in s^{-1}. Substituting this into equation (8.19) gives:

$$k_r = k_q [Q] \tag{8.21}$$

From this and the values for k_r and k_q calculated by using the two different methods, the critical concentrations can be calculated. For method 1 the value obtained for the critical concentration is $6.4 \times 10^{-4} M$ and for method 2 the value obtained is $7.5 \times 10^{-4} M$.

From equation 8.7 R_0 was found to be 8.5 nm for method 1 and 8.1 nm for method 2. The average measured value for R_0 is therefore 8.3 nm. This is slightly higher than the value of 7.0 nm obtained from the overlap integral. This may be due to errors in the measurements of the quantum yield and of

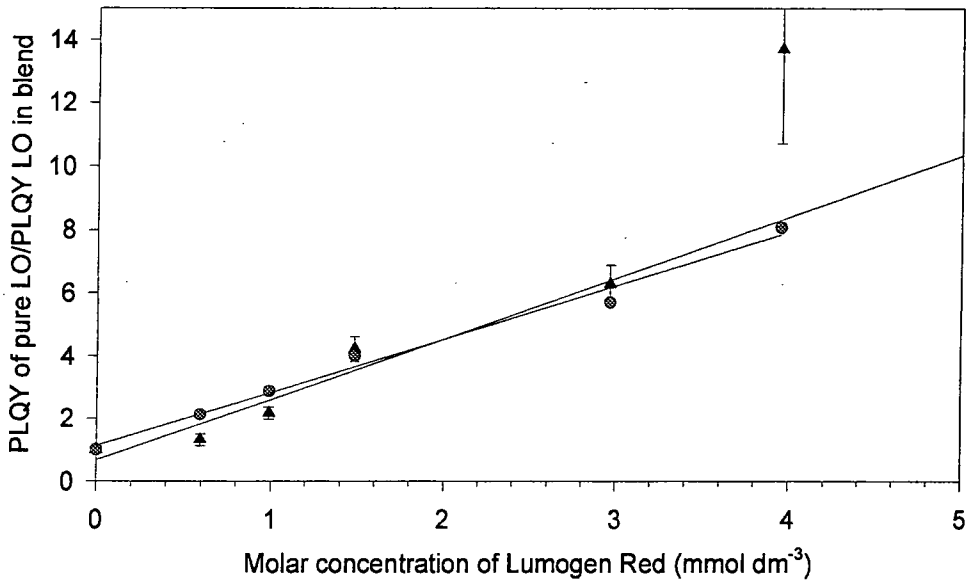

Figure 8.19: Quantum yield measurements as a function of concentration.

the decay time. There may also be donor-donor transfer which could result in a larger value of R_0 than that determined by the overlap integral [15]. These results also compare well with work by Sharma [34] who measured the decay time of the lumogen orange in lumogen orange/lumogen red blends in PMMA. He obtained a value of 6.5 nm for the Foïster radius.

8.7 Discussion

The measurements of the energy transfer rate described above can be used to understand why there is a discontinuity in the peak position of the ASE

as a function of concentration. The discontinuity seen in the ASE data may be due to competition between the energy transfer from the lumogen orange to the lumogen red and the stimulated emission mechanism. At low concentrations of lumogen red, the rate of energy transfer is small as the inter-molecular distance is large. The stimulated emission decay rate is the preferred channel for decay and therefore ASE from the lumogen orange is observed. At higher concentrations the rate of energy transfer is also higher so energy transfer becomes more efficient than stimulated emission as a decay pathway. The excitation will be transferred to the lumogen red before ASE is produced. Therefore for blends with high concentrations of lumogen red, the ASE peak is observed at the same wavelength as for the pure lumogen red film i.e. 620 nm.

The graph in figure 8.14 shows that the discontinuity in the position of the ASE spectra occurs at a doping level of 10% (1×10^{-3}M). Using this value an estimate can be made for the lifetime of the stimulated emission. At this concentration the stimulated emission rate is equal to the rate of energy transfer. Using the value of $5.0 \pm 0.2 \times 10^{11} \mathrm{s}^{-1}\mathrm{mol}^{-1}\mathrm{dm}^3$ for the rate coefficient and a concentration of 1×10^{-3}M, the stimulated emission rate is $4.9 \pm 0.2 \times 10^8 s^{-1}$. The stimulated emission lifetime is therefore 2.0 ns. This is shorter than the spontaneous emission lifetime which has a value of 3.6 ns measured by Sharma [34].

8.8 Conclusion

Thin films of blends of lumogen orange and lumogen red in a PMMA host matrix have been made and through absorption and photoluminescence measurements it has been shown that efficient energy transfer takes place from the donor (lumogen orange) to the acceptor (lumogen red). This has been successfully quantified by fitting the absorption and photoluminescence spectra as a sum of the pure lumogen orange and the pure lumogen red spectra. The Förster radius was calculated using the overlap integral technique and found to be 7.0 $\pm$1.0 nm.

The ASE properties for blends of different concentrations of lumogen red were investigated. The results show that the spectral position of the ASE depends on the concentration of the lumogen red in the blend. For low concentrations the peak of the ASE is observed at around 580 nm and for high concentrations it is observed at 620 nm. The concentration of lumogen red where the shift takes place is 10% = 1×10^{-3}M.

In order to understand the energy transfer dynamics, the rate of energy transfer has been measured using two different methods. The PLQY of the lumogen orange component of the emission was measured as a function of lumogen red concentration. Using this technique, the rate of energy transfer was found to be $5.4 \pm 0.2 \times 10^{11} \mathrm{s}^{-1}\mathrm{mol}^{-1}\mathrm{dm}^3$ and from this the value of R_0 was calculated to be 8.5 nm. The second method involved measuring the decay rate of the luminescence from the lumogen orange. Using this technique the rate of energy transfer was found to be $4.6 \pm 0.2 \times 10^{11} \mathrm{s}^{-1}\mathrm{mol}^{-1}\mathrm{dm}^3$. From this the value of R_0 was calculated to be 8.1 nm. These results show that both measurements give a Förster radius close to the value obtained from the overlap integral.

These values for the energy transfer rate were used to estimate the rate at which the excited state is de-excited. The concentration at which the rate

of stimulated emission is equal to the rate of energy transfer, was shown by the ASE data to be 10%. This was used to estimate the rate of stimulated emission and was found to be $4.9 \pm 0.2 \times 10^8 s^{-1}$.

These results show that energy transfer can be used effectively to control the emission wavelength.

Bibliography

[1] B.H. Soffer and B.B. McFarland. *Applied Physics Letters*, 10:266, 1967.

[2] H. Kogelnik and C.V. Shank. *Applied Physics Letters*, 18:152, 1971.

[3] A. Dogariu, D. Vacar, and A.J Heeger. *Physical Review B*, 58:10218, 1998.

[4] E.S. Maniloff, A.V. Klimov, and D.W. McBranch. *Physical Review B*, 56:1876, 1997.

[5] G.J. Denton, N. Tessler, N.T. Harrison, and R.H. Friend. *Physics Review Letters*, 78:733, (1997).

[6] S.V. Frolov, M. Liess, P.A. Lane, W. Gellerman, Z.V. Vardeny, M. Ozaki, and Yoshino K. *Physics Review Letters*, 78:4285, 1997.

[7] F. Hide, M. A. Diazgarcia, B. J. Schwartz, M. R. Andersson, Q. B. Pei, and A. J. Heeger. *Science*, 273(5283):1833, 1996.

[8] B. Schweitzer, G. Wegmann, H. Giessen, D. Hertel, H. Bassler, R. F. Mahrt, U. Scherf, and K. Mullen. *Applied Physics Letters*, 72(23):2933–2935, 1998.

[9] X. Long, M. Grell, A. Malinowski, D. D. C. Bradley, M. Inbasekaran, and E. P. Woo. *Optical Materials*, 9(1-4):70–76, 1998.

[10] V. Doan, V. Tran, and B. J. Schwartz. *Chemical Physics Letters*, 288(2-4):576–584, 1998.

[11] Cario and Franck. *Zeitschrift der Physik*, 17:202, 1923.

[12] S. E. Shaheen, B. Kippelen, N. Peyghambarian, J. F. Wang, J. D. Anderson, E. A. Mash, P. A. Lee, N. R. Armstrong, and Y. Kawabe. *Journal Of Applied Physics*, 85(11):7939–7945, 1999.

[13] H. Mattoussi, H. Murata, C. D. Merritt, Y. Iizumi, J. Kido, and Z. H. Kafafi. *Journal Of Applied Physics*, 86(5):2642–2650, 1999.

[14] V. G. Kozlov, V. Bulovic, P. E. Burrows, M. Baldo, V. B. Khalfin, G. Parthasarathy, S. R. Forrest, Y. You, and M. E. Thompson. *Journal Of Applied Physics*, 84(8):4096–4108, 1998.

[15] U. Lemmer, A. Ochse, M. Deussen, R. F. Mahrt, E. O. Gobel, H. Bassler, P. H. Bolivar, G. Wegmann, and H. Kurz. *Synthetic Metals*, 78(3):289–293, 1996.

[16] G. Dicker, A. Hohenau, W. Graupner, S. Tasch, M. Graupner, A. Hermetter, B. Schlicke, N. Schulte, A. D. Schluter, U. Scherf, K. Mullen, and G. Leising. *Synthetic Metals*, 102(1-3):873–874, 1999.

[17] R. Gupta, M. Stevenson, M. D. McGehee, A. Dogariu, V. Srdanov, J. Y. Park, and A. J. Heeger. *Synthetic Metals*, 102(1-3):875–876, 1999.

[18] A. Dogariu, R. Gupta, A. J. Heeger, and H. Wang. *Synthetic Metals*, 100(1):95–100, 1999.

[19] R. S. Deshpande, V. Bulovic, and S. R. Forrest. *Applied Physics Letters*, 75(7):888–890, 1999.

[20] G. Seybold and G. Wagonblast. *Dyes Pigmants*, 11:303, 1989.

[21] S. Demmig and H. Langhals. *Chemische Berichte-Recueil*, 121(2):225–230, 1988.

[22] A. Rademacher, S. Markle, and H. Langhals. *Chemische Berichte-Recueil*, 115(8):2927–2934, 1982.

[23] M. D. Rahn, T. A. King, A. A. Gorman, and I. Hamblett. *Applied Optics*, 36(24):5862–5871, 1997.

[24] J. Ivri, Z. Burshtein, E. Miron, R. Reisfeld, and M. Eyal. *IEEE Journal Of Quantum Electronics*, 26(9):1516–1520, 1990.

[25] M. D. Rahn and T. A. King. *Applied Optics*, 34(36):8260–8271, 1995.

[26] A.A. Turro N.J. Lamola. *Energy Transfer and Organic Photochemistry.* Interscience Publishers, 1969.

[27] G. Gaviola and P. Pringsheim. *Zeitschrift der Physik*, 24:24, 1924.

[28] T. Forster. *Annalen der Physik.*, 2:55, 1948.

[29] T. Forster. *Discussions Faraday Soc.*, 27:7, 1959.

[30] *An Introduction to Error Analysis.* Oxford University Press, 1982.

[31] N. C. Greenham, I. D. W. Samuel, G. R. Hayes, R. T. Phillips, Yarr Kessener, S. C. Moratti, A. B. Holmes, and R. H. Friend. *Chemical Physics Letters*, 241(1-2):89–96, 1995.

[32] J. C. deMello, H. F. Wittmann, and R. H. Friend. *Advanced Materials*, 9(3):230 (4 pages), 1997.

[33] S. Liu and L.L. Hench. *Proceedings of the Society of Photo-optical Instrumentation*, 1758:14, 1992.

[34] P Sharma. *Polymeric Thin Films for Integrated optics.* PhD thesis, 1992.

Chapter 9

Conclusions

Lasers and amplifiers made from conjugated polymers have the potential to revolutionise the communications industry. These semi-conducting materials, which demonstrate strong amplification over a broad gain bandwidth are easy to process and will be of great importance in future devices. For this reason, the work in this thesis has investigated the factors which affect the gain in conjugated polymers and perylene dyes. An investigation of the stimulated emission characteristics of MEH-PPV, a red emitting polymer has shown that the mechanism for the spectral line-narrowing (SLN) is amplified spontaneous emission (ASE). The gain coefficient was measured to be 4 cm^{-1} and the loss coefficient at 620 nm was 10 cm^{-1}. Measurements also showed that there was no effect of excitation wavelength on the position of the ASE.

The effect of temperature on the absorption, photoluminescence and ASE characteristics of MEH-PPV films were also investigated. Films spun from both THF and CB were compared and it was found that the film morphology affected the temperature dependence of the films. A smaller shift of the ASE peak position compared to the PL for both THF and CB films was observed. The two possible explanations for this are: (1) the ASE originates from ordered sites whereas PL is due to all sites and (2) the position of the net

gain is influenced by other processes such as excited state absorption.

It was also shown that the absorption peak had the same temperature dependence as the PL with the thermal energy kT subtracted. This is evidence that the excitons migrate until they are within kT of the lowest energy sites in the sample.

It was found that the spectral position of the ASE could be controlled by 31 nm which corresponds to a bandwidth of 25 THz. This was achieved by changing the film thickness close to the cut-off thickness for waveguiding. Modeling of the waveguide modes in the asymmetric waveguide showed that the cut-off thickness determines the wavelength of the ASE peak for thin films, whereas for thick films the peak of the ASE is determined by the position of the maximum gain. A technique for measuring the cut-off thickness of the polymer films was used and good agreement with the modeled data was observed.

The process of energy transfer in organic films is potentially very useful in that both the pump and the emission wavelength can be controlled. Efficient energy transfer (Förster transfer) was observed between two perylene dyes (lumogen orange and lumogen red). The energy transfer dynamics were investigated in blends of these chromophores doped into the host matrix PMMA. The position of the ASE was found to depend on the lumogen red (acceptor) concentration. Below an acceptor concentration of 1×10^{-3}M the ASE was observed at 580 nm (originating from the lumogen orange) and above the ASE was at 620 nm (originating from the lumogen red). The energy transfer coefficient was measured using two different techniques to be $5 \pm 0.2 \times 10^{11} \text{mol}^{-1}\text{dm}^3$. This was used to estimate the rate of stimulated emission at $4.9 \times 10^8 s^{-1}$.

In the future work could focus on the mechanism for spectral line-narrowing, as although the current opinion is that ASE is responsible for the dramatic narrowing of the emission spectrum no work has showed conclusively that

this is the case. Experiments would have to be carefully designed to distinguish between ASE and spontaneous emission processes. It would also be interesting to investigate energy transfer in more detail, especially as a mechanism for controlling the emission wavelength, and this could be extended to polymer systems.

Appendix A

Papers published as a result of this thesis

- Photophysics of an alkyl substituted poly(p-phenylenevinylene) A.K. Sheridan, I.D.W. Samuel, A.Bleyer, D.D.C. Bradley,Synthetic Metals, 101 pp 259 (1999).
- Tuneability of the ASE in thin organic films. A.K.Sheridan, G.A.Turnbull, D.D.C.Bradley, I.D.W.Samuel, Synthetic Metals, in press
- The temperature dependence of the spectral line narrowing and photoluminescence of MEH-PPV, A.K.Sheridan, J.M. Lupton, I.D.W. Samuel, D.D.C. Bradley, Synthetic Metals 111-112 pp 533 (2000).
- The effect of temperature on the spectral line narrowing in MEH-PPV, A.K. Sheridan, J.M. Lupton, I.D.W. Samuel, D.D.C. Bradley, Chemical Physics Letters, 322 pp51 (2000)
- Tunability of amplified spontaneous emission through control of the waveguide mode-structure in conjugated polymer films A.K. Sheridan,

G.A. Turnbull, A. Safonov, and W.L. Barnes, I. D. W. Samuel, Physical Review B 62 pt18 pp R11929 (2000)

Appendix B

Papers published from related work:

- Comparison of the electronic properties of poly[2-(2'-ethylhexyloxy)-1,4-phenylenevinylene], prepared by different precursor polymer routes, S-C. Lo, A.K. Sheridan, I.D.W. Samuel, P.L.Burn, The Journal of Materials Chemistry 9, No.9, pp 2165 (1999)
- Comparison of precursor polymer routes to and electronic properties of phyenyacetylene derivatised poly[2-(2'-ethylhexyloxy)-1,4-phenylenevinylene], S-C. Lo, A.K. Sheridan, I.D.W. Samuel, P.L.Burn. , The Journal of Materials Chemistry, 10 pp 275 (2000)
- Effect of different precursor routes on the electronic properties of poly[2-(2'-ethylhexyloxy)-1,4-phenylenevinylene] and poly[2-(2'-ethylhexyloxy)-5-(phenylethynyl)-1,4-phenylenevinylene] S-C. Lo, A.K. Sheridan, I.D.W. Samuel, P.L.Burn. Abstracts of papers of the American Chemical Society, 218, No.Pt2, pp.551-POLY (1999).
- Tuning the opto-electronic properties of pyridine-containing polymers for light emitting devices, C. Wang, M. Kiliziraki, J.A. Macbride, M.

R. Bryce, L.E. Horsburgh, A.K. Sheridan, A. P. Monkman, I.D.W. Samuel. Advanced Materials, 12 No.3 pp 217 (2000).

- Conjugated polymer and dye molecules investigated by means of photo thermal deflection spectroscopy, L.O. Palson, P.D. Wood, A.K.Sheridan, I.D.W.Samuel. Chemical Physics Letters, submitted.